

Integrated spectroscopy of the *Herschel* Reference Survey.

The spectral line properties of a volume-limited, K-band selected sample of nearby galaxies^{*}

A. Boselli¹, T.M. Hughes², L. Cortese³, G. Gavazzi⁴, V. Buat¹

¹ Laboratoire d'Astrophysique de Marseille - LAM, Université d'Aix-Marseille & CNRS, UMR7326, 38 rue F. Joliot-Curie, 13388 Marseille Cedex 13, France e-mail: Alessandro.Boselli@oamp.fr, Veronique.Buat@oamp.fr

² Kavli Institute for Astronomy & Astrophysics, Peking University, Beijing 100871, P.R. China e-mail: tmhughes@pku.edu.cn

³ European Southern Observatory, Karl-Schwarzschild Str. 2, 85748 Garching bei Muenchen, Germany e-mail: lcortese@eso.org

⁴ Università di Milano-Bicocca, piazza della Scienza 3, 20126, Milano, Italy e-mail: giuseppe.gavazzi@mib.infn.it

ABSTRACT

We present long-slit integrated spectroscopy of 238 late-type galaxies belonging to the *Herschel* Reference Survey, a volume limited sample representative of the nearby universe. This sample has a unique legacy value since ideally defined for any statistical study of the multifrequency properties of galaxies spanning a large range in morphological type and luminosity. The spectroscopic observations cover the spectral range 3600-6900 Å at a resolution $R \approx 1000$ and are thus suitable for separating the underlying absorption from the emission of the $H\beta$ line as well as the two [NII] lines from the $H\alpha$ emission. We measure the fluxes and the equivalent widths of the strongest emission lines ([OII] λ 3727, $H\beta$, [OIII] λ 4959 and [OIII] λ 5007, [NII] λ 6548, $H\alpha$, [NII] λ 6584, [SII] λ 6717 and [SII] λ 6731). The data are used to study the distribution of the equivalent width of all the emission lines, of the Balmer decrement $C(H\beta)$ and of the observed underlying Balmer absorption under $H\beta$ ($E.W.H\beta_{abs}$) in this sample. Combining these new spectroscopic data with those available at other frequencies, we also study the dependence of $C(H\beta)$ and $E.W.H\beta_{abs}$ on morphological type, stellar mass and stellar surface density, star formation rate, birthrate parameter and metallicity in galaxies belonging to different environments (fields vs. Virgo cluster). The distribution of the equivalent width of all the emission lines, of $C(H\beta)$ (or equivalently of $A(H\alpha)$) and $E.W.H\beta_{abs}$ are systematically different in cluster and field galaxies. The Balmer decrement increases with stellar mass, stellar surface density, metallicity and star formation rate of the observed galaxies, while it is unexpectedly almost independent from the column density of the atomic and molecular gas. The dependence of $C(H\beta)$ on stellar mass is steeper than that previously found in other works. The underlying Balmer absorption does not significantly change with any of these physical parameters.

Key words. Galaxies: spiral; Galaxies: ISM; ISM: dust, extinction

1. Introduction

A complete understanding of the matter cycle in galaxies, i.e. of the process that transforms the primordial atomic gas into molecular clouds where stars are formed, and of the metal production and the formation of dust grains requires a multifrequency analysis. Indeed, the atomic gas can be directly observed using the 21 cm emission line, while the molecular component is generally traced by the emission of carbon monoxide emission lines. Star formation can be quantified under some assumptions through the observations of the ionised hydrogen or of the UV stellar continuum emitted by the youngest stellar populations. Dust, formed by the aggregation of metals produced in the final phases of stellar evolution and injected into the interstellar medium by stellar winds and supernovae explosions, absorbs the stellar radiation and re-emits the acquired energy in the infrared domain (e.g. Boselli 2011).

With the aim of studying the matter cycle in galaxies of different morphological type and luminosity, we have defined a K-band selected, volume limited sample of nearby galaxies, the *Herschel* Reference Survey (HRS; Boselli et al. 2010a), to be observed in guaranteed time with the SPIRE instrument (Griffin et al. 2010) on board of *Herschel* (Pilbrat et al. 2010). This

sample, which includes just over three hundreds objects, is ideally defined for characterising the statistical properties of normal, nearby galaxies. Given the tight relation between the near-infrared bands and the total stellar mass of galaxies (Gavazzi et al. 1996), the choice of the K band secures a stellar mass selection. The sample, which includes both isolated galaxies and objects in the Virgo cluster, is also appropriate for studying the effects of the environment on galaxy evolution (Boselli & Gavazzi 2006).

Since the definition of the sample, which is extensively described in Boselli et al. (2010a), we are making a huge effort at gathering multifrequency data spanning the whole range of the electromagnetic spectrum to offer to the astronomical community a complete and homogeneous set of data suitable for any kind of statistical analysis. Near infrared and optical images are already available thanks to the 2MASS (Jarrett et al. 2003; Skrutskie et al. 2006) and SDSS (Adelman-McCarthy et al. 2008) surveys. The SPIRE imaging data at 250, 350 and 500 μ m of the whole sample, collected during the first year of *Herschel*, have been recently published in a dedicated paper (Ciesla et al. 2012). A cycle 6 GALEX legacy survey has been completed (Cortese et al. 2012a). Combined with the data obtained during the Virgo cluster survey (GUViCS; Boselli et al. 2011), this provides FUV and NUV magnitudes for most of the HRS galaxies. We are also undertaking an $H\alpha$ + [NII] imaging survey at San Pedro Martir,

^{*} Based on observations collected at the Observatoire de Haute Provence (OHP) (France), operated by the CNRS

Mexico (Boselli et al., in prep.) and a $^{12}\text{CO}(1-0)$ survey of the star forming spirals of the sample with the 12 m Kitt Peak radio telescope. The present paper is devoted to the publication of the long-slit, integrated spectroscopy of the late-type systems obtained with the 1.93 m telescope of the Observatoire de Haute Provence.

Given the complete nature of the *Herschel* Reference Survey, we use these data to make a statistical analysis of the spectroscopic properties of a mass-selected sample of nearby galaxies in different environments. We study the distribution of the equivalent width of the different emission lines. The equivalent widths are normalised indices and are thus ideally defined for a direct comparison of galaxies of different size and luminosity. We focus our attention on the analysis of the Balmer decrement. This index traces the attenuation of the emission lines due to dust. Its importance resides in the fact that, when far infrared data are missing, it is often used in cosmological surveys to quantify the amount of dust attenuation of the stellar emission with the Calzetti law (Calzetti 2001). Spectroscopic surveys are allowing the measurement of this quantity for galaxies at higher redshift (e.g. Caputi et al. 2008; Ly et al. 2012). We also analyse the statistical properties of the underlying Balmer absorption due to the absorption of the stellar continuum in the atmosphere of warm A-type stars (Poggianti & Barbaro 1997; Thomas et al. 2004). This index, crucial for an accurate measure of the Balmer decrement, is often used as an indicator of the mean age of the underlying stellar population. In an accompanying paper (Hughes et al. 2012), we analyse the stellar mass - metallicity relation in the same complete sample of nearby galaxies and its dependence on the environment. Several papers based on the exploitation of the SPIRE data of the HRS have been published in the *Herschel* dedicated A&A special issue or in more recent communications. Some of these are focused on the study of the statistical properties of the HRS sample: in Cortese et al. (2011a) and Cortese et al. (2012b) we analyse the HI gas and dust scaling relations of the whole sample. The far infrared colours and the spectral energy distributions are discussed in Boselli et al. (2010b) and Boselli et al. (2012), while the dust properties of the early-type systems in Smith et al. (2012a). Some of these works are already taking advantage of the spectroscopic data presented here.

The spectroscopic data presented in this work, as well as those collected at other frequencies, will be made available to the community through the dedicated HeDaM database (<http://hedam.oamp.fr/>; Roehlly et al. 2012).

2. The sample

The *Herschel* Reference Survey is a SPIRE guaranteed time key project aimed at observing with *Herschel* a complete, K-band selected ($K \leq 8.7$ mag for early-types, $K \leq 12$ for type \geq Sa), volume limited ($15 \leq D \leq 25$ Mpc) sample of nearby galaxies at high galactic latitude. The sample, which is extensively presented in Boselli et al. (2010a), is composed of 322 galaxies out of which 260 are late-type systems¹. Figure 1 shows the distribution of the different morphological classes within the HRS. The K-band selection has been chosen as a proxy for galaxy stellar mass (Gavazzi et al. 1996). The sample includes objects in environments of different density, from the core of the Virgo

¹ With respect to the original sample given in Boselli et al. (2010a), we removed the galaxy HRS 228 whose new redshift indicates it as a background object. We also revised the morphological type for three galaxies that moved from the early- to late-type class: NGC 5701, now classified as Sa, and NGC 4438 and NGC 4457 now Sb.

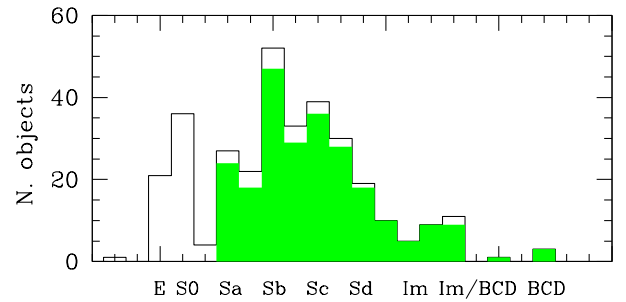


Fig. 1. Distribution in morphological type of all the HRS galaxies (solid line) and of the late-type systems with available spectroscopic data (green).

cluster, to loose groups and fairly isolated systems. As defined, the present sample is ideal for any statistical study of the mean galaxy population of the nearby universe.

This paper is focused on the late-type galaxies of the sample. We present new spectroscopic observations of 134 galaxies², and we combine this new dataset with the one already published by our team for Virgo cluster objects (Gavazzi et al. 2004) or available in the literature (Kennicutt 1992a, 1992b; Jansen et al. 2000; Moustakas & Kennicutt 2006; Moustakas et al. 2010) with the purpose of providing the most complete and homogeneous list of spectroscopic parameters of these late-type systems. The resulting spectroscopic sample is fairly complete since it includes 238 out of the 260 late-type systems (see Figure 1).

3. Observations

Late-type HRS galaxies have been observed during 51 nights in the years 2004-2009 using the 1.93 m telescope of the Observatoire d'Haute Provence (OHP; see Table 1). Data were acquired using a telescope configuration and sky conditions similar to those of Gavazzi et al. (2004). Observations were carried out using the CARELEC spectrograph and a grism with a dispersion of 133 \AA/mm corresponding to 1.8 \AA/pixel . The spectrograph is equipped with a 2048×1024 EEV CCD with a pixel of 13.5 \mu m , and a spatial scale of $0.58 \text{ arcsec/pixel}$. Galaxies were observed using a 5 arcmin slit of width of 2.5 arcsec, adapted for the typical seeing conditions (2-3 arcsec). To obtain data representative for the whole galaxy, most targets have

² Four other galaxies with data available in the literature have been also observed, bringing the total number of observed objects to 138.

Table 1. Logbook of the observations

Date	N. of galaxies
17-25/4/2004	4
4-10/3/2005	18
11-22/4/2007	69
3-9/3/2008	23
25-31/3/2009	24

been observed in drift-scan mode, i.e. with the slit, generally parallel to the galaxy major axis, drifting over the optical surface of the galaxy³. For those few objects with angular size larger than the size of the slit, the drift was done in the direction perpendicular to the major axis. Drifting was obtained by slewing manually several times the telescope between two extreme positions checked on one offset star or on the galaxy itself. Not unexpectedly spectra obtained in this way have lower S/N ratio than traditional long-slit spectra of similar integration time, because a large fraction of the time is spent on low surface brightness regions. Bright stars overposed on the disc of the galaxies were avoided, whenever possible, during the observations, or identified as high-surface brightness regions in the spectra and removed during the data reduction. Our spectra cover the wavelength range 3600-6900 (from [OII] to [SII]) with a resolution of $R \approx 1000$. Observations were taken either in photometric conditions or through thin cirrus⁴. Typical integration times are of 900-3600 sec, depending on the surface brightness of the target. The spectra were calibrated using the spectrophotometric standards Feige 34 and Hz 44 from the catalogue of Massey et al. (1988) observed twice on each night.

The general properties of the target galaxies and the log-book of the observations are presented in Table 7. Each column contains:

- Column 1: *Herschel* Reference Sample (HRS) name, from Boselli et al. (2010a).
- Columns 2-6: Name as in the Catalogue of Galaxies and Clusters of Galaxies (CGCG; Zwicky et al. 1961-1968), Virgo Cluster Catalogue (VCC; Binggeli et al. 1985), Uppsala General Catalogue (UGC; Nilson 1973), New General Catalogue (NGC) or Index Catalogue (IC) (Dreyer 1888, 1908).
- Column 7, 8: J2000 right ascension and declination, from NED.
- Column 9: Distance in Mpc, determined assuming galaxies in Hubble flow outside the Virgo cluster (with $H_0 = 70 \text{ km s}^{-1} \text{ Mpc}^{-1}$) or according to their membership to the different Virgo cluster substructures as indicated by Gavazzi et al. (1999) (17 Mpc for Virgo A and for all the other clouds with the exception of Virgo B, taken at 23 Mpc).
- Column 10: Morphological classification, from NED.
- Column 11: Total 2MASS K-band magnitude (Jarrett et al. 2003; Skrutskie et al. 2006).
- Column 12: Optical isophotal diameter D_{25} (25 mag arcsec⁻²), in arcmin, from NED.
- Column 13: Heliocentric radial velocity, in km s^{-1} , from NED.

³ No drift has been done on perfectly edge-on galaxies and on a few other objects.

⁴ The 2006 run was totally lost due to bad weather conditions.

- Column 14: Cluster or cloud membership, from Gavazzi et al. (1999) for Virgo, and Tully (1988) or Nolthenius (1993) whenever available, or from our own estimate otherwise (Boselli et al. 2010a).
- Column 15: Observing run.
- Column 16: Photometric quality, classed as either photometric (P), transparent (T) or thin Cirrus (C).
- Column 17: Integration time (as number of exposures \times individual exposure time).

4. Data reduction

In order to form a homogeneous dataset with the existing observations of Gavazzi et al. (2004), we apply the same data reduction method to the new observations presented in this work. The reduction of the observations from the raw, two-dimensional images into calibrated, one-dimensional spectra is performed using standard tasks within the IRAF⁵ package. Bias subtraction is applied using the median of several bias frames and the median of exposures of quartz lamps is used for correcting the flat-field. Cosmic rays are removed by using COSMICRAY. Under visual inspection, remaining extended features are manually removed and any bad pixel is masked.

The wavelength calibration is carried out using IDENTIFY, REIDENTIFY and FITCOORD on combined exposures of helium and argon lamps, typically using 20-30 arc lines. The calibration solution is then applied to the science frames using TRANSFORM. Using measurements of sky emission lines to test the accuracy of the calibration, we find the typical error in the solution being 0.1 - 0.2 Å. We manually correct the calibrations for systematic offsets, thus reducing the typical wavelength calibration errors to $\leq 0.5 \text{ Å}$.

Subtraction of the sky background from the two-dimensional images is performed with the BACKGROUND task and then the one-dimensional spectra are extracted using APSUM to define an aperture along which the signal is integrated.

The flux calibration to transform the measured intensities into flux densities is performed by the STANDARD, SENSFUNC and CALIBRATE tasks. The standard star frames, taken of Feige 34 and Hz 44 on each observing night, are used to determine the sensitivity function of the detector. The STANDARD task integrates the standard star observations over calibration bandpasses and the measurements are corrected for atmospheric extinction using the reference extinction data in IRAF. The observational measurements from these bandpasses are then compared with the standard reference observations to determine the system sensitivity as a function of wavelength. The calibration factor used to convert from the measured intensities into flux densities at each wavelength is determined with SENSFUNC.

The CALIBRATE task uses these sensitivity functions to convert the observed intensities at each wavelength in each spectra into flux densities, i.e. with units of $\text{erg cm}^{-2} \text{ s}^{-1} \text{ Å}^{-1}$, corrected for atmospheric extinction. Finally, each spectra is transformed to the rest frame wavelength. Two template spectra are chosen to represent absorption-line objects or emission-line objects, and these templates are converted to their rest frame wavelength.

⁵ IRAF is the Image Analysis and Reduction Facility made available to the astronomical community by the National Optical Astronomy Observatories, which are operated by AURA, Inc., under contract with the U.S. National Science Foundation. STSDAS is distributed by the Space Telescope Science Institute, which is operated by the Association of Universities for Research in Astronomy (AURA), Inc., under NASA contract NAS 5-26555.

The `FXCOR` task cross-correlates the template spectrum to the remaining spectra of each object type, thus determining the relative shift for each spectra. This shift is then applied with `DOPCOR`. Due to the manual drifting of the telescope during the observations, however, we are in the impossibility of reconstructing the absolute flux within a given aperture of the observed galaxies. For this reason we normalise all spectra to their mean intensity between $\lambda = 5400 - 5600 \text{ \AA}$. The typical signal to noise of the reduced spectra, measured using the `DER_SNR` package⁶, ranges in between $S/N \sim 15$ and 70 , but is significantly lower in the blue range ($\lambda \leq 4000 \text{ \AA}$: $S/N \sim 5-20$) because of the low sensitivity of the EEV CCD. The observed spectra of all HRS galaxies, including those with data available in the literature, are given in Fig. 19 in order of increasing HRS name.

⁶ http://www.stecf.org/software/ASTROsoft/DER_SNR/

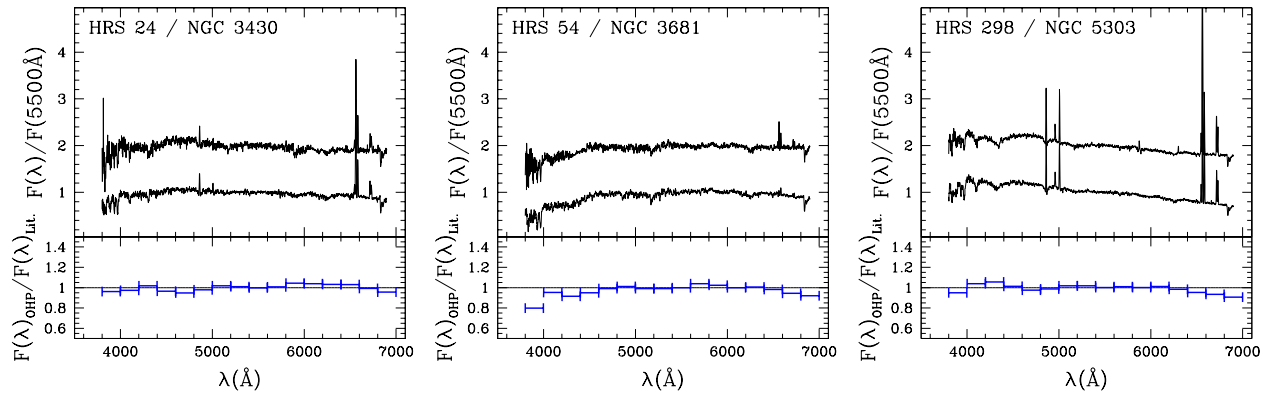


Fig. 2. Comparison between the spectra of HRS 24, 54 and 298 observed multiple times between 2007 and 2009 (upper and lower spectra, respectively). The lower panel shows the ratio of the two measurements in 200 \AA wide bins (blue line).

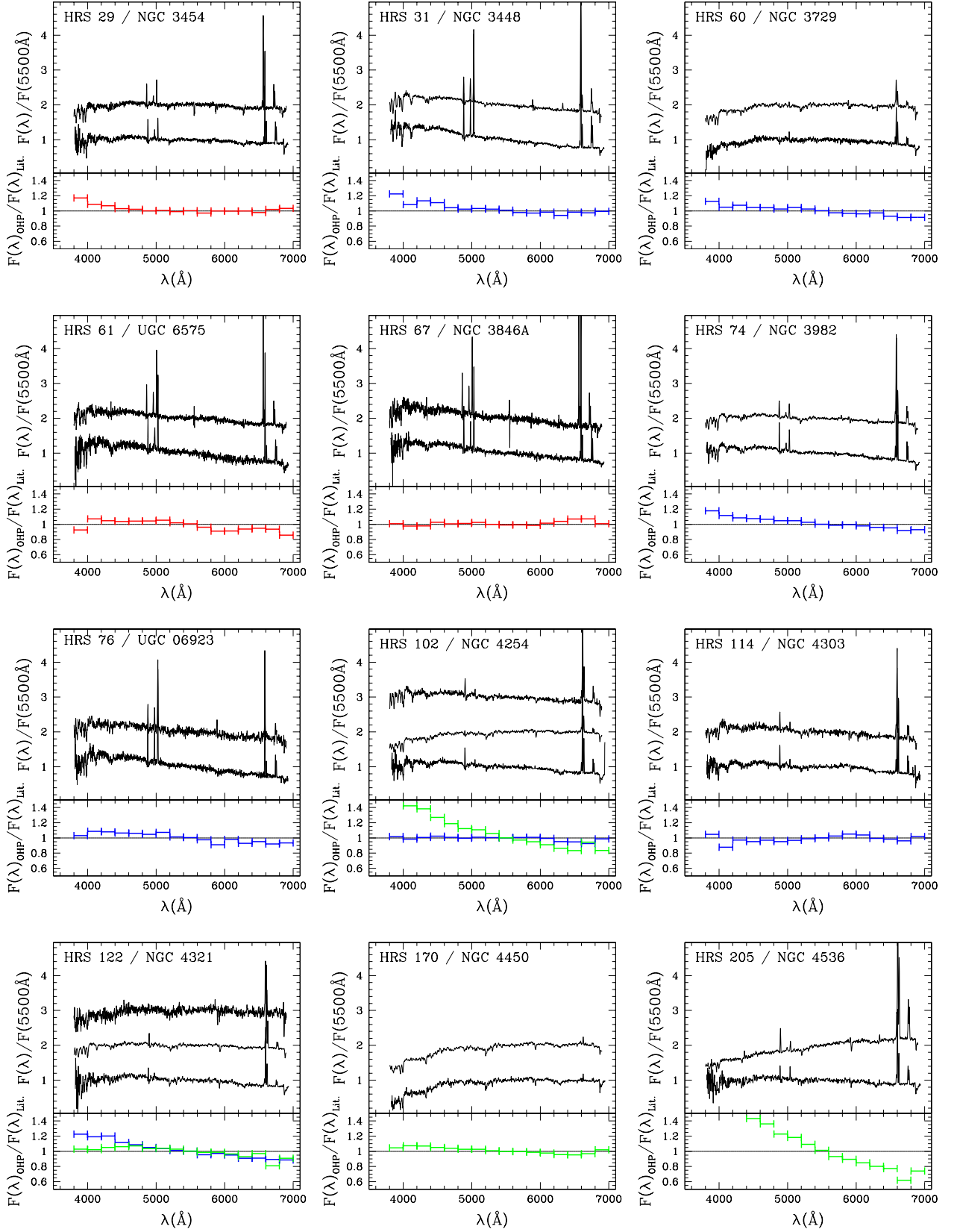


Fig. 3. Comparison between the spectra of galaxies observed in this work or in Gavazzi et al. (2004) (lower spectra) and with data available in the literature (upper spectra). The ratio of the different spectra is given in the lower panel, in bins 200 Å wide. Different colour codes are used when data are from Moustakas et al. (2010) (green), Moustakas & Kennicutt (2006) (blue) and Jansen et al. (2000) (red). Whenever two independent spectra are available in the literature (HRS 102, 122 and 217), they are given from top to bottom following the order Moustakas & Kennicutt (2006), Moustakas et al. (2010), this work or Gavazzi et al. (2004).

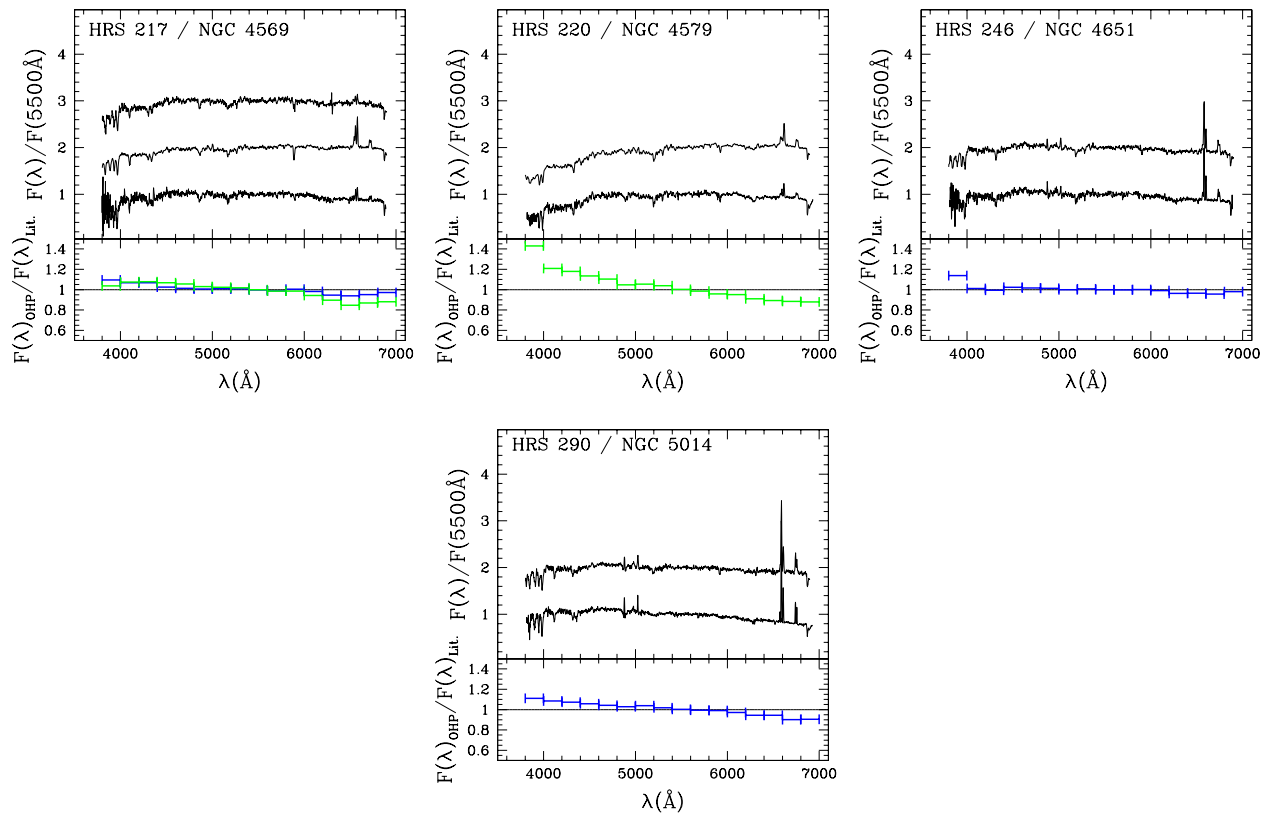


Fig. 3. Continued.

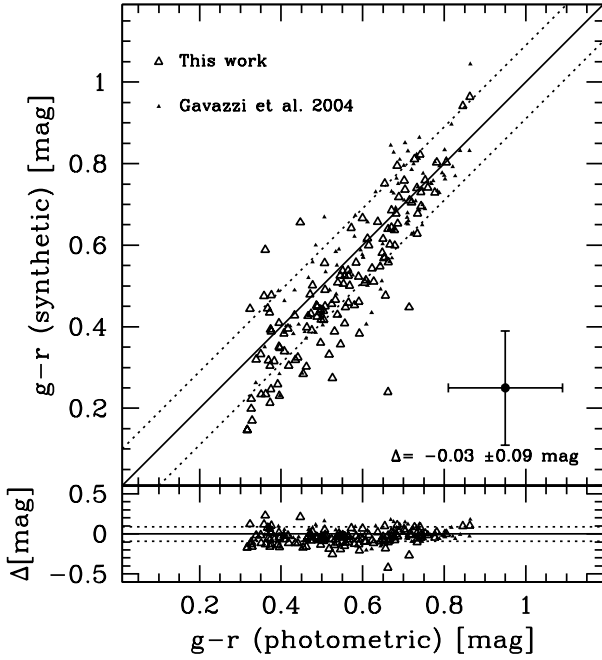


Fig. 4. Comparison between the photometric and the spectroscopic $g-r$ colours for galaxies observed in this work (empty triangles) and in Gavazzi et al. (2004) (filled triangles). The solid line gives the 1:1 relationship and the dotted lines the 1 sigma uncertainty. The cross indicates a typical error bar of 0.14 mag on the colour, corresponding to $\sim 10\%$ uncertainty in each band.

4.1. Spectrophotometric accuracy

We first test the spectrophotometric quality of our spectra by comparing multiple observations of the same galaxy both from our survey and the literature. Over the course of our observing campaign, only three objects in our sample have been observed two or more times using the drift-scan technique and spectra were derived using the same reduction method. We normalize each pair of spectra to the mean flux around 5500 \AA and calculate the flux ratio in 200 \AA wide bins, in order to check for any variation in continuum shape. In Fig. 2, we compare the multiple observations of these three galaxies. We find that the relative scatter in the observations is 3.2% with a slight wavelength dependence (see Table 2). The relative scatter of the red portion ($\lambda > 5500 \text{ \AA}$) of the spectrum is around 3.1% , and this increases to 3.6% at the blue end ($\lambda < 5500 \text{ \AA}$). The largest discrepancy occurs at $\lambda < 4000 \text{ \AA}$, where the difference in one object reaches $\sim 20\%$. In the red ($\lambda > 6800 \text{ \AA}$) the differences are $\leq 15\%$. Although we are limited by the low number of objects for comparison, it appears that the largest discrepancies occurs in a galaxy observed in cirrus conditions (HRS 54).

Ten galaxies observed in this survey and six in Gavazzi et al. (2004) have integrated spectroscopy data available in the literature from Jansen et al. (2000), Moustakas & Kennicutt (2006) and Moustakas et al. (2010). We compare our results in Fig. 3. Despite various differences in how these sets of spectra were obtained, we find an average relative difference of 7.0% with some wavelength dependence present for some objects (see Table 2). The relative scatter of the red portion ($\lambda > 5500 \text{ \AA}$) of the spectrum is around 5.7% , and it increases to 8.9% at the blue end ($\lambda < 5500 \text{ \AA}$).

The Moustakas et al. (2010) spectra are typically redder than our spectra. The differences between our and the Moustakas et al. (2010) spectra reach $\sim 60\%$ at $\lambda \sim 4000 \text{ \AA}$ and 35% at $\lambda \sim 7000 \text{ \AA}$ in HRS 205, while is generally $\leq 20\%$ and $\leq 15\%$ in the same spectral domain when our data are compared to Moustakas & Kennicutt (2006) and Jansen et al. (2000). This large difference might result from the fact that the Moustakas et al. (2010) spectra are limited to the radial strip observed by Spitzer within the SINGS project. These strips cover the inner regions and are thus significantly less extended than the optical discs of the observed galaxies. Because of the colour gradient, these inner spectra are redder, as clearly evident in NGC 4254 (HRS 102). Here, our and the Moustakas & Kennicutt (2006) spectra, encompassing the whole galaxy disc, are consistent within 5% at all wavelengths, and are both significantly bluer than the one of Moustakas et al. (2010) which is limited to the inner disc. If we limit the comparison of our spectra with those published in Moustakas & Kennicutt (2006) and Jansen et al. (2000), the difference in the spectra reduces to $\sim 4.4\%$, with 5.2% in the blue and 4.1% in the red.

Contrary to what is found in the comparison of multiple observations of the same galaxies done within this survey (see above), we do not see any strong systematic difference between galaxies observed in photometric (HRS 29, 67, 102, 114, 122, 217; mean difference 3.8%) or cirrus conditions (HRS 246; 2.3%) also when the comparison is limited to $\lambda < 4000 \text{ \AA}$ and $\lambda > 6800 \text{ \AA}$ ⁷.

We further test our spectrophotometric accuracy by comparing magnitudes synthesized from our spectra to the recently published broadband photometry from Cortese et al. (2012a). Synthesized spectroscopic $g-r$ colours were obtained by deconvolving the continua with the profiles of the g and r SDSS filters. Figure 4 shows the comparison between the photometric and the spectroscopic $g-r$ colours synthesized for all the HRS galaxies with available photometric data. The mean offset is 0.03 mag with a rms scatter of 0.09 mag . Overall the agreement between the two sets of data is good, considering that the error on the photometric magnitudes is of the order of $\sim 10\%$. A systematic difference is however present for the bluest galaxies, where the synthetic colours are bluer than the photometric ones by $\leq 0.1 \text{ mag}$. To summarise, we find that the errors on the continuum in our data are of $\leq 20\%$ for $\lambda < 4000 \text{ \AA}$, $\leq 15\%$ for $\lambda > 6800 \text{ \AA}$, and $\leq 10\%$ elsewhere. These uncertainties are consistent with those previously reported in the literature (see Gavazzi et al. 2004; Moustakas & Kennicutt 2006).

5. Emission line flux measurements

5.1. Contribution of the underlying Balmer absorption

We measure the emission lines of each spectra by visually inspecting them using `SPLIT`, and obtain a measurement of the relative flux and equivalent width for the detected emission lines. The typical signal-to-noise of the emission lines, measured as the ratio of the peak flux of the line and the sigma measured for the continuum either sides of the line, is $S/N \geq 20$ for $H\alpha$, $S/N \sim 3-12$ for the other lines with exception of the $[OIII]$ lines where $S/N \sim 2-8$ due to the low sensitivity of the CCD shortward of 4000 \AA . The $H\beta$ line often displays underlying stellar absorption which must be corrected for, otherwise the measured flux of the emission line is underestimated (see Fig. 8 of Gavazzi et al. 2004). The underlying absorption also affects the other main

⁷ This comparison is done excluding the Moustakas et al. (2010) data.

Table 2. Comparison with spectra available in the literature or with multiple observations

Spectral range	All	J00+MK06	J00	MK06	M10	Repeated
3700-7000 Å	7.0%	4.4%	3.7%	4.6%	12.5%	3.2%
3700-5500 Å	8.9%	5.2%	3.9%	5.7%	16.9%	3.1%
5500-7000 Å	5.7%	4.1%	4.1%	4.1%	9.1%	3.6%

Balmer line, $H\alpha$.

Different techniques have been proposed in the literature for removing the contribution of the underlying Balmer absorption to the emission lines. Moustakas & Kennicutt (2006) and Moustakas et al. (2010) proposed to fit the observed spectra of galaxies with population synthesis models using different star formation histories and then subtract them from the observed spectra to obtain pure line emission spectra. Their analysis has shown that, because of quite different star formation histories, the equivalent width of the $H\beta$ underlying absorption of star forming galaxies can vary in between 3.9 and 5.9 Å. Using this technique, they estimate that the mean underlying Balmer absorption in their sample of galaxies is $E.W.H\beta_{abs} = 4.4 \pm 0.63$ Å and $E.W.H\alpha_{abs} = 2.80 \pm 0.38$ Å, respectively (Moustakas & Kennicutt 2006).

Our spectra are unfortunately quite noisy in the blue range, shortward of ~ 4000 Å. Furthermore the HRS sample includes bright, massive galaxies characterised by a high surface brightness as well as relatively low luminosity, low surface brightness objects. The set of spectroscopic data in our hand is thus quite non homogeneous in terms of S/N. Since the accuracy of the fit depends on the S/N (Oh et al. 2011), these spectra can be hardly used without other photometric data to constrain the star formation history of the target galaxies and measure the underlying Balmer absorption using population synthesis models.

Moreover, the fitting procedures using population synthesis models have also their own limits. Groves et al. (2012) have indeed shown that, for a fixed age of the underlying stellar population, different population synthesis models give differences in the $H\beta$ and $H\alpha$ Balmer absorption lines up to $\sim 2-3$ Å. There are also indications that the use of different fitting procedures can lead to different measurements of line emission, in particular whenever the emission is weak (Oh et al. 2011). For these reasons we prefer to adopt a simpler approach by directly measuring the underlying absorption in the $H\beta$ line from the spectra, and use a constant correction for the $H\alpha$ line.

Indeed the spectral resolution and the sensitivity of our data allow us to directly measure the underlying absorption under $H\beta$ in most of the target galaxies (181/238). The comparison of direct measurements on the spectra with those determined using population synthesis models on SDSS data done by Cid Fernandes et al (2005) produced very consistent results. The $H\beta$ absorption feature is deblended from the emission line using `SPLIT`. To be consistent with Gavazzi et al. (2004), a mean additive correction of 1.8 in flux and -1.4 Å in EW is applied to those $H\beta$ lines where underlying absorption is not detected. These values correspond to the fraction of the (broader) absorption feature that lies under the emission feature.

The spectral resolution, combined with the contamination of the two [NII] lines, however, prevent the measurement of the underlying $H\alpha$ absorption. Their measurement is thus quite tricky since the three lines tend to overlap at the continuum. Hence, the $H\alpha$ and [NII] lines are all measured by simultaneously fit-

ting gaussian profiles to each line in the triplet using the same baseline fit to the continuum. For the underlying absorption we adopt a fixed correction of $E.W.H\alpha_{abs} = 2.80$ Å for all galaxies, a value consistent with the mean value of Moustakas & Kennicutt (2006). This correction can be simply added to the observed emission line as:

$$E.W.H\alpha_{corr}(\text{Å}) = E.W.H\alpha_{obs} + 2.8 \quad (1)$$

for the equivalent width, where $E.W.H\alpha_{corr}$ is the corrected equivalent width and $E.W.H\alpha_{obs}$ the observed one, and

$$f(H\alpha)_{corr} = f(H\alpha)_{obs} \times \left(1 + \frac{2.8}{E.W.H\alpha_{obs}}\right) \quad (2)$$

for the flux. We remark that this correction is significantly larger than the one determined by Gavazzi et al. (2011) using the SDSS spectra of 881 passive galaxies in the Coma supercluster ($E.W.H\alpha_{abs} = 1.3$ Å). For consistency, the same correction is applied to the Gavazzi et al. (2004) data.

To quantify any possible systematic effect due to this assumption for the determination of the $H\alpha$ line emission, as well as in the direct measurement of $H\beta$, we have run the MILES population synthesis models (Vazdekis et al. 2010) assuming two different star formation histories, the Sandage law, whose analytical form is presented in Gavazzi et al. (2001) and Boselli (2011), and that determined by the chemo-spectrophotometric models of Boissier & Prantzos (1999), presented in Buat et al. (2008). Although not tuned to reproduce any possible effect due to the interaction with the environment, these star formation laws are well adapted for representing galaxies with a smooth secular evolution as expected for our K-band selected sample (Boissier & Prantzos 2000; Boissier et al. 2001; 2003; Gavazzi et al. 2001; Boselli et al. 2001). The MILES population synthesis models have been chosen because they have the sufficient spectral resolution (2.51 Å) necessary for this analysis. The Sandage law is indicised on a delayed exponential time scale τ , while the Boissier & Prantzos (1999) star formation history on the stellar mass. We have thus run the MILES population synthesis models for 5 different τ (2, 5, 8, 10, 20 Gyr)⁸ and stellar masses ($\log M_{star} = 8.89, 9.92, 10.52, 10.94, 11.25 M_{\odot}$), and assuming two different metallicities ($Z = Z_{\odot}$; $Z = 1/4Z_{\odot}$). These parameters are representative of the dynamic range observed in our sample (Boselli et al. 2012; Hughes et al. 2012). We have then measured the equivalent width of the $H\alpha$ and $H\beta$ underlying Balmer absorption lines of the different model galaxies consistently with what done on the real data. We have also checked that the results do not depend on the resolution, as claimed by Moustakas & Kennicutt (2006), by degrading the resolution from the nominal value of 2.51 Å, down to 3 Å, 4 Å and 6 Å⁹. The results

⁸ The value of τ gives the typical age of the peak of star formation in this delayed exponentially declining star formation history.

⁹ The following analysis is based on the 3 Å resolution data.

of this exercise are shown in Fig. 5. Figure 5 shows the expected variation of the equivalent width of the $H\alpha$ (upper panel) and $H\beta$ (middle panel) lines as a function of τ (left) and M_{star} (right). The lower histograms show the expected distribution for the whole galaxy sample, and for galaxies separated in two bins of metallicity ($12+\log(O/H) \leq 8.5$, blue; $12+\log(O/H) > 8.5$, red, with metallicities taken from Hughes et al. 2012). The threshold in metallicity ($12+\log(O/H) = 8.5$) has been chosen to include \simeq the same number of objects in the 2 defined bins. For a solar neighborhood metallicity of $Z_{\odot} = 8.69$ (Asplund et al. 2009), the $Z = 1/4 Z_{\odot}$ metallicity of the models shown in the lower and middle panels corresponds to $12+\log(O/H) = 8.09$, a value below the lower limit in the range of metallicities observed in our sample.

Figure 5 shows that overall the observed values of $E.W.H\beta_{abs}$ are consistent with those predicted by population synthesis models for the ranges of τ and/or M_{star} covered by the HRS galaxies ($3 \leq E.W.H\beta_{abs} \leq 6.5$). There is, however, a systematic difference in the observed distribution of metal poor (blue) and metal rich (red) galaxies, the former with higher values of $E.W.H\beta_{abs}$ than the latter (histogram in the right panel of the middle row). Overall this systematic difference is opposite to that predicted by population synthesis models. However, this difference between models and observations might partly be due to the fact that the $E.W.H\beta_{abs}$ decreases with increasing mass, making metal rich, massive galaxies with $E.W.H\beta_{abs}$ comparable to those of metal poor, low mass systems. The values of $E.W.H\beta_{abs}$ determined by fitting Bruzual & Charlot (2003) population synthesis models to the observed spectra by Moustakas & Kennicutt (2006) are slightly lower than those measured in our data (see sect. 7.5) or those predicted by the MILES models for solar metallicities, but perfectly match the dynamic range covered by the MILES population synthesis models for $Z = 1/4 Z_{\odot}$ metallicities. Figure 5 thus indicates that the difference in the estimate of the equivalent width of the Balmer absorption under $H\beta$ determined fitting different population synthesis models (Bruzual & Charlot 2003 vs. Vazdekis et al. 2010; $\simeq 2 \text{ \AA}$) is expected to be comparable to the width of the distribution of the observed values ($\sim 1.5 \text{ \AA}$) shown in sect. 7.5.

In the expected range of τ and M_{star} covered by the HRS galaxies, the MILES population synthesis models indicate that $E.W.H\alpha_{abs}$ varies between 2.3 and 3.5 \AA , consistently with the values determined by Moustakas & Kennicutt (2006) ($E.W.H\alpha_{abs} 2.8 \pm 0.38 \text{ \AA}$). Variations with the metallicity are at most of 0.3 \AA , thus $\lesssim 10 \%$ of the $E.W.H\alpha_{abs}$. Sandage model star formation histories give values of $E.W.H\alpha_{abs}$ in the range 2.3-3 \AA , slightly lower than those predicted by the Boissier & Prantzos models ($2.6 \leq E.W.H\alpha_{abs} \leq 3.5 \text{ \AA}$) in the range of τ and M_{star} expected for the HRS galaxies. With the data in our hand we are at present in the impossibility of identifying which between the two models (Sandage vs. Boissier & Prantzos) better reproduces the observations, making the choice of a constant value of $E.W.H\alpha_{abs}$ reasonable. Figure 5 shows that the adoption of a constant value of $E.W.H\alpha_{abs}$ might induce systematic effects in the dataset presented and analysed in this work. These effects, however, should be very minor. The mean equivalent width of the $H\alpha$ line measured from our spectra is of the order of 25 \AA (see sect. 7.2), thus significantly larger than any possible systematic variation in $E.W.H\alpha_{abs}$ ($\lesssim 0.4 \text{ \AA}$). The other emission lines might be affected through the extinction correction based on the Balmer decrement. The $H\alpha$ over $H\beta$ ratio, however, can be measured only whenever both the $H\alpha$ and $H\beta$ lines are detected. Figure 6 shows that this is the case only whenever $E.W.H\alpha_{emi} \gtrsim$

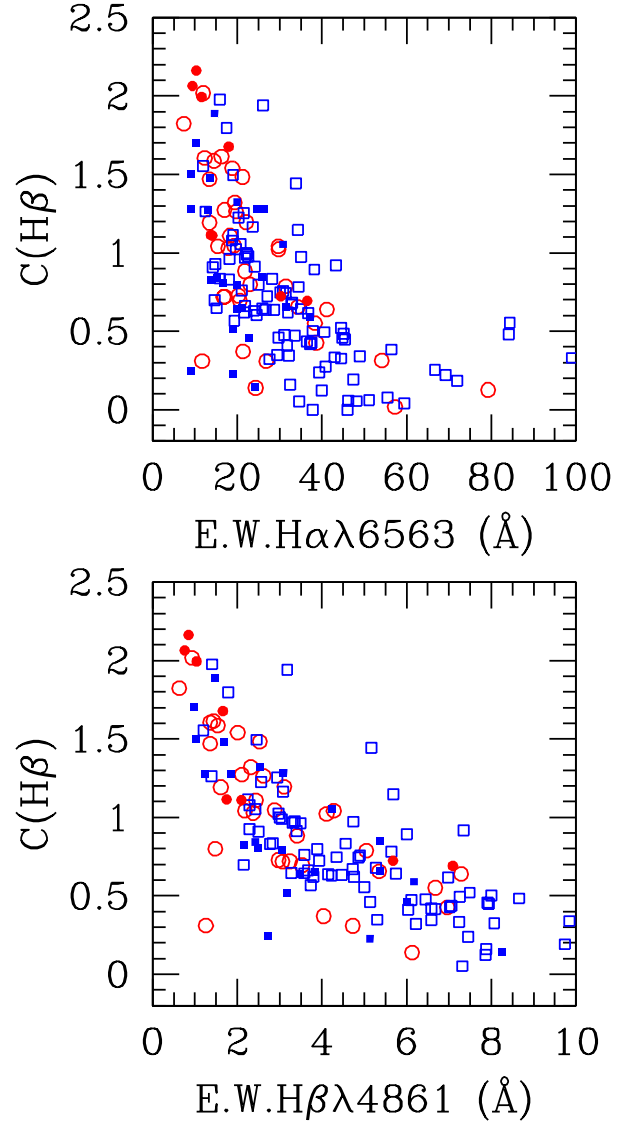


Fig. 6. Observed variation of the Balmer decrement $C(H\beta)$ as a function of the $H\alpha$ (upper panel) and $H\beta$ (middle panel) equivalent widths, in \AA . Red symbols indicate HI-deficient cluster galaxies ($HI - def > 0.4$), blue ones HI-normal, field objects ($HI - def \leq 0.4$). Filled symbols indicate galaxies hosting an AGN, empty symbols normal galaxies. The typical uncertainty on $C(H\beta)$ ranges from ~ 0.3 for $E.W.H\beta_{abs} > 2 \text{ \AA}$ to 0.5 below.

10 \AA . Systematic errors of $\lesssim 0.4 \text{ \AA}$ on $H\alpha$ are small compared to the mean uncertainty on the line emission measurements ($\simeq 10\text{-}20 \%$) and could thus be neglected in the following analysis. Although possibly present (Rosa-Gonzalez et al. 2002), we do not apply any correction due to stellar absorption in other emission lines.

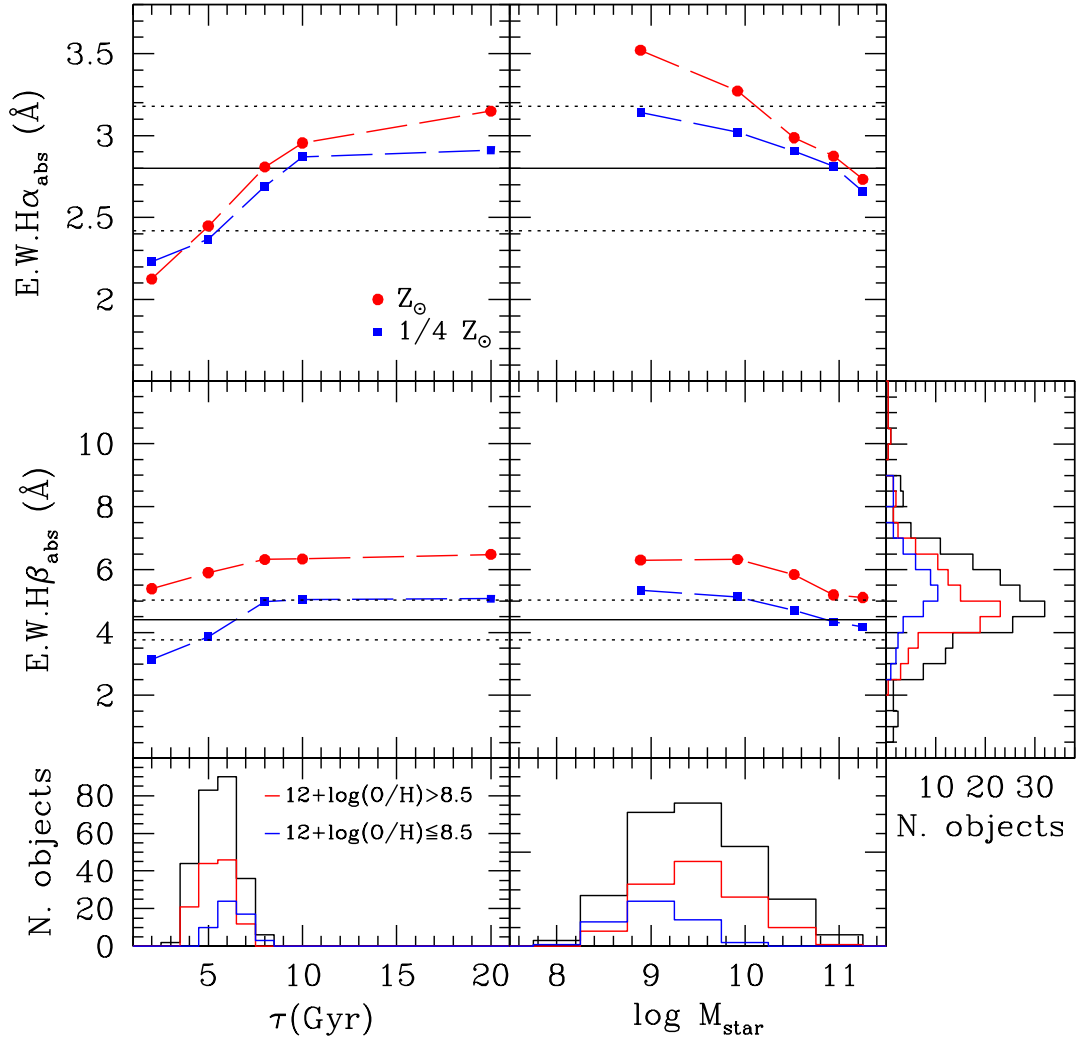


Fig. 5. Variation of the equivalent width of the H α (upper panel) and H β (middle panel) Balmer absorption lines, in \AA , predicted by the MILES population synthesis models, as a function of the delayed exponentially declining time scale τ for a Sandage law (left) and of the stellar mass for the Boissier & Prantzos (2000) chemo-spectrophotometric models of galaxy secular evolution (right). The red line is for solar metallicities, the blue one for $Z = 1/4 Z_{\odot}$. The Balmer absorption lines are measured for five different τ (2, 5, 8, 10, 20 Gyr) and stellar masses ($\log M_{\text{star}} = 8.89, 9.92, 10.52, 10.94, 11.25 M_{\odot}$). The horizontal solid and dotted lines give the mean value \pm the standard deviation of $E.W.H\alpha_{\text{abs}}$ ($2.8 \pm 0.38 \text{ \AA}$) and $E.W.H\beta_{\text{abs}}$ ($4.4 \pm 0.63 \text{ \AA}$) of Moustakas & Kennicutt (2006) for their sample of galaxies. The lower panel gives the expected distribution of τ and M_{star} for the late-type HRS galaxies analysed in this work. The values of τ are estimated using the $\tau - L_H$ luminosity relation given in Gavazzi et al. (2002): $\log \tau = -0.149 \times \log L_H + 2.221$. The blue and red histograms give the observed distribution of HRS galaxies with metallicity $12 + \log(\text{O}/\text{H}) \leq 8.5$ and $12 + \log(\text{O}/\text{H}) > 8.5$, respectively. The right histogram in the middle row shows the distribution of the observed underlying Balmer absorption at H β for the whole sample (black) and for metal poor (blue) and metal rich (red) galaxies.

5.2. Line uncertainties

An empirical way of quantitatively checking the quality of the line emission measurements is that of comparing the observed distribution of the $[\text{OIII}]\lambda 4959/[\text{OIII}]\lambda 5007$ and of the $[\text{NII}]\lambda 6548/[\text{NII}]\lambda 6584$ flux line ratios to the theoretical values (1/3; Osterbrock & Ferland 2005). This comparison is done in Figure 7, where the $[\text{OIII}]\lambda 4959/[\text{OIII}]\lambda 5007$ and the $[\text{NII}]\lambda 6548/[\text{NII}]\lambda 6584$ flux line ratios are plotted versus the equivalent width of the $[\text{OIII}]\lambda 5007$ and $[\text{NII}]\lambda 6584$ lines, respectively. Figure 7 shows that the ratios of the two doublets are close to the theoretical values for large equivalent widths, with

a scatter from the expected relations increasing with decreasing intensity of the emission lines. We do not see any evident systematic difference in the ratios of galaxies hosting an AGN, consistent with the idea that the nuclear contribution is generally minor in these integrated spectra (see Sect. 7.2). For the $[\text{NII}]\lambda 6548/[\text{NII}]\lambda 6584$ line doublet, the mean ratio for the whole sample (including the data of Gavazzi et al. 2004) differs from the theoretical value by less than 10%, with a mean scatter of $\sim 20\%$ (see Table 3). The difference with respect to the theoretical values for our new set of data significantly reduces for galaxies with $E.W.[\text{NII}]\lambda 6548 > 2 \text{ \AA}$ ($[\text{NII}]\lambda 6548/[\text{NII}]\lambda 6584 = 0.32 \pm 0.04$).

Table 3. Line ratios: comparison with theoretical values

Line ratio	Sample	Condition	N. object	ratio
[NII] λ 6548/[NII] λ 6584	T.W. + G04	-	191	0.31 \pm 0.07
	T.W.	-	118	0.31 \pm 0.06
	T.W. + G04	[NII] λ 6548 > 2 Å	86	0.33 \pm 0.06
	T.W.	[NII] λ 6548 > 2 Å	55	0.32 \pm 0.04
	T.W. + G04	[NII] λ 6548 > 3 Å	39	0.33 \pm 0.06
	T.W.	[NII] λ 6548 > 3 Å	21	0.33 \pm 0.02
	T.W. + G04	[NII] λ 6548 \leq 2 Å	105	0.30 \pm 0.08
	T.W.	[NII] λ 6548 \leq 2 Å	63	0.30 \pm 0.08
[OIII] λ 4959/[OIII] λ 5007	T.W. + G04	-	85	0.42 \pm 0.11
	T.W.	-	62	0.40 \pm 0.10
	T.W. + G04	[OIII] λ 4959 > 3 Å	40	0.39 \pm 0.11
	T.W.	[OIII] λ 4959 > 3 Å	24	0.35 \pm 0.04
	T.W. + G04	[OIII] λ 4959 \leq 3 Å	45	0.44 \pm 0.11
	T.W.	[OIII] λ 4959 \leq 3 Å	38	0.44 \pm 0.11

The ratio [OIII] λ 4959/[OIII] λ 5007 of our new observations is close to the theoretical value whenever E.W.[OIII] λ 4959 \geq 3 Å ([OIII] λ 4959/[OIII] λ 5007 = 0.35 \pm 0.04), while is significantly larger below this limit, or whenever the data of Gavazzi et al. (2004) are included (see Table 3). An accurate inspection of the spectra suggests that this discrepancy is due to a systematic overestimate of the [OIII] λ 4959 line for E.W.[OIII] λ 4959 < 3 Å resulting from the contamination of an important NaI sky line (λ 4983 Å; Osterbrock & Martel 1992) which falls close to this emission line at the typical redshift of our targets¹⁰.

The deviations of the [OIII] and [NII] line ratios from the expected values can be used to quantify the uncertainty in the line emission measurement. Here we make the conservative assumption that the uncertainty in the line ratio is totally due to the measure of the weakest of the two lines of the doublet. This test indicates that the mean uncertainty in the measure of the [NII] line intensity for the new observations presented here (T.W.) is \leq 6% whenever the equivalent width of the emission line is larger than 3 Å, \leq 12% for equivalent widths larger than 2 Å and increases to \leq 24 % below. The uncertainty in the [OIII] λ 4959 is \leq 12% whenever the equivalent width of the emission line is larger than 3 Å, but it increases to \sim 35 % with a systematic trend (the line emission is overestimated) for smaller equivalent widths. The errors are slightly larger whenever the data of Gavazzi et al. (2004) are included (T.W.+G04). These uncertainties are comparable to those obtained with the same test using the integrated spectra of Jansen et al. (2000) or those quoted by Moustakas & Kennicutt (2006) who measured [OIII] λ 4959/[OIII] λ 5007 ratios within \pm 4% from the theoretical value whenever E.W.[OIII] λ 4959 \geq 3 Å. They are also consistent with the uncertainties derived by the comparison with narrow band imaging data (see Sect. 6.2). As previously mentioned, the large uncertainty in the [OIII] λ 4959 line is related to the contamination of a strong NaI sky line at λ 4983 Å¹¹. Given that the signal to noise in the spectra around 4800-5000 Å is comparable to that at \sim 6500 Å, we can as-

sume that the mean uncertainties in the measurement of the [OIII] λ 5007 and H β lines are comparable to those determined for the [NII] lines. This is also valid for the [SII] lines. On the other hand, given the noise of the spectra below 4000 Å and the observed systematic difference at these short wavelengths with respect to other sets of data available in the literature (\leq 20%), the uncertainty on the measurements of the [OIII] λ 3727 Å line is significantly larger (we indeed detected only emission lines with equivalent widths \geq 10 Å), at best of 20% but never exceeding 50%.

5.3. Balmer decrement

The emission line intensities can be corrected for internal extinction using the Balmer decrement $C(H\beta)$. With the H β line corrected for underlying absorption, the Balmer decrement is given by (Lequeux et al. 1981):

$$C(H\beta) = \left[\log \left(\frac{H\alpha}{H\beta} \right)_{theor} - \log \left(\frac{H\alpha}{H\beta} \right)_{obs} \right] / f(H\alpha) \quad (3)$$

where $\log (H\alpha/H\beta)_{theor}$ is the theoretically expected ratio between H α and H β , $\log (H\alpha/H\beta)_{obs}$ is the observed value and $f(H\alpha)$ is the reddening function relative to H β . The theoretical ratio depends on the electron density n and the gas temperature T . Assuming that $T = 10000$ K and $n = 100$ e cm⁻³ and that all the Lyman line photons are absorbed by the diffuse gas located around the emitting star (case B from Osterbrock & Ferland 2006), which are values typical of HII regions, then $(H\alpha/H\beta)_{theor} = 2.86$. The measured line fluxes can be corrected for internal extinction using the relation:

$$\log \left(\frac{\lambda}{H\beta} \right)_{corr} = \log \left(\frac{\lambda}{H\beta} \right)_{obs} + C(\lambda) \times f(\lambda) \quad (4)$$

and adopting the reddening function $f(\lambda)$ of Fitzpatrick & Massa (2007) (see Table 4). In those galaxies where H β is undetected, we do not derive an upper limit to $C(H\beta)$ based on the H α equivalent width, as in Gavazzi et al. (2004), since these estimates are very uncertain. We present in Table 8 the observed line emission fluxes (normalised to H α) of the main emission lines detected in our spectra, i.e. [OIII] λ 3727 Å, H β 4861 Å, [OIII] λ 4959 and

¹⁰ The comparison of observed flux ratios with the expected theoretical values allowed us to identify a few spurious measurements in Gavazzi et al. (2004). For these galaxies, indicated with a note in the following Tables, we have remeasured fluxes and equivalent widths.

¹¹ Given that the sky emission strongly contaminates only the [OIII] λ 4959 line, its emission can be deduced with a smaller uncertainty from the [OIII] λ 5007 Å line assuming a constant ratio.

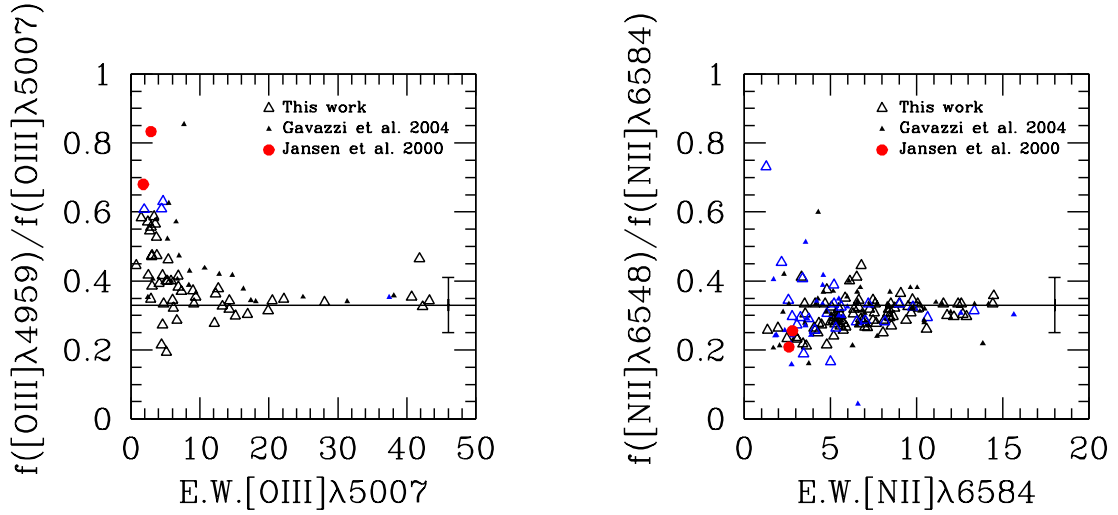


Fig. 7. The relationship between the $[\text{OIII}]\lambda 4959/[\text{OIII}]\lambda 5007$ flux line ratio and the equivalent width of $[\text{OIII}]\lambda 5007$ (left) and of the $[\text{NII}]\lambda 6548/[\text{NII}]\lambda 6584$ flux line ratio and the equivalent width of $[\text{NII}]\lambda 6584$ (right). The solid line gives the theoretical value ($1/3$). Empty triangles are for galaxies observed in this work, filled triangles for those presented in Gavazzi et al. (2004), red dots for objects in Jansen et al. (2000). Galaxies hosting an AGN are marked with a blue symbol. The vertical line indicates a 18% error in the flux line emission line.

Table 4. Extinction coefficients for optical emission lines, from Fitzpatrick & Massa (2007)

line	λ Å	$k_{MW}(\lambda)^a$	$f(\lambda)^{a,b}$
$[\text{OII}]$	3727/29	4.751	+0.324
H β	4861	3.588	0.000
$[\text{OIII}]$	4959	3.497	-0.025
$[\text{OIII}]$	5007	3.452	-0.038
$[\text{NII}]$	6548	2.524	-0.294
H α	6563	2.517	-0.297
$[\text{NII}]$	6584	2.507	-0.301
$[\text{SII}]$	6717	2.444	-0.319
$[\text{SII}]$	6731	2.437	-0.321

Notes: adapted from Boselli (2011).

a) $k(\lambda)$ and $f(\lambda)$ are determined assuming $R_{MW}(V)=3.08$.

b) $f(\lambda)$ is relative to H β .

$[\text{OIII}]\lambda 5007$ Å, $[\text{NII}]\lambda 6548$ Å, H α 6563 Å, $[\text{NII}]\lambda 6584$ Å, $[\text{SII}]\lambda 6717$ Å and $[\text{SII}]\lambda 6731$ Å. Table 8 is arranged as follow:

- Column 1: *Herschel* Reference Sample (HRS) name.
- Column 2: References for the data: 1: this work; 2: Gavazzi et al. (2004); 3: Moustakas et al. (2010); 4: Moustakas & Kennicutt (2006); 5: Jansen et al. (2000); 6: Kennicutt (1992a; 1992b).
- Column 3: $E(B - V)$, from Schlegel et al. (1998).
- Column 4: Balmer decrement $C(H\beta)$. The contribution of the Milky Way is subtracted using the Galactic extinction map of Schlegel et al. (1998) combined with the Fitzpatrick & Massa (2007) Galactic extinction law¹².
- Columns 5-13: Observed line intensities normalized to H α . We normalise to H α since this is the only line detected in all emission line galaxies.

¹² The values of $C(H\beta)$ differ from those of Gavazzi et al. (2004) because those published in that paper include the Galactic extinction and have been measured using a different Galactic extinction law.

We also present in Table 9 the corresponding equivalent widths of the main emission lines detected in our spectra. Table 9 is arranged as follow:

- Column 1: *Herschel* Reference Sample (HRS) name.
- Column 2: References for the data: 1: this work; 2: Gavazzi et al. (2004); 3: Moustakas et al. (2010); 4: Moustakas & Kennicutt (2006); 5: Jansen et al. (2000); 6: Kennicutt (1992a; 1992b).
- Column 3: $E(B - V)$, from Schlegel et al. (1998).
- Columns 4-12: Equivalent widths (in Å).
- Column 13: Equivalent width of the underlying H β absorption (in Å).

6. Comparison with the literature

6.1. Comparison with integrated spectra

A few HRS galaxies have been observed using the same drift scan technique adopted in this work by Kennicutt (1992a; 4 objects), Jansen et al. (2000; 5), Moustakas & Kennicutt (2006; 16) and Moustakas et al. (2010; 8). Their integrated spectroscopic data are given in Tables 10 and 11 and can be compared to those obtained in this work or in Gavazzi et al. (2004). Figure 8 shows the relationship between the equivalent width (left) and the normalised flux (right) of the most important emission lines for galaxies in common. We consider here the data published in Gavazzi et al. (2004) together with those collected in this more recent observational campaign, as both datasets have been taken using the same telescope with the same instrumental configuration.

Figure 8 shows that for the galaxies in common, the different sets of data are consistent within the quoted errors. There is, however, a systematic difference in the normalised fluxes of the $[\text{NII}]$ and $[\text{SII}]$ lines with Moustakas et al. (2010), who give values larger than those obtained in this work or in Gavazzi et al. (2004). The largest differences are observed in galaxies hosting

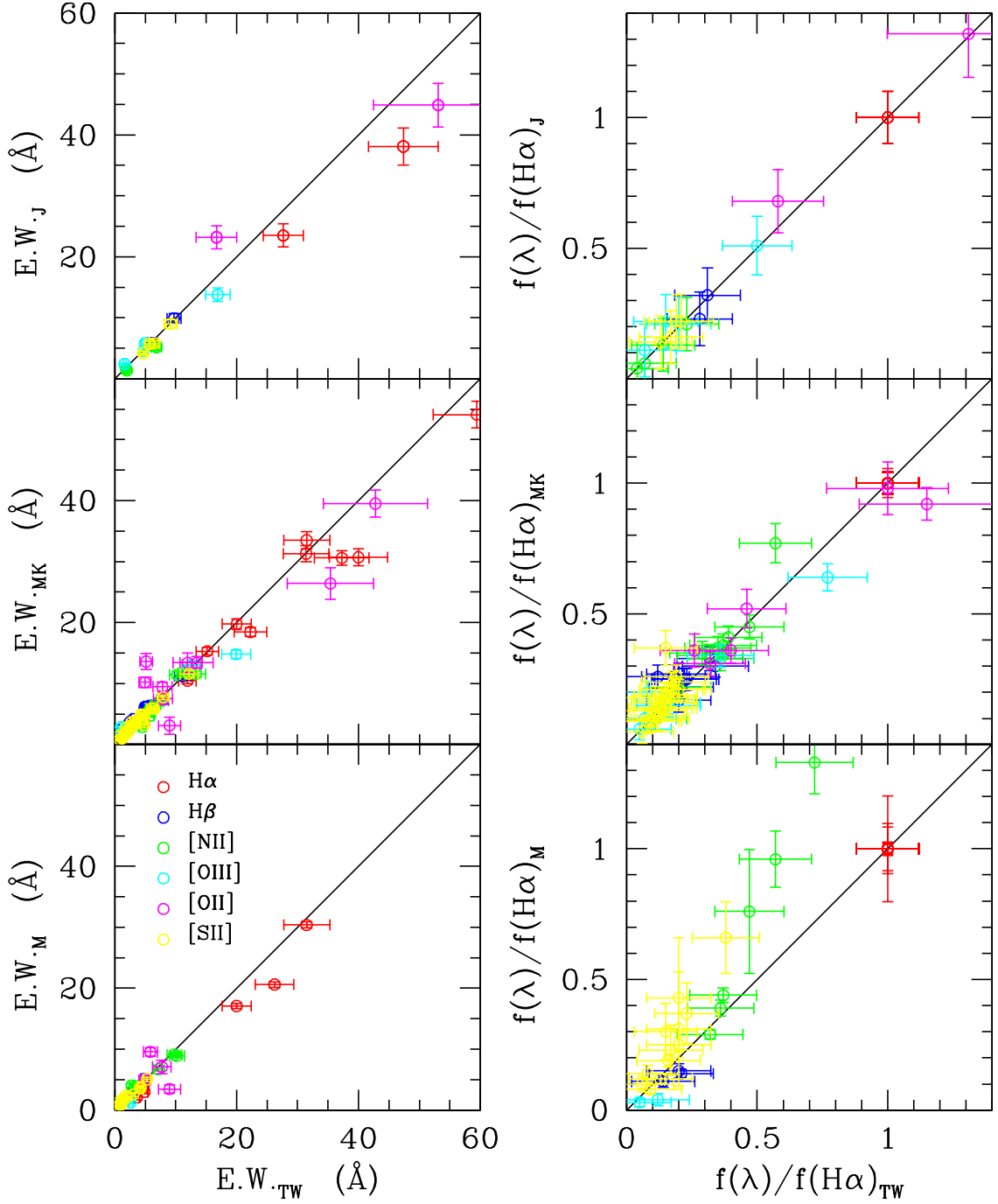


Fig. 8. The comparison between the equivalent width (left) and the normalised flux (right) of the main emission lines measured in this work (TW) with those available in the literature from Jansen et al. (2000; J; upper panel), Moustakas & Kennicutt (2006; MK; middle panel) and Moustakas et al. (2010; M; lower panel). Different colour codes are used for the different emission lines: red symbols for $H\alpha$; blue for $H\beta$, green for $[NII]_{6548}$ and $[NII]_{6584}$ Å, cyan for $[OIII]$ and 5007 Å, magenta for $[OII]_{3727}$ Å, and yellow for $[SII]_{6717}$ and 6731 Å (the two lines composing a doublet are plotted with the same symbol). The solid line shows the 1:1 relationship.

an AGN (NGC 4579, NGC 4569 and NGC 4450). AGNs are characterised by larger $[NII]/H\alpha$ and $[SII]/H\alpha$ line ratios than star forming discs (e.g. Kewley et al. 2006). Given that the integrated spectra of Moustakas et al. (2010) are covering only a radial strip (including the nucleus) which is just a fraction of the optical disc covered by our observations, we expect that the contamination of the central AGN to the total emission is more important in Moustakas et al. (2010) than in our data. The mean

ratio of the fluxes normalised to $H\alpha$ of the galaxies in common with Jansen et al. (2000) and Moustakas & Kennicutt (2006) is of 0.93 ± 0.18 , while that of the equivalent width is of 1.01 ± 0.30 , and drops to 1.00 ± 0.22 excluding the most uncertain $[OII]$ line. These differences are consistent with the errors on the different line emission estimated in the previous section.

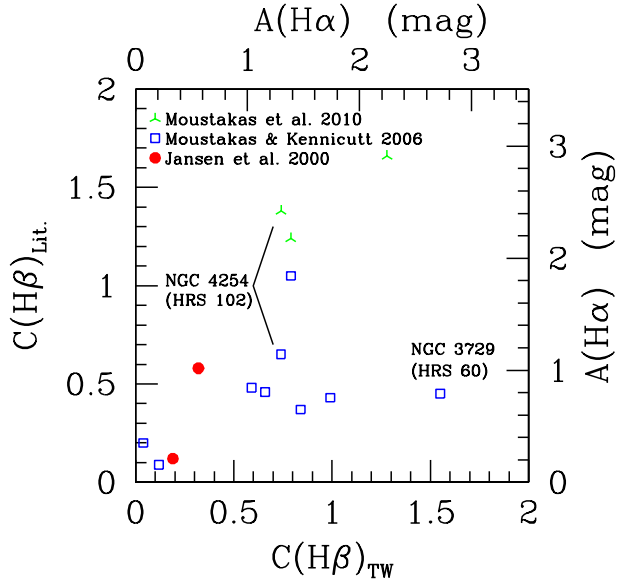


Fig. 9. The comparison between the Balmer decrement $C(H\beta)$ (or equivalently $A(H\alpha)$) measured in this work (TW) with that obtained using data available in the literature (Lit). Green three points crosses are for data from Moustakas et al. (2010), blue open squares from Moustakas & Kennicutt (2006) and red filled dots from Jansen et al. (2000). The typical uncertainty on $C(H\beta)$ from our measurements is 0.3-0.5.

Figure 9 shows the relationship between $C(H\beta)$ Balmer decrement for 8 HRS galaxies in the literature with detected $H\alpha$ and $H\beta$ lines. The poor statistics prevents us to see whether the agreement between the different sets of data is satisfactory. The most discrepant values are those relative to NGC 4254 (HRS 102) and NGC 3729 (HRS 60). NGC 4254 has been observed by Moustakas et al. (2010) and Moustakas & Kennicutt (2006), yielding to $C(H\beta) = 1.38$ and 0.65 , respectively. These values can be compared to $C(H\beta) = 0.74$ as determined from our own data. If we consider the difference between the two values obtained by the team of Moustakas as indicative of the uncertainty on this value or of any systematic difference related to the observed region, we can conclude that our value is consistent with their measurements. NGC 3729 is the HRS galaxy within the Moustakas & Kennicutt (2006) sample with the lowest value of $H\beta$ E.W. ($H\beta$ E.W. = 1.2 \AA from this work, $H\beta$ E.W. = 2.56 \AA from Moustakas & Kennicutt (2006)). The mean ratio of the $C(H\beta)$ determined from this work to those given in the literature for galaxies in common is of $C(H\beta)_{T.W.}/C(H\beta)_{Lit.} = 1.13 \pm 0.65$. The scatter in the ratio is slightly larger than an error of ~ 0.3 - 0.4 determined from the uncertainty in the measurements of the $H\alpha$ and $H\beta$ lines. We thus conclude that the total uncertainty on $C(H\beta)$ from our data is of 0.3-0.5, with the largest uncertainties for the highest values of the Balmer decrement.

6.2. Comparison with $H\alpha + [NII]$ narrow band imaging

Most of the late-type HRS galaxies have been recently observed in imaging mode using narrow band interferential filters using the San Pedro Martir 2.1m telescope (Boselli et al. in prep.). Those in the Virgo cluster have narrow band imaging

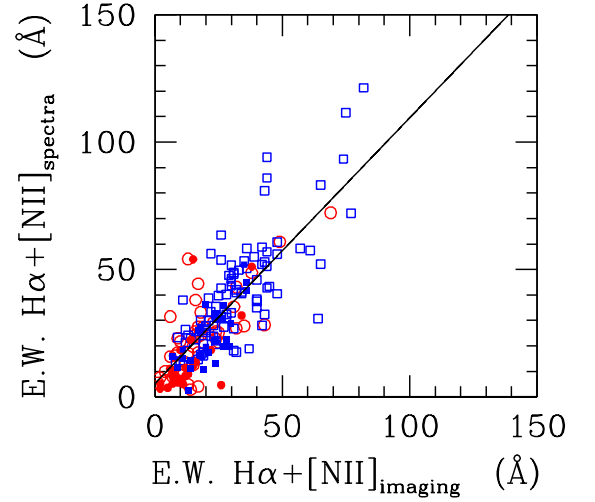


Fig. 10. The comparison between the E.W. $H\alpha + [NII]$ obtained in our spectroscopic survey with those obtained in imaging mode by Boselli et al. (in preparation) for 198 galaxies in common. Blue crosses are for star forming galaxies with a normal HI gas content ($HI - def \leq 0.4$), open red circles for HI-deficient objects ($HI - def > 0.4$). Filled symbols indicate galaxies hosting an AGN. The solid line shows the linear fit $E.W.H\alpha + [NII]_{spectra} = 1.040(\pm 0.058)E.W.H\alpha + [NII]_{imaging} + 5.370(\pm 1.766)$ ($r=0.79$). The typical uncertainty in the equivalent width measured from spectroscopic data is 12-18%, in imaging mode is $\sim 20\%$.

data from Koopmann et al. (2001), Boselli et al. (2002a), Boselli & Gavazzi (2002) and Gavazzi et al. (2002; 2006). $H\alpha + [NII]$ equivalent widths¹³ obtained with integrated spectroscopy can be thus directly compared to those obtained in imaging mode (Fig. 10). To take into account that the imaging data do include the contribution of the underlying absorption, the spectroscopic $H\alpha + [NII]$ equivalent width is defined as:

$$E.W.H\alpha + [NII]_{spectra} = E.W.H\alpha + E.W.[NII]_{6548} + E.W.[NII]_{6564} - E.W.H\alpha_{abs} \quad (5)$$

where $E.W.H\alpha_{abs} = 2.8 \text{ \AA}$ (see previous section).

Figure 10 shows that the $E.W.H\alpha + [NII]_{spectra}$ obtained in integrated spectroscopic mode are consistent with those obtained in imaging mode. The best fit to the data gives $E.W.H\alpha + [NII]_{spectra} = 1.040(\pm 0.058)E.W.H\alpha + [NII]_{imaging} + 5.370(\pm 1.766)$ ($r=0.79$). It also indicates that the drift scan spectroscopy is tracing the global properties of the observed galaxies.

7. Analysis

Because of its definition, the HRS sample can be used to trace the line emission statistical properties of a volume limited, K-band selected sample of nearby late-type galaxies spanning a large range in stellar mass, luminosity, morphological type and belonging to different environments (cluster vs. fields). In this

¹³ The interferential filters have a FWHM of $\sim 80 \text{ \AA}$ and thus encompass the nearby $[NII]$ lines at 6548 and 6584 \AA .

section we study the mean statistical properties of the HRS sample and the dependence of the derived spectral parameters (emission line equivalent widths, Balmer decrement, line diagnostics, underlying Balmer absorption) as a function of different physical parameters (morphological type, stellar mass and surface density, birthrate parameter, metallicity, star formation rate and gas column density).

7.1. Ancillary data and the derived physical parameters

Different sets of multifrequency data are required to characterise the physical properties of the target galaxies. Near-IR and optical photometry, taken from 2MASS (Jarrett et al. 2003), GOLDMine (Gavazzi et al. 2003) or NED, are used to estimate total stellar masses using the colour-dependent recipes given in Boselli et al. (2009). The near-IR photometry is also used to measure the H-band effective surface brightness $\mu_e(H)$ (in mag arcsec⁻²), defined as the mean surface brightness within the effective radius (radius including half of the total stellar light; see Gavazzi et al. (2000)). This entity gives a direct measure of the intensity of the general interstellar radiation field, i.e. the intensity of the radiation emitted by the bulk of the stellar component. Stellar masses, combined with UV GALEX (Boselli et al. 2011; Cortese & Hughes 2009; Hughes & Cortese 2009) and H α +[NII] imaging data (Boselli et al. in prep.), are also used to quantify different direct tracers of the star formation history of the galaxies. This is done by measuring the birthrate parameter b (Kennicutt et al. 1994), that in a closed box model can be defined as in Boselli et al. (2001):

$$b = \frac{SFR}{\langle SFR \rangle} = \frac{SFR t_0 (1 - R)}{M_{star}} \quad (6)$$

with t_0 the age of the galaxy (13 Gyr) and R the returned gas fraction, here assumed to be $R=0.3$ (Boselli et al. 2001). As remarked in Boselli et al. (2012), the birthrate parameter is equivalent to the specific star formation rate $SSFR$. The star formation rate is measured using extinction corrected H α + [NII] imaging data and FUV GALEX images using the prescription described in Boselli et al. (2009). The current set of spectroscopic data is used to correct H α + [NII] fluxes for the [NII] contamination and the Balmer decrement. UV data are corrected for dust attenuation using the prescriptions of Cortese et al. (2008) based on the far infrared to UV flux ratios. Star formations are then determined using the UV and H α calibrations of Kennicutt (1998). We assume an escape fraction of zero and a fraction of ionising photons absorbed by dust before ionising the gas of zero ($f=1$). Although unphysical (see Boselli et al. 2009), this choice has been done to allow a direct comparison with the results obtained in the literature using other star formation rates determined using H α data. These works generally assume $f=1$. Our most recent results indicate that $f \sim 0.6$ (Boselli et al. 2009). When both H α and UV data are available, the SFR is determined as the mean value.

As defined, b measures the ratio of the ionising (photons with $\lambda < 912 \text{ \AA}$) to non ionising ($\lambda = 1.65 \text{ \mu m}$) radiation and is thus a direct tracer of the hardness of the interstellar radiation field. Galaxies with a b parameter > 1 have a present day star formation activity more important than their mean star formation activity since their birth. They are characterised by very blue colours and thus have hard interstellar radiation fields.

The birthrate parameter is proportional to the specific star formation rate $SSFR$ defined as (Brinchmann et al. 2004):

$$SSFR = \frac{SFR}{M_{star}} = \frac{b}{t_0(1 - R)} \quad (7)$$

This parameter is also important since it is often used to discriminate the far infrared properties of galaxies in blind infrared cosmological surveys such as H-GOODS and H-ATLAS (e.g. Elbaz et al. 2011; Smith et al. 2012b). We thus use either of the two parameters in the following analysis.

Gas metallicities, $12+\log(O/H)$, are derived using the set of data described in this paper as indicated in Paper II (Hughes et al. 2012). We follow the conversions of Kewley & Ellison (2008) for five different metallicity calibrations from the literature and adopt the PP04 O3N2 calibration on the [NII] and [OIII] emission lines (Pettini & Pagel 2004) as the base metallicity. We then determine the average oxygen abundance in units of $12+\log(O/H)$ for each galaxy. Integrated HI gas data, available for almost the totality of the late-type galaxies of the sample, are used to detect those objects that might have suffered any kind of perturbation induced by the Virgo cluster environment. Interferometric data, mainly taken in order of preference from VIVA (Chung et al. 2009a), Cayatte et al. (1994) and Warmels (1986), are used to measure HI gas column densities (in $M_{\odot} \text{ pc}^{-2}$). For the VIVA galaxies, column densities are determined using the isophotal HI radius¹⁴. For the sake of homogeneity, we normalise the HI column densities given in Cayatte et al. (1994) and in Warmels (1986) by calculating the mean ratio of the column densities measured for galaxies in common with the VIVA survey. This gives $\log \Sigma_{HI}(VIVA) = 0.92 (\pm 0.58) \log \Sigma_{HI}(Cayatte)$ ¹⁵ and $\log \Sigma_{HI}(VIVA) = 1.04 (\pm 0.45) \log \Sigma_{HI}(Warmels)$. ¹²CO(1-0) imaging data are available for a small fraction of the HRS galaxies. We estimate H₂ gas column densities using the set of data of Chung et al. (2009b). For consistency with the HI, column densities are measured using the isophotal radius. The total H₂ gas mass is estimated using the relation:

$$M(H_2)(M_{\odot}) = 3.922 \times 10^{-17} X_{CO} D^2 S_{CO} (\text{Jy km s}^{-1}) \quad (8)$$

where X_{CO} is the CO to H₂ conversion factor, in units of $\text{mol cm}^{-2} (\text{K km s}^{-1})^{-1}$. Here we use the H-band luminosity dependent calibration of Boselli et al. (2002b).

To quantify the effects of the environment on the statistical properties of the HRS galaxies we code them according to their HI gas content. There are indeed strong indications that this gas component is removed during the interactions of galaxies with the hostile cluster environment (Boselli & Gavazzi 2006). We assume as normal, unperturbed objects those with an HI-deficiency parameter $HI-def \leq 0.4$, where $HI-def$ is defined as the difference in logarithmic scale between the expected and the observed HI mass of a galaxy of given angular size and morphological type (Haynes & Giovanelli 1984). HI-deficiencies for all the target galaxies have been measured using the recent calibrations of Boselli & Gavazzi (2009).

¹⁴ For the galaxy HRS 102 (NGC 4254) we use the effective radius since the isophotal radius gives HI column densities a factor of ~ 1000 larger than those determined by Cayatte et al. (1994). The effective radius is indeed more representative of the HI distribution within the disc of this galaxy.

¹⁵ We exclude in the measure of the mean gas column density ratio the galaxy HRS 257 (NGC 4698) for which the difference in the gas column density with Cayatte et al. (1994) is of \sim a factor of 10.

7.2. Line diagnostic

Spectral line emission is often used to characterise, using different diagnostic diagrams, the nature of the emitting source. The set of data in our hands allow us to construct two of the three mostly used diagnostic diagrams, the $[\text{OIII}]\lambda 5007/\text{H}\beta$ vs. $[\text{NII}]\lambda 6584/\text{H}\alpha$ and the $[\text{OIII}]\lambda 5007/\text{H}\beta$ vs. $[\text{SII}]\lambda 6717-6731/\text{H}\alpha$ (Fig. 11). To discriminate active galaxies from normal, star forming objects here we use the recent definitions of Kewley & Ellison (2008).

Despite the presence of a large fraction of active galaxies in the sample¹⁶, the diagnostic diagrams shown in Fig. 11 indicate that the integrated spectra of the HRS galaxies are mainly those of star forming objects (HII), with a few composite spectra (Comp). Only one galaxy, NGC 4388, has an integrated spectrum typical of a Seyfert galaxy. This galaxy is a well known edge-on Seyfert 2 galaxy located close to M86.

The analysis of Fig. 11 does not show any strong systematic difference between gas poor and gas rich late-type galaxies in the $[\text{OIII}]\lambda 5007/\text{H}\beta$ vs. $[\text{NII}]\lambda 6584/\text{H}\alpha$ diagram. There might be a slight (hardly quantifiable) shift towards high $[\text{SII}]\lambda 6717-6731/\text{H}\alpha$ ratios in the $[\text{OIII}]\lambda 5007/\text{H}\beta$ vs. $[\text{SII}]\lambda 6717-6731/\text{H}\alpha$ diagram of the HI-deficient objects (red circles). If real, we think that this mild difference between gas rich and gas poor objects comes from the fact that in HI-deficient objects star formation is suppressed in the outer disc (Boselli et al. 2006; Boselli & Gavazzi 2006). In these objects HII regions, from where most of the line emission comes from, are located only in the inner disc. 63 out of the 260 HRS late-type galaxies are known to host an AGN (Seyfert, LINER or retired AGN). The contribution of the nuclear emission to the integrated spectrum is thus more important in HI-deficient objects than in gas rich systems. Despite the contribution of the AGN to the integrated spectra is minor, objects hosting an active nucleus should be removed in any study of the physical properties of the ISM since their line emission can be partly contaminated by the nuclear activity. The *Herschel* Reference Survey, however, has been designed not only to gather a complete set of multifrequency data ideal for the study the physical properties of the ISM in nearby galaxies, but also for providing a well defined reference for high redshift studies. In these studies of distant, unresolved galaxies the spectra cover a large fraction of the galaxy disc and are thus directly comparable to the integrated spectra obtained in this work (Kobulnicky et al. 1999). For this reason we keep in the following analysis the whole galaxy sample, but we clearly identify and remove active galaxies whenever necessary for the physical interpretation of the data.

7.3. Emission lines equivalent widths

The equivalent widths are useful parameters in statistical analysis since they are normalised entities only moderately sensitive to internal attenuation (in the hypothesis that line and the continuum are equally attenuated). The $\text{H}\alpha$ equivalent width, historically used in the study of the star formation activity of galaxies (e.g. Kennicutt 1983a), for instance, is tightly related to the birthrate parameter and the specific star formation rate. Figure 12 shows the distribution of the equivalent width of all the emission lines detected in our survey. The black solid line gives the distribution of the whole sample and can thus be considered as the typical distribution of a K-band selected sample of nearby

¹⁶ The nuclear data necessary for this classification are available for 233/260 of the late-type galaxies analysed in this work.

late-type galaxies. The number of objects (shown in each single panel in Fig. 12) indicates whether the distribution can be considered as representative (the whole sample is composed of 260 objects). The blue line gives the distribution of the galaxies with a normal HI content ($\text{HI} - \text{def} \leq 0.4$) while the red one that of HI-deficient objects. The Kolmogorov-Smirnov test indicates that the probability that the HI-normal and HI-deficient distributions are driven by the same parent distribution is not null only for $[\text{OIII}]\lambda 3727 \text{ \AA}$ and $[\text{OIII}]\lambda 4959 \text{ \AA}$. These two lines, however, are detected only in a few HI-deficient cluster galaxies. The observed distributions of these two lines, whose detection rate is low compared to the other lines, might thus not be representative in particular for the quiescent, HI-deficient cluster objects. We also remind that the equivalent width of the $[\text{OIII}]\lambda 4959 \text{ \AA}$ line can be significantly overestimated (by $\sim 40\%$) whenever the $\text{E.W.}[\text{OIII}]\lambda 4959 \leq 3 \text{ \AA}$ (see Sect. 5.2).

A systematic difference in the mean $\text{H}\alpha$ equivalent width of HI-normal and HI-deficient galaxies has been already observed in nearby clusters by Kennicutt (1983b) and Gavazzi et al. (1991; 2002; 2006). This is the first evidence for a systematic difference in the distribution of the equivalent widths of the other emission lines. The observed difference in the $\text{H}\beta$ line is not surprising since, as $\text{H}\alpha$, $\text{H}\beta$ is a direct tracer of star formation. $[\text{OIII}]$, $[\text{NII}]$ and $[\text{SII}]$ are not directly related to star formation since in galaxies they can be ionised by shocks (e.g. Dopita & Sutherland 1996). Furthermore, their intensity also depends on metallicity (Kewley & Ellison 2008).

7.4. Balmer decrement

The Balmer decrement gives a direct measure of the dust extinction of the hydrogen emission lines within HII regions. The importance of this quantity resides in the fact that, under the assumption that all emission lines come from the same HII regions, it can be used to correct for dust extinction all UV, optical and near-IR emission lines of galaxies. At the same time the Balmer decrement is related to the far-IR to UV flux ratio and is thus often used for correcting the UV to near-IR stellar continuum in star forming galaxies when far infrared data are not available (Calzetti 2001). Figure 13 traces the distribution of the Balmer decrement $C(\text{H}\beta)$ (see eq. 3), or equivalently of $A(\text{H}\alpha)$ ($A(\text{H}\alpha) = 1.754 C(\text{H}\beta)$), in the HRS sample. We include in the following analysis all galaxies with detected $\text{H}\alpha$ and $\text{H}\beta$ emission lines without any restriction on their equivalent width. This choice is dictated by the fact that any cut in the $\text{H}\beta$ line to restrict the analysis to high quality data would induce a systematic bias in the analysed sample. There is indeed a tight correlation between $C(\text{H}\beta)$ and $\text{E.W.}\text{H}\beta_{\text{emi}}$ (shown in Fig. 6) indicating that the most uncertain values are those relative to the high attenuations. We remind that the mean uncertainty in the measure of $C(\text{H}\beta)$ is $\sim 0.3-0.5$.

Figure 13 shows an asymmetric distribution with values of $C(\text{H}\beta)$ from 0 to ~ 2 ($0 \leq A(\text{H}\alpha) \leq 3.5 \text{ mag}$) peaked at $C(\text{H}\beta) = 0.79 \pm 0.49$ ($A(\text{H}\alpha) = 1.38 \pm 0.87 \text{ mag}$) when the whole sample is considered, $C(\text{H}\beta) = 0.74 \pm 0.47$ ($A(\text{H}\alpha) = 1.30 \pm 0.82 \text{ mag}$) if AGN are excluded. This value is smaller than the values obtained by Moustakas et al. (2006) ($0 \leq A(\text{H}\alpha) \leq 2.5 \text{ mag}$, with a mean value of $A(\text{H}\alpha) 0.51 \pm 0.50$) but fairly consistent with Kennicutt (1992b) ($A(\text{H}\alpha) \simeq 1$), or with Boselli et al. (2001) for a subsample of normal, late-type galaxies such as those analysed in this work extracted from the spectroscopic

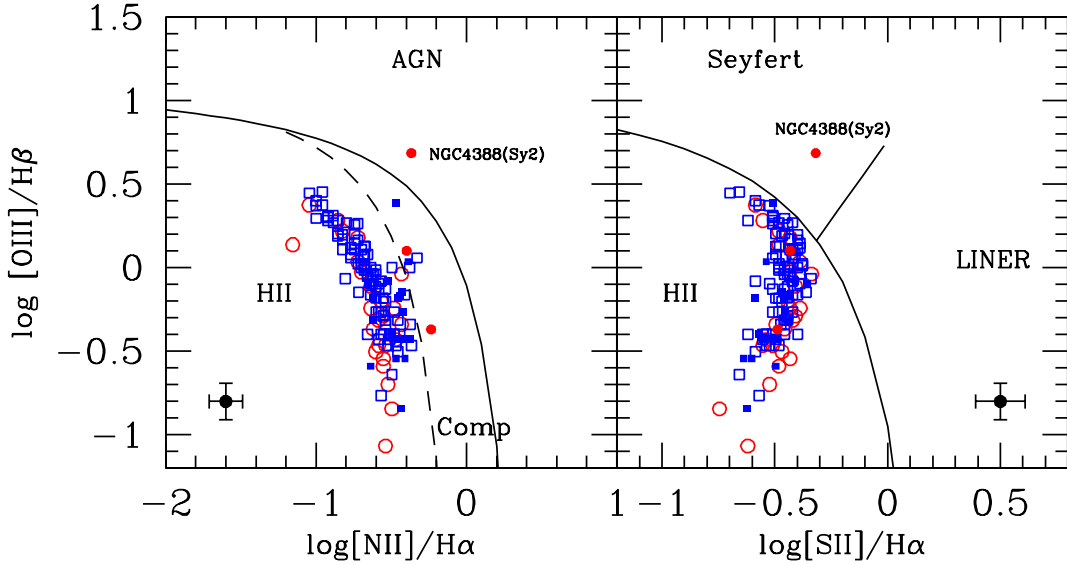


Fig. 11. The emission line diagnostic diagrams $[\text{OIII}]\lambda 5007/\text{H}\beta$ vs. $[\text{NII}]\lambda 6584/\text{H}\alpha$ and $[\text{OIII}]\lambda 5007/\text{H}\beta$ vs. $[\text{SII}]\lambda 6717-6731/\text{H}\alpha$ for all HRS galaxies. The solid and dashed lines gives the limits between star forming (HII), active (AGN, Seyfert, LINER) and composite galaxies of Kewley & Ellison (2008). Blue symbols are for galaxies with a normal HI gas content ($HI - def \leq 0.4$), red symbols for HI-deficient objects ($HI - def > 0.4$). Filled symbols are for galaxies hosting an AGN.

atlas of Kennicutt (1992b) ($A(H\alpha) = 0.78 \pm 0.47 \text{ \AA}$)¹⁷. We see a systematic difference between HI-deficient cluster galaxies ($C(H\beta) = 1.00 \pm 0.54$; $A(H\alpha) = 1.76 \pm 0.94$ mag for the whole sample, $C(H\beta) = 0.94 \pm 0.51$; $A(H\alpha) = 1.65 \pm 0.89$ mag excluding AGN) and field, HI-normal objects ($C(H\beta) = 0.71 \pm 0.45$; $A(H\alpha) = 1.24 \pm 0.80$ mag for the whole sample, $C(H\beta) = 0.66 \pm 0.43$; $A(H\alpha) = 1.16 \pm 0.75$ mag excluding AGN). A Kolmogorov-Smirnov test indicates that the probability that the two distributions are driven by the same parent distribution is only of 0.15-0.30%.

The $\text{H}\alpha$ and $\text{H}\beta$ emission lines used to trace the distribution given in Fig. 13 can be measured in 178 out of the 238 HRS late-type galaxies with spectroscopic data. In a large fraction of our sample (60 over 238 observed galaxies, 25%), the $\text{H}\beta$ emission line is not detected. This can be explained by the fact that the $\text{H}\beta$ line is intrinsically 2.86 times less intense than the $\text{H}\alpha$ line, thus hardly detectable in low surface brightness objects with low signal to noise spectra. These galaxies are generally low mass (Gavazzi et al. 1996), metal poor objects (Tremonti et al. 2004), where dust attenuation is very low (Boselli et al. 2009; see also Fig. 14). The presence of low surface brightness objects in our sample where $C(H\beta)$ cannot be measured might thus bias the observed $C(H\beta)$ distribution given in Fig. 13 towards highly attenuated objects. At the same time, however, the $\text{H}\beta$ line can be undetected in highly attenuated objects where $\text{H}\alpha/\text{H}\beta \gg 2.86$. The two effects should compensate each other, and the resulting mean value of $C(H\beta)$ and $A(H\alpha)$ given above should thus be representative of the entire sample. At the same time we do not have any reason to believe that any systematic bias can

be at the origin of the observed distribution of HI-deficient and HI-normal objects. We have to remark, however, that because of the metallicity gradient in late-type galaxies, the inner disc of cluster objects, whose ISM is unaffected during the interaction with the hostile environment (Boselli et al. 2006; Cortese et al. 2011b), is characterised by a higher dust extinction than the metal poor outer disc. The contribution of this outer disc in the integrated value of $C(H\beta)$ only in unperturbed field objects might thus explain their systematic lower values with respect to HI-deficient systems.

We can study how the Balmer decrement $C(H\beta)$ depends on different intrinsic quantities characterising the observed galaxies. For this purpose we plot in Fig. 14 the relationship between the Balmer decrement $C(H\beta)$ and the morphological type, the stellar mass M_{star} , the H band effective surface brightness $\mu_e(H)$, the birthrate parameter b , the metallicity index $12+\log(\text{O}/\text{H})$, and the star formation rate. Different symbols are used to indicate normal (empty) from active (filled) galaxies. Table 5 gives the Spearman correlation coefficients of the relations between the Balmer decrement and these physical parameters for the whole sample, while Table 6 the best fit for the different subsamples of galaxies with a normal HI gas content ($HI - def \leq 0.4$) and HI-deficient objects ($HI - def > 0.4$) as well as for star forming galaxies and for AGNs.

The analysis of Fig. 14 and of Table 5 and 6 indicates that: 1) Despite a huge dispersion in the distribution of $C(H\beta)$, the attenuation of the emission lines is more important in early-type spirals (Sa-Sc) than in late-type Im and BCD (Stasinska et al. 2004). This evidence is consistent with the decrease of the attenuation of the stellar continuum determined using the far-IR to UV flux ratio ($A(FUV)$) with increasing morphological type observed by Buat & Xu (1996) and Cortese et al. (2008). In early-type spirals ($\leq \text{Sbc}$) we do not observe any strong

¹⁷ The values of Kennicutt (1992b) and Boselli et al. (2001) have been measured without accounting for any $\text{H}\alpha$ underlying absorption and are thus systematically underestimated with respect to the values given in this work.

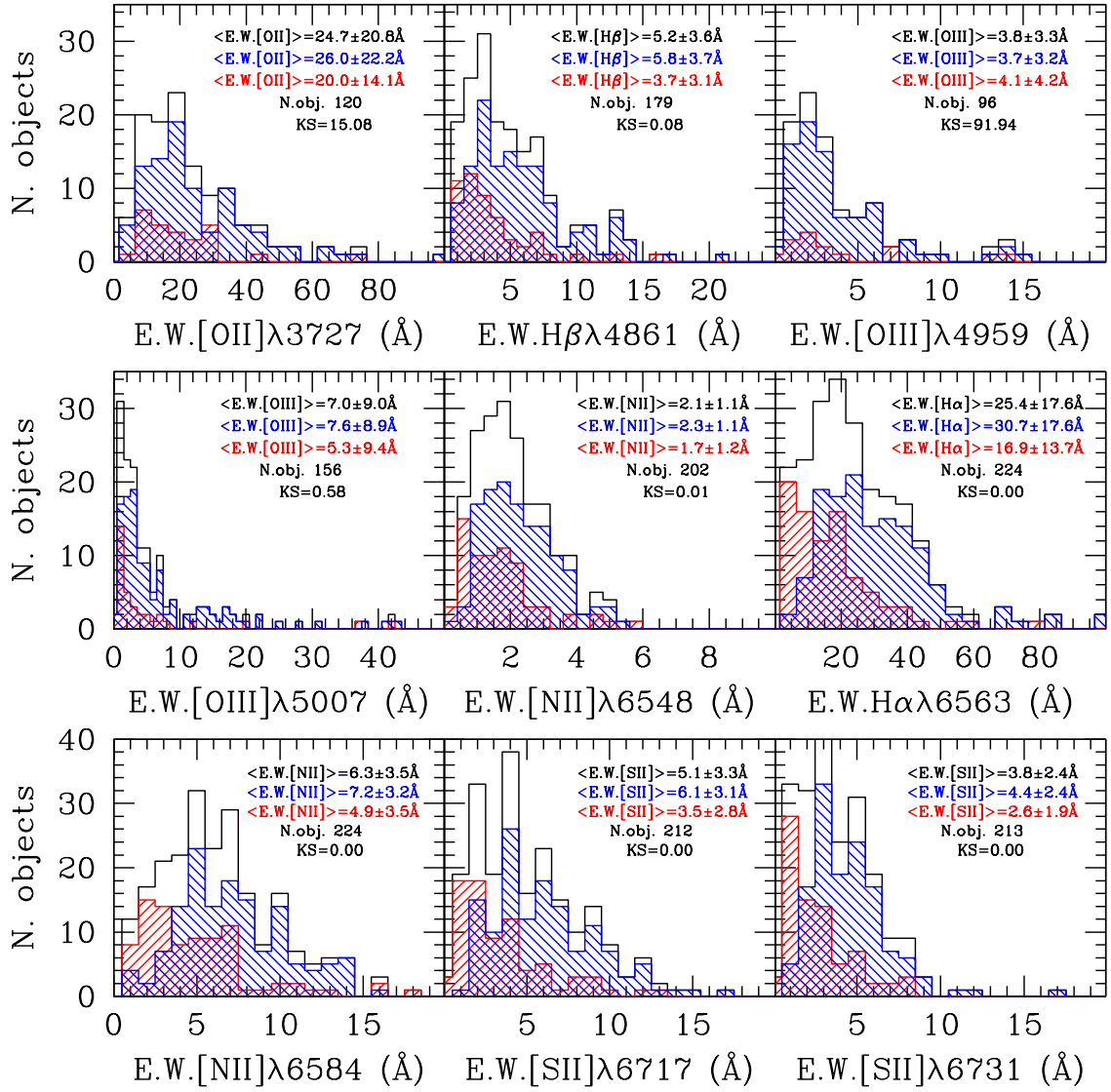


Fig. 12. The distribution of the equivalent width of the different emission lines in the HRS sample. The black line indicates the whole sample of late-type galaxies, the blue line that of galaxies with a normal HI gas content ($HI - def \leq 0.4$) and the red one that of HI-deficient Virgo cluster objects ($HI - def > 0.4$). Each panel gives the total number of available data, the mean value of the equivalent width for the whole distribution (black) and separately for galaxies with a normal HI gas content ($HI - def \leq 0.4$; blue) and for HI-deficient objects (red), and the probability that the HI-normal and HI-deficient galaxy distributions are driven by the same parent distribution, as derived by the Kolmogorov-Smirnov (KS) test.

systematic difference between cluster HI-deficient and field normal objects. Later morphological types, however, are mainly objects with a normal gas content. We can thus deduce that the observed systematic difference in the $C(H\beta)$ distribution shown in Fig. 13 can also be due to the lack of HI-deficient late-type spirals. The lack of this class of objects in the HRS can be easily explained considering that these low mass systems are rapidly transformed into quiescent ellipticals in the Virgo cluster after a ram pressure stripping event able to remove their total gas content and quenching their star formation activity (Boselli et al. 2008a,b).

2) $C(H\beta)$ increases with the stellar mass. The polynomial fit to the data of HI-normal galaxies (blue solid line), given in Table 6 and shown in Fig. 14, is comparable with that obtained

by Boselli et al. (2009) on a similar set of data or with the median values determined by Stasinska et al. (2004) on SDSS data¹⁸. It is, however, significantly steeper than those obtained using SDSS data by Gilbank et al. (2010; black dotted line) and Garn & Best (2010). Part of this difference is due to the fact that the two works use different extinction laws, the first Seaton (1979) which underestimates the extinction by $\sim 13\%$, the second (Calzetti et al. 2000) by 30% . The difference in stellar mass resulting from the adoption of different recipes is of the order of ≈ 0.1 in dex. Despite possible uncertainties resulting from the transformation of M_B absolute magnitudes

¹⁸ The $C(H\beta)$ values determined from Stasinska et al. (2004) assuming the same Galactic extinction law used in this work ranges from ~ 0.77 at $\log M_{star} \sim 9.37$ to $C(H\beta) \sim 1.05$ at $\log M_{star} \sim 10.57$.

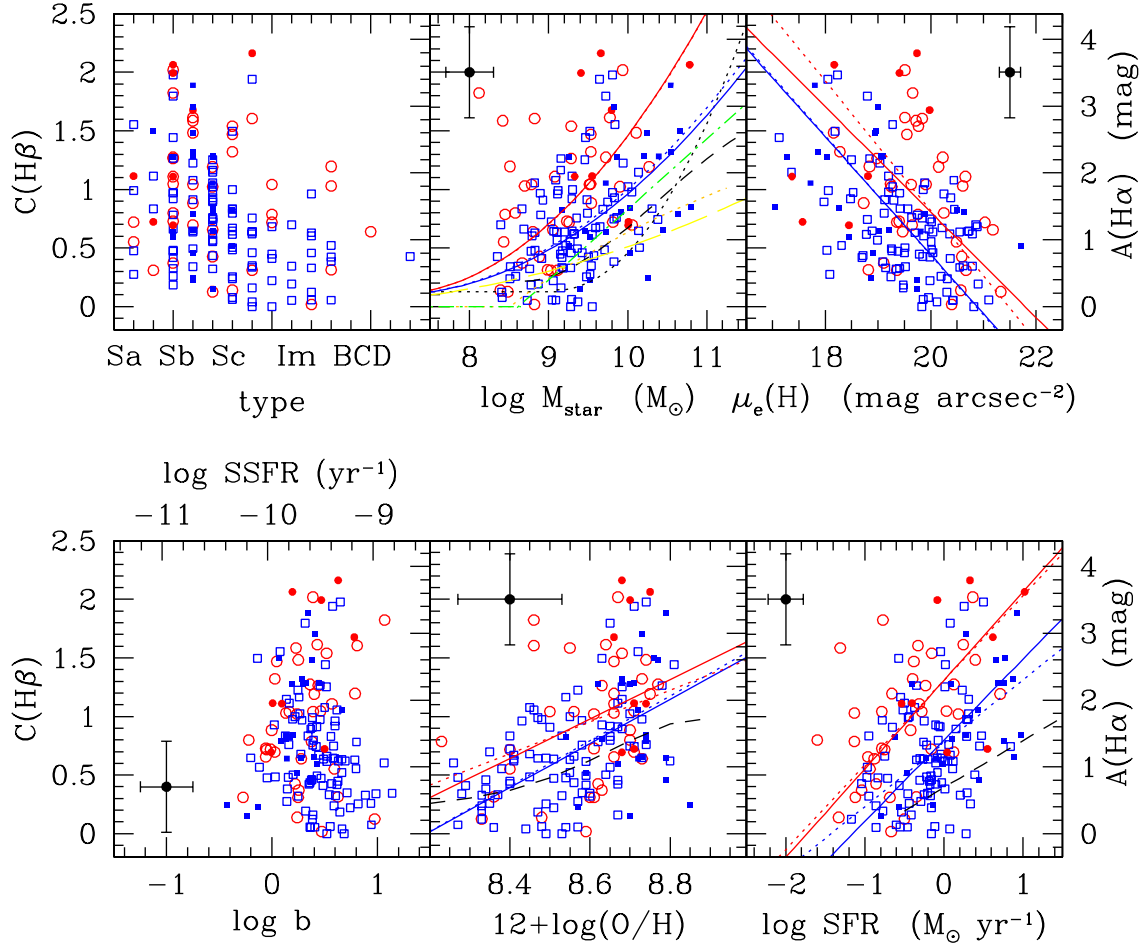


Fig. 14. The relationship between the Balmer decrement $C(H\beta)$ and different parameters characterising the observed galaxies. From left to right, upper line: the morphological type, the logarithm of the total stellar mass (in M_{\odot}), the H band effective surface brightness (in mag arcsec^{-2}); lower line: the logarithm of the birthrate parameter b or equivalently the specific star formation rate $SSFR$, the metallicity index $12+\log(O/H)$ and the star formation rate SFR (in $M_{\odot} \text{ yr}^{-1}$). Blue symbols are for galaxies with a normal HI gas content ($HI - def \leq 0.4$), red symbols for HI-deficient objects ($HI - def > 0.4$). Filled symbols are for galaxies hosting an AGN. The black cross shows the typical uncertainty on the data. The blue and red lines indicate the best fit to the data for HI-normal and HI-deficient galaxies respectively whenever evident correlations are present. Solid lines indicate the best fit obtained including all galaxies, the dotted lines excluding those objects hosting an AGN. The black dotted line indicates the relation obtained by Gilbank et al. (2010) using SDSS data (increased by 13 % to take into account the difference between the two extinction laws used in their (Seaton 1979) and our work (Fitzpatrick & Massa 2007)). The black short-dashed line indicates the relationships obtained by Garn & Best (2010) using SDSS, increased by 30 % to take into account the difference between our extinction law and that used in their work (Calzetti et al 2000). The orange dotted line is the best fit for $0.75 \leq z \leq 1.5$ galaxies given by Dominguez et al. (2012), the yellow, long-dashed line is the relation obtained by Lee et al. (2009) once B band absolute magnitudes are transformed into stellar masses using the relations $\log L_H = -0.455 \times M_B + 1.289$ and $B - V = 0.711 \times \log L_H - 4.439$, combined with the relations given in Boselli et al. (2009) for measuring stellar masses. The green dotted-dashed line is the best fit given in Boselli et al. (2009).

into stellar masses, the difference between our data for isolated, unperturbed galaxies with the fit of Lee et al. (2009) is mainly due to selection effects. Indeed, to avoid objects with very uncertain data Lee et al. (2009) use only galaxies not hosting an AGN and with an equivalent width of the $H\beta$ emission line larger than 5 \AA . Applying the same selection criteria, our data roughly match the fit given by Lee et al. (2009). Our sample, however, is dominated by galaxies with $E.W.H\beta \leq 5 \text{ \AA}$, and the same selection would thus drop the sample with useful data to $\sim 1/3$ of the total sample (see for example Fig. 6 and 12).

Furthermore, this selection criterium might introduce a strong selection bias since low $H\beta$ emission lines might come from galaxies with a strong attenuation. To check whether the high $C(H\beta)$ values determined in our sample are driven mainly by uncertainties in the measurement of the $H\beta$ line or are rather indicative of high attenuations, we have inspected the spectra and the images of those objects with $C(H\beta) > 1.5$. Ten out of the 17 galaxies with $C(H\beta) > 1.5$ are edge-on galaxies with prominent dust lanes (HRS 21, 23, 149, 197, 233, 264, 273, 284, 308, 323), where the attenuation is expected to be very

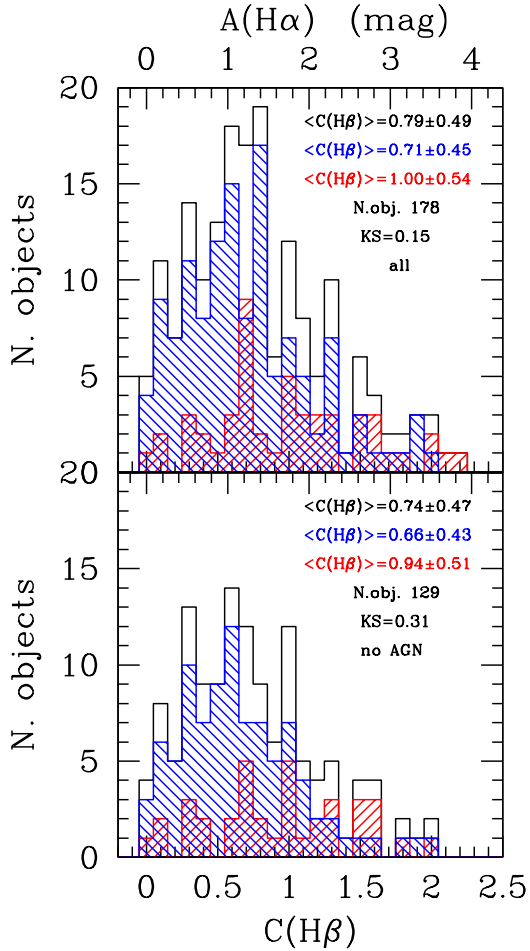


Fig. 13. The distribution of the Balmer decrement $C(H\beta)$ or $A(H\alpha)$ for the whole the HRS sample (above) and excluding AGNs (below). The black line indicates the whole sample of late-type galaxies, the blue line that of galaxies with a normal HI gas content ($HI-def \leq 0.4$) and the red one that of HI-deficient Virgo cluster objects ($HI-def > 0.4$).

important (Xiao et al. 2012). Furthermore the quality of the spectra of these 17 galaxies is sufficiently good to get fairly accurate measurements. We also checked whether the inclusion of active galaxies (AGN, Seyferts, LINERS and retired following the classification of Stasinska et al. (2008)) might change the results. The fits given in Table 6 do not change significantly including or not these active galaxies, consistent with the fact that our integrated spectra are representative of entire galaxies and thus typical of star forming regions (see Sect. 7.2).

Variations of the $H\alpha$ over $H\beta$ ratio with the total B band luminosity has been reported by Moustakas et al. (2006) on both their sample of nearby galaxies with integrated spectra (Moustakas & Kennicutt 2006) and on a much larger SDSS sample of star forming objects. Variations with the r band luminosity has been also reported by Stasinska et al. (2004). This trend is similar to the increase of $A(FUV)$ with the H band luminosity, proxy for the total stellar mass, observed by Cortese et al. (2006) or that reported by Iglesias-Paramo et al. (2007) or Salim et al. (2007) in the local universe, and by Ly et al. (2012) at $z \sim 0.4$.

3) Our Balmer decrement vs. stellar mass relation for isolated galaxies is significantly steeper than that of Dominguez et al. (2012) for objects in the redshift range $0.75 \leq z \leq 1.5$, indicative of a significant evolution.

4) The Balmer decrement increases with the H band effective surface brightness of the target galaxies. Once again, these results agrees with the variation of the dust attenuation of the stellar continuum $A(FUV)$ with $\mu_e(H)$ observed by Cortese et al. (2006) and Johnson et al. (2007) or with the $\log(H\alpha/H\beta)$ vs. r -band surface brightness relation found on SDSS galaxies by Stasinska et al. (2004).

5) Although we do not observe any obvious relation between the Balmer decrement and the birthrate parameter b , the most active galaxies in star formation ($b \gtrsim 4$) all have $C(H\beta) \lesssim 0.5$. We should remark, however, that the dynamic range sampled in b is quite small because relatively quiescent late-type galaxies are generally undetected in $H\beta$. A qualitatively similar behavior has been previously observed between the far infrared to UV flux ratio and b by Martin et al. (2007), and between $\log(H\alpha/H\beta)$ and the $H\alpha$ equivalent width, proxy of the birthrate parameter, by Stasinska et al. (2004).

6) As the stellar attenuation $A(FUV)$, $C(H\beta)$ increases with the gas metallicity (Stasinska et al. 2004; Cortese et al. 2006; Johnson et al. 2007; Garn & Best 2010; Xiao et al. 2012). This relationship is expected, given that metals are the major constituents of dust grains.

7) There is an evident but dispersed trend between $C(H\beta)$ and the star formation rate of galaxies. This trend has been already observed by Wang & Heckman (1996), Sullivan et al. (2001), Perez-Gonzalez et al. (2003), Stasinska et al. (2004), Garn & Best (2010) and Xiao et al. (2012). Variations of the dust attenuation measured using the far infrared to UV flux ratio with different tracers of the star formation activity have been also reported by Wang & Heckman (1996), Buat et al. (2005), Iglesias-Paramo et al. (2006).

8) The observed trends are shared by galaxies with a normal HI gas content (blue squares) and HI-deficient objects (red circles). Consistently with the distributions shown in Fig. 13, however, HI-deficient galaxies tend to have slightly higher values of $C(H\beta)$ than normal objects. We also observe the well know decrease of the star formation activity of cluster galaxies with respect to that of unperturbed field objects due to the removal of the atomic gas reservoir (Gavazzi et al. 2002; Boselli & Gavazzi 2006; Boselli et al. 2006, 2008a).

9) We do not see in any of these relations any strong systematic difference between galaxies hosting an AGN and normal, star forming objects.

All these results seem robust vs. the uncertainty in the determination of the Balmer decrement, which is of the order of 0.3-0.5.

Semi-analytical models of galaxy evolution often quantify the dust attenuation within galaxies by means of their total gas column density (e.g. Guiderdoni et al. 1998). Although limited to a very small subsample of objects having high resolution HI and CO data, we can test whether this assumption is valid in normal, star forming galaxies such as those belonging to the HRS. Figure 15 shows the relationships between the Balmer decrement $C(H\beta)$ and the molecular and atomic gas column densities. We do not consider the total gas column density which is obviously dominated by the molecular gas phase (see Figure 15).

The Balmer decrement does not depend on the HI and H_2 gas column density. Given the small number of galaxies with HI and CO imaging data, however, and the small dynamic range sampled in $C(H\beta)$, Σ_{HI} and Σ_{H_2} , we cannot exclude that we do

Table 5. Spearman correlation coefficients ρ of the relations between the Balmer decrement and the underlying $H\beta$ absorption and the physical parameters for all galaxies (Fig. 14 and 18)

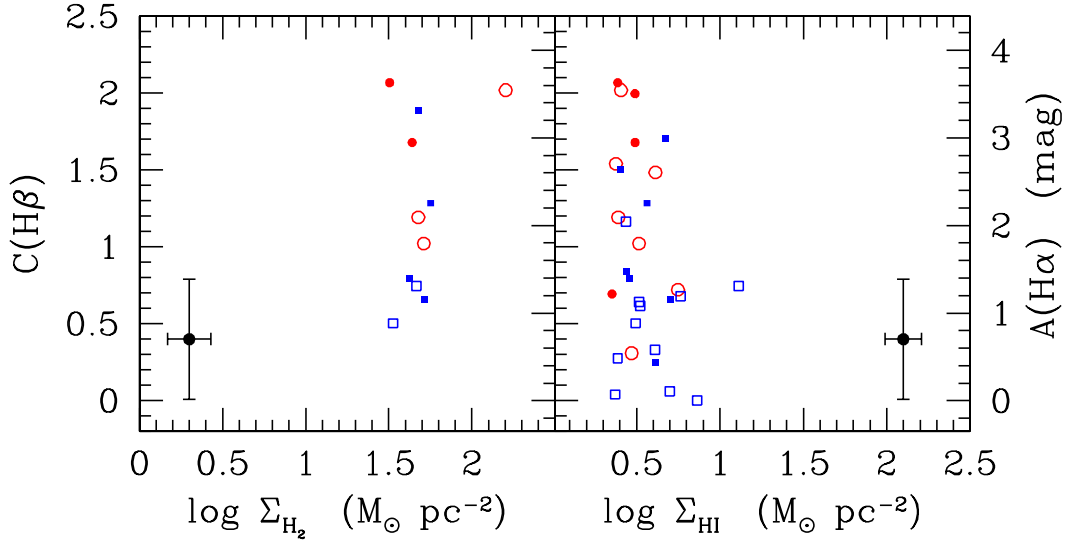
Variable Units	$\log M_{star}$ M_{\odot}	$\mu_e(H)$ AB mag arcsec $^{-2}$	$\log b$	$12+\log(O/H)$	$\log SFR$ $M_{\odot} \text{ yr}^{-1}$
All galaxies					
$C(H\beta)$	0.39	-0.38	-0.16	0.49	0.33
$E.W.H\beta_{abs}$	-0.16	0.08	0.04	-0.31	-0.07
Excluding AGN					
$C(H\beta)$	0.35	-0.36	-0.22	0.50	0.25

Notes: determined using both HI-normal and HI-deficient galaxies.

Table 6. Relationships between $C(H\beta)$ and the different physical parameters (Fig. 14)

Sample	All galaxies		Excluding AGN	
	Regression	ρ	Regression	ρ
Non-deficient	$C(H\beta) = 0.096 \times \log M_{star}^2 - 1.344 \log M_{star} + 4.804$	0.41	$C(H\beta) = 0.100 \times \log M_{star}^2 - 1.400 \log M_{star} + 5.000$	0.39
Deficient	$C(H\beta) = 0.151 \times \log M_{star}^2 - 2.114 \log M_{star} + 7.499$	0.40	$C(H\beta) = 0.151 \times \log M_{star}^2 - 2.110 \log M_{star} + 7.484$	0.33
Non-deficient	$C(H\beta) = -0.503 \times \mu_e(H) + 10.500$	-0.43	$C(H\beta) = -0.510 \times \mu_e(H) + 10.631$	-0.41
Deficient	$C(H\beta) = -0.450 \times \mu_e(H) + 9.806$	-0.23	$C(H\beta) = -0.554 \times \mu_e(H) + 11.893$	-0.30
Non-deficient	$C(H\beta) = 1.882 \times [12 + \log O/H] - 15.413$	0.48	$C(H\beta) = 1.929 \times [12 + \log O/H] - 15.798$	0.48
Deficient	$C(H\beta) = 1.681 \times [12 + \log O/H] - 13.482$	0.36	$C(H\beta) = 1.352 \times [12 + \log O/H] - 10.674$	0.35
Non-deficient	$C(H\beta) = 0.692 \times \log SFR + 0.797$	0.39	$C(H\beta) = 0.541 \times \log SFR + 0.772$	0.27
Deficient	$C(H\beta) = 0.756 \times \log SFR + 1.308$	0.47	$C(H\beta) = 0.722 \times \log SFR + 1.307$	0.48

Notes: linear relations are determined using a bisector fit.


Fig. 15. The relationship between the Balmer decrement $C(H\beta)$ and the atomic (right) and molecular (left) hydrogen column density (in $M_{\odot} \text{ pc}^{-2}$). Blue symbols are for galaxies with a normal HI gas content ($HI - def \leq 0.4$), red symbols for HI-deficient objects ($HI - def > 0.4$). Filled symbols are for galaxies hosting an AGN. The black cross shows the typical uncertainty on the data.

not see any relation just because of the poor statistics. Indeed quite dispersed variations have been already reported in the literature between $A(FUV)$ and the total gas column density (Xu et al. 1997; Boquien et al., in prep.), although based on data of much lower quality.

The Balmer decrement can be compared to other standard tracers of the dust attenuation within galaxies. Among these, the most widely used are the far-IR to UV flux ratio (Buat & Xu 1996, Gordon et al. 2000, Witt & Gordon 2000), and the slope of the UV spectrum β (Meurer et al. 1999, Calzetti et al. 2000, Calzetti 2001). The far-IR to UV flux ratio has been generally measured using FUV GALEX and either IRAS or Spitzer IR

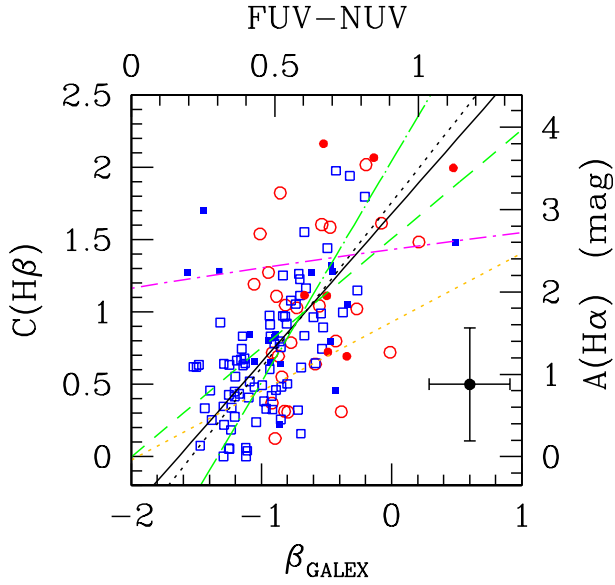


Fig. 16. The relationship between the Balmer decrement $C(H\beta)$ and the UV slope β_{GALEX} determined using GALEX data. Blue symbols are for galaxies with a normal HI gas content ($HI - def \leq 0.4$), red symbols for HI-deficient objects ($HI - def > 0.4$). Filled symbols are for galaxies hosting an AGN. The black cross shows the typical uncertainty on the data. The black solid line indicates the best bisector fit to our data when all galaxies are included, the dotted line excluding AGNs. The orange dotted line shows the fit obtained by Hao et al. (2011), the green dotted-long dashed line and the dashed line the best fit for normal and starburst galaxies by Cortese et al. (2006), and the magenta dotted-short-dashed line that of GAMA/H-ATLAS galaxies of Wijesinghe et al. (2011).

data for different samples of galaxies. Owing to the advent of the *Herschel* space mission, which is producing imaging data in the 70 to 500 μm spectral domain, we can significantly increase the quality of the measure of the total far-IR luminosity of nearby galaxies using spectral energy distribution fitting codes. The SPIRE observations of the HRS galaxies have been recently completed (Ciesla et al. 2012.). PACS observations, more critical for the determination of the total far-IR luminosity since they cover the 70-170 μm spectral domain, just started. For this reason we will postpone the investigation of the relationship of the $C(H\beta)$ vs. total far-IR to UV flux ratio to a future communication. Here we focus on the comparison of the Balmer decrement with the slope of the UV spectrum β , defined as in Overzier et al. (2011):

$$\beta_{\text{GALEX}} = 2.22[FUV - NUV] - 2.0 \quad (9)$$

where FUV and NUV are the GALEX data in the far ($\lambda = 1539 \text{ \AA}$) and near ($\lambda = 2316 \text{ \AA}$) UV bands, corrected for galactic extinction using the Schlegel et al. (1998) Milky Way extinction map and the Fitzpatrick & Massa (2007) extinction law. Figure 16 shows the relationship between the Balmer decrement $C(H\beta)$ and the β_{GALEX} parameter for the HRS galaxies.

Figure 16 shows a very dispersed correlation between the two variables (bisector fit: $C(H\beta) = 1.03 \times \beta_{\text{GALEX}} + 1.68$;

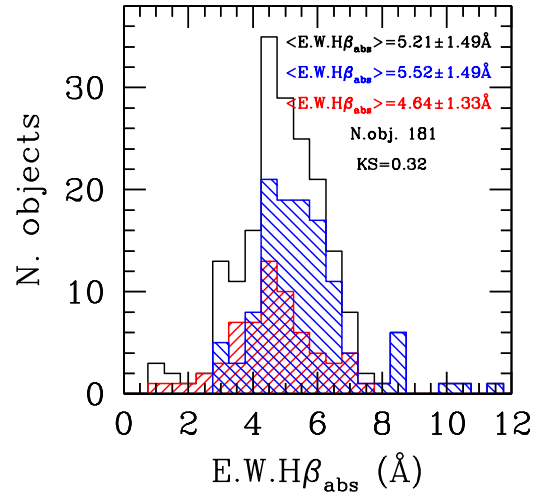


Fig. 17. The distribution of the equivalent width of the $H\beta$ underlying absorption line (in \AA) in the HRS sample. The black line indicates the whole sample of late-type galaxies, the blue line that of galaxies with a normal HI gas content ($HI - def \leq 0.4$) and the red one that of HI-deficient Virgo cluster objects ($HI - def > 0.4$).

Spearman coefficient $\rho = 0.56$) shared by HI-deficient and HI-normal galaxies (solid line). A very similar relation is obtained excluding those galaxies hosting an AGN (bisector fit: $C(H\beta) = 1.14 \times \beta_{\text{GALEX}} + 1.75$; Spearman coefficient $\rho = 0.61$). Given the large dispersion of the observed relation, our data are \sim consistent with the best fit of Cortese et al. (2006) for normal galaxies (dotted-long dashed line), and with that of starbursts (dashed line). Although roughly matching their extremely dispersed data, our fit is completely inconsistent with the best fit given by the GAMA/H-ATLAS collaboration by Wijesinghe et al. (2011; dotted-short-dashed line). This significant difference in the fit (but not necessarily in the data) might be partly due to the quite uncertain aperture corrections necessary to transform nuclear emission line data from GAMA/H-ATLAS to integrated values. The best fit given by Hao et al. (2011) is significantly flatter than the relation observed in our data. It is worth noticing that the Hao et al. sample, however, spans a smaller range in Balmer decrement ($A(H\alpha) \lesssim 2$) than ours, and at the same time includes quite a few objects with $\beta_{\text{GALEX}} \gtrsim 0$.

7.5. Underlying Balmer absorption

The underlying Balmer absorption features observed in the spectra of galaxies are often used as direct tracers of the mean age of the underlying stellar populations since they are due to the absorption of the stellar continuum in the atmosphere of warm A-type stars (Poggianti & Barbaro 1997; Thomas et al. 2004; Le Borgne et al. 2004). Thanks to the spectral resolution of CARELEC, the $H\beta$ line is easily observable in the spectra of the HRS galaxies. We can thus trace the distribution of the equivalent width of the $H\beta$ underlying absorption in a complete, volume limited sample of nearby galaxies. Figure 17 shows the distribution of the E.W. $H\beta_{\text{abs}}$ for the 181/260 late-type galaxies where this feature has been observed and measured.

The mean value of the distribution is $E.W.H\beta_{abs} = 5.21 \pm 1.49 \text{ \AA}$, a value consistent with that measured by Gavazzi et al. (2004) ($E.W.H\beta_{abs} = 5.7 \pm 1.9 \text{ \AA}$). By fitting population synthesis models to the observed spectra of their galaxies, Moustakas & Kennicutt (2006) found a mean $E.W.H\beta_{abs} = 4.40 \pm 0.63 \text{ \AA}$, while Moustakas et al. (2010) give $E.W.H\beta_{abs} = 2.5 \pm 1.0 \text{ \AA}$. Combining the integrated spectra of Kennicutt (1992b) with their own measurements of dwarf irregular galaxies, Kobulnicky et al. (1999) found $E.W.H\beta_{abs}$ ranging from 1 and 6 \AA , with a mean value of $E.W.H\beta_{abs} = 3 \pm 2 \text{ \AA}$. Smaller values have been obtained for BCD galaxies by Izotov et al. (1994) ($0.0 \leq E.W.H\beta_{abs} \leq 3.5$), or for extragalactic HII regions by McCall et al. (1985) ($E.W.H\beta_{abs} = 1.4 \pm 0.2 \text{ \AA}$). Figure 17 also shows a systematic significant difference between the distribution of the underlying Balmer absorption at $H\beta$ of galaxies with a normal HI gas content ($E.W.H\beta_{abs} = 5.52 \pm 1.49 \text{ \AA}$) and HI-deficient objects ($E.W.H\beta_{abs} = 4.64 \pm 1.33 \text{ \AA}$). A Kolmogorov-Smirnov test indicates that the probability that the two distributions are driven by the same parent distribution is only of 0.32%. We are not aware of any other systematic study of any possible dependence of the $E.W.H\beta_{abs}$ index observed in late-type galaxies belonging to different environments. Variations of $E.W.H\beta_{abs}$ as a function of the environment have been reported in Smith et al. (2009) for dwarf early-type galaxies. This work has shown that dwarf ellipticals belonging to the core of the Coma cluster have, on average, stronger $H\beta$ absorption lines than similar objects at the cluster periphery. All these evidences are consistent with the predictions of our chemo-spectrophotometric models of galaxy evolution especially tailored to take into account the effects of the interaction with the cluster environment (Boselli et al. 2006; 2008a, 2008b). These models predict that ram pressure stripping is able to remove a fraction of the cold gas component quenching, on relatively short time scales ($\lesssim 1 \text{ Gyr}$), the activity of star formation. The quenching of the star formation activity induces a decrease of the equivalent width of the $H\beta$ absorption line on time scales of the order of 0.5-0.8 Gyrs, as depicted in Fig. 20 of Boselli et al. (2008a). Late-type HI-deficient galaxies are thus expected to have a lower equivalent width of the $H\beta$ absorption line than gas-rich star forming systems of similar luminosity, as indeed shown in Fig. 17.

Figure 18 shows how the underlying absorption of the $H\beta$ line is related to other physical parameters characterising the sample galaxies. The Spearman regression coefficients of the different relations are given in Table 5. Figure 18 and Table 5 do not show any evident strong trend between $E.W.H\beta_{abs}$ and any of the parameters, not even the birthrate parameter b , which is tightly related to star formation history of galaxies. There are however some indications that the $H\beta$ underlying absorption is barely anticorrelated to the metallicity of the parent galaxy ($\rho = -0.31$). Variations of the equivalent width of the $H\beta$ absorption line with the r band absolute magnitude have been reported by Smith et al. (2009) for the early-type galaxy population in the Coma cluster. A direct comparison of our results with those of Smith et al. (2009) is, however, difficult because our sample is limited to the late-type galaxy population while their includes only early-types. In unperturbed late-type galaxies the underlying absorption comes mainly from A-type stars formed through a rather constant star formation activity, while in elliptical galaxies these stars have been produced by the last, and generally short-lived, episode of star formation. Despite the fact that the $H\beta$ equivalent width of the underlying absorption is tightly connected to the mean age of the underlying stellar population, a direct interpretation of this index and of its variations in terms of age is

quite difficult in star forming systems such as those analysed in this work. As depicted in Fig. 5, in late-type galaxies $E.W.H\beta_{abs}$ is expected to be fairly constant for objects with stellar masses $10^{8.8} \lesssim M_{star} \lesssim 9^{9.8} M_{\odot}$, which is the stellar mass range mainly covered by our sample. A small decrease of the $E.W.H\beta_{abs}$ is expected only for higher stellar masses, where the decrease of the star formation over cosmic time has been sufficiently rapid to produce any effect. For comparison, Le Borgne et al. (2004) give the variation of the $H\beta$ equivalent width as a function of the stellar age for an instantaneous burst, representative of the star formation history of massive ellipticals or globular clusters. As previously mentioned, however, the equivalent width of the $H\beta$ absorption line also depends on metallicity (higher values of $E.W.H\beta_{abs}$ are expected in metal-rich systems, see Fig. 5). Given the mass-metallicity relation observed also in our sample (Hughes et al. 2012), any variation of $E.W.H\beta_{abs}$ with stellar age is neutralized by the dependence of $E.W.H\beta_{abs}$ on the metallicity. For the same reason we expect that any possible dependence of the observed $E.W.H\beta_{abs}$ with any tracer of the star formation activity of the parent galaxies (SFR , b and indirectly $12+\log(O/H)$) is removed by the combined dependence of this parameter on age and metallicity.

8. Conclusions

We present new long-slit integrated spectroscopy in the spectral range 3600-6900 \AA at a resolution $R \approx 1000$ of 138 late-type galaxies belonging to the *Herschel* Reference Survey. Combined with those already collected by our team (Gavazzi et al. 2004) or those available in the literature, these observations provide us with spectroscopic data for 238 out of the 260 late-type galaxies of the sample. The completeness of the observations allow us to make a statistical analysis of the spectroscopic properties of a complete, K-band selected, volume limited sample of nearby galaxies ($15 \leq D \leq 25 \text{ Mpc}$) spanning a large range in morphology and luminosity, and belonging to different environments (Virgo cluster vs. field).

This analysis has shown systematic differences in the spectroscopic properties of normal, gas rich field late-type galaxies and cluster HI-deficient objects. HI-deficient ($HI-def > 0.4$) Virgo cluster galaxies have, on average, equivalent widths of all the sampled emission lines significantly smaller than those of similar objects with a normal HI content. The observed difference in those lines sensitive to the present day star formation activity ($H\alpha$, $H\beta$) is a further confirmation that the star formation activity of cluster galaxies is quenched whenever the gas reservoir is removed during any interaction with the hostile environment (e.g. Boselli & Gavazzi 2006). The observed difference in the other lines ($[OIII]$, $[NII]$ and $[SII]$) is probably a geometrical effect due to the smaller extension of the emitting disc of HI-deficient galaxies linked to the suppression of star formation in the outer disc (e.g. Boselli et al. 2006).

This analysis also shows that the Balmer decrement is systematically higher in HI-deficient cluster galaxies with respect to field objects with a normal gas content. This difference might be due to two different effects: 1) a lack of HI-deficient low luminosity, late-type spirals and 2) the mean extinction of gas and dust truncated discs observed in HI-deficient objects is higher than in normal, field galaxies just because measured only in the metal rich inner disc. We also observe that the underlying Balmer absorption is systematically lower in cluster, HI-deficient objects than in field galaxies.

The Balmer decrement is correlated with the stellar mass, the stellar surface density, the metallicity and the star formation rate

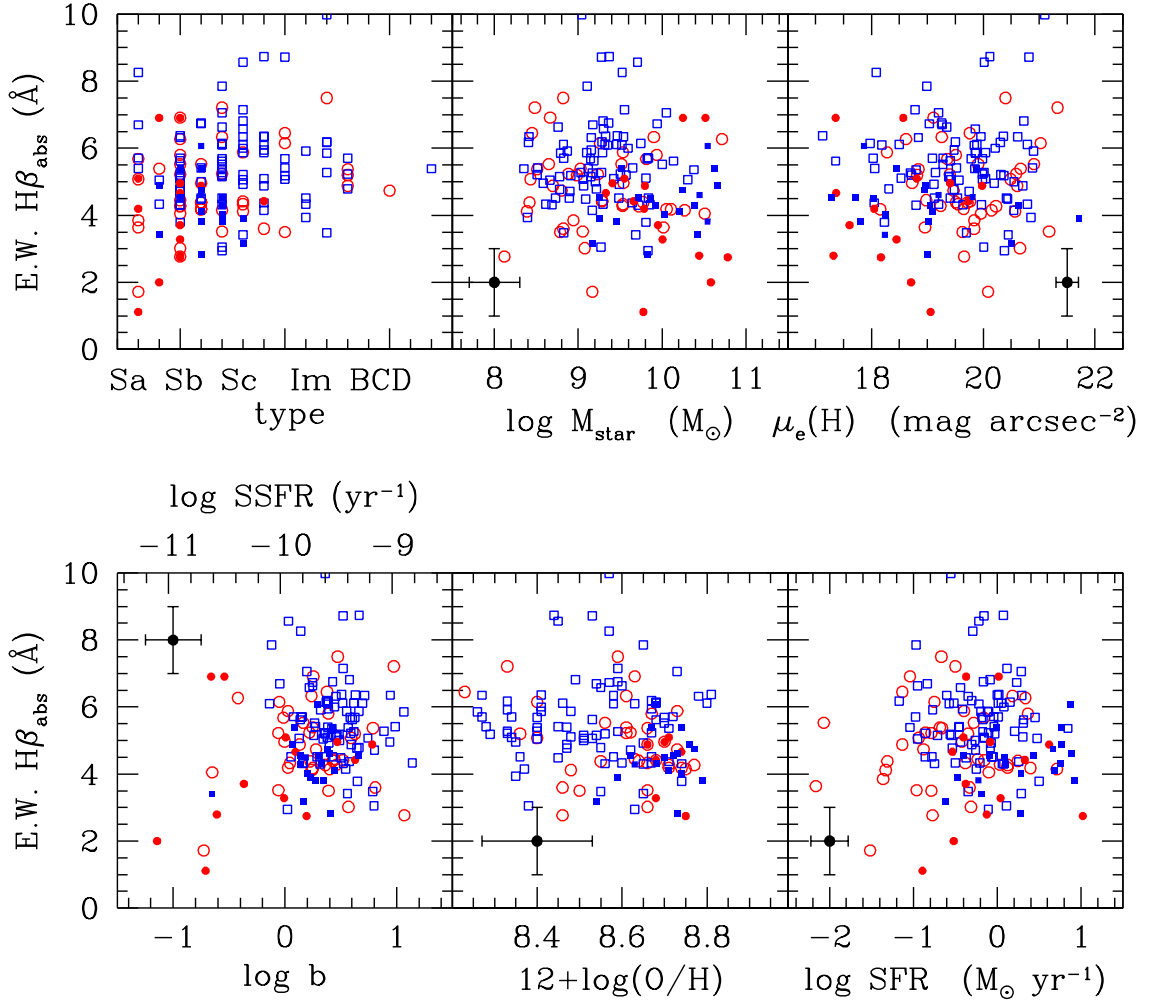


Fig. 18. The relationship between the underlying Balmer absorption $E.W.H\beta_{abs}$ and different parameters characterising the observed galaxies. From left to right, upper line: the morphological type, the logarithm of the total stellar mass (in M_{\odot}), the H band effective surface brightness (in mag arcsec^{-2}); lower line: the logarithm of the birthrate parameter b , or equivalently the specific star formation rate $SSFR$, the metallicity index $12+\log(O/H)$, and the star formation rate (in $M_{\odot} \text{yr}^{-1}$). Blue symbols are for galaxies with a normal HI gas content ($HI-def \leq 0.4$), red symbols for HI-deficient objects ($HI-def > 0.4$). Filled symbols indicate galaxies hosting an AGN. The black cross shows the typical uncertainty on the data for a galaxy of equivalent width of 5 \AA .

of the observed galaxies. The correlation with stellar mass is significantly steeper than that determined in other works based either on integrated spectroscopy or SDSS data. Although dust is tightly associated to the gaseous phase of the interstellar medium, we do not observe any relation between the Balmer decrement and the column density of the atomic and molecular gas. On the contrary, the underlying Balmer absorption looks almost independent from stellar mass, stellar surface density, birthrate parameter, star formation rate and gas metallicity. We also observe a relation, although scattered, between the Balmer decrement and the slope of the UV spectrum, an independent tracer of the UV attenuation in galaxies. The relation is consistent with that found in different samples of resolved, nearby galaxies, but is significantly different from that determined for the GAMA/H-ATLAS collaboration. The huge dispersion observed in all these relations clearly indicates that none of the sampled physical parameters can be used without introducing a large uncertainty as a proxy of the dust attenuation in galaxies.

This result might thus have major implications in the interpretation of spectro-photometric data gathered in cosmological surveys and in the calibration of semi-analytical models of galaxy evolution.

Acknowledgements. We are grateful to the anonymous referee for the accurate and detailed reviewing and for the constructive comments that significantly helped to increase the quality of the manuscript. We want to thank the OHP telescope operators J. Taupenas et J.P. Troncin for their invaluable support during the observations and the PNCG for their generous allocation of time at the OHP telescope. A.B thanks the ESO visiting program committee for inviting him at the Garching headquarters for a two months staying. We are also grateful to P. Anders, S. Boissier, M. Boquien, L. Ciesla and M. Fossati for their help during the preparation of the figures. We thank R. Jansen for providing us with the fits files of HRS galaxies in common. TMH acknowledges the support of a Kavli Research Fellowship. The research leading to these results has received funding from the European Community's Seventh Framework Programme (FP7/2007-2013) under grant agreement No 229517. This research has made use of the NASA/IPAC Extragalactic Database (NED) which is operated by the Jet Propulsion Laboratory, California Institute of Technology, under contract with the National Aeronautics and Space Administration and of the

GOLDMine database (<http://goldmine.mib.infn.it/>). IRAF is distributed by the National Optical Astronomy Observatory, which is operated by the Association of Universities for Research in Astronomy (AURA) under cooperative agreement with the National Science Foundation.

References

- Adelman-McCarthy , J., Agueros, M., Allam, S., et al., 2008, *ApJS*, 175, 297
 Binggeli, B., Sandage, A. and Tammann, G. A., 1985, *AJ*, 1985, 90, 1681
 Boissier, S., Prantzos, N., 1999, *MNRAS*, 307, 857
 Boissier, S., Prantzos, N., 2000, 312, 398
 Boissier, S., Boselli, A., Prantzos, N., Gavazzi, G., 2001, *MNRAS*, 321, 733
 Boissier, S., Prantzos, N., Boselli, A., Gavazzi, G., 2003, *MNRAS*, 346, 1215
 Boselli, A., 2011, in "A Panchromatic View of Galaxies", Wiley-VCH, Berlin (ISBN-10: 3-527-40991-2)
 Boselli, A., Gavazzi, G., 2002, *A&A*, 386, 124
 Boselli, A., Gavazzi, G., 2006, *PASP*, 118, 517
 Boselli, A., Gavazzi, G., 2009, *A&A*, 508, 201
 Boselli, A., Gavazzi, G., Donas, J., Scodreggio, M., 2001, *AJ*, 121, 753
 Boselli, A., Iglesias-Paramo, J., Vilchez, J.M., Gavazzi, G., 2002a, *A&A*, 386, 134
 Boselli, A., Lequeux, J., Gavazzi, G., 2002b, *A&A*, 384, 33
 Boselli, A., Boissier, S., Cortese, L., et al., 2006, *ApJ*, 651, 811
 Boselli, A., Boissier, S., Cortese, L., Gavazzi, G., 2008a, *ApJ*, 674, 742
 Boselli, A., Boissier, S., Cortese, L., Gavazzi, G., 2008b, *A&A*, 489, 1015
 Boselli, A., Boissier, S., Cortese, L., Buat, V., Hughes, T., Gavazzi, G., 2009, *ApJ*, 706, 1527
 Boselli, A., Eales, S., Cortese, L., Bendo, G., Chanial, P., Buat, V., Davies, J., Auld, R., et al., 2010a, *PASP*, 122, 261
 Boselli, A., Ciesla, L., Buat, V., et al., 2010b, *A&A*, 518, L61
 Boselli, A., Boissier, S., Heinis, S., et al., 2011, *A&A*, 528, 107
 Boselli, A., Ciesla, L., Cortese, L., et al., 2012, *A&A*, 540, 54
 Brinchmann, J., Charlot, S., White, S., et al., 2004, *MNRAS*, 351, 1151
 Bruzual, G., Charlot, S., 2003, *MNRAS*, 344, 1000
 Buat, V., Xu., C., 1996, *A&A*, 306, 61
 Buat, V., Iglesias-Paramo, J., Seibert, M., et al., 2005, *ApJ*, 619, L51
 Buat, V., Boissier, S., Burgarella, D., et al., 2008, *A&A*, 483, 107
 Calzetti, D., 2001, *PASP*, 113, 1449
 Calzetti, D., Armus, L., Bohlin, R., Kinney, A., Koornneef, J., Storchi-Bergmann, T., 2000, *ApJ*, 533, 682
 Caputi, K., Lilly, S., Ausser, H., et al., 2008, *ApJ*, 680, 939
 Cayatte, V., Kotanyi, C., Balkowski, C., van Gorkom, J., 1994, *AJ*, 107, 1003
 Cid Fernandes, R., Abilo, M., Sodre, L., Stasinska, G., Gomes, J., 2005, *MNRAS*, 358, 363
 Chung, A., van Gorkom, J., Kenney, J., Crowl, H., Vollmer, B., 2009a, *AJ*, 138, 1741
 Chung, E., Rhee, M., Kim, H., Yun, M., Heyer, M., Young, J., 2009b, *ApJS*, 184, 199
 Ciesla, L., Boselli, A., Smith, M., et al., 2012, *A&A*, 540, 52
 Cortese, L., Hughes, T., 2009, 400, 1225
 Cortese, L., Boselli, A., Buat, V., et al. 2006, *ApJ*, 637, 242
 Cortese, L., Boselli, A., Franzetti, P., Decarli, R., Gavazzi, G., Boissier, S., Buat, V., 2008, *MNRAS*, 386, 1157
 Cortese, L., Catinella, B., Boissier, S., Boselli, A., Heinis, S., 2011a, *MNRAS*, 415, 1797
 Cortese, L., Davies, J., Pohlen M., et al., 2011b, *A&A*, 518, L49
 Cortese, L., Boissier, S., Boselli, A., et al., 2012a, *A&A*, 544, 101
 Cortese, L., Ciesla, L., Boselli, A., et al., 2012b, *A&A*, 540, 42
 Dominguez, A., Siana, B., Henry, A., et al., 2012, *astroph/1201.1867*
 Dopita, M., Sutherland, R., 1996, *ApJS*, 102, 161
 Dreyer, J.L.E., 1888, *MmRAS*, 49, 1
 Dreyer, J.L.E., 1908, *MmRAS*, 59, 105
 Elbaz, D., Dickinson, M., Hawang, H., et al., 2011, *A&A*, 533, 119
 Fitzpatrick, E., Massa, D., 2007, *ApJ*, 663, 320
 Garn, T., Best, P., 2010, *MNRAS*, 409, 421
 Gavazzi, G., Boselli, A., Kennicutt, R., 1991, *AJ*, 101, 1207
 Gavazzi, G., Pierini, D., Boselli, A., 1996, *A&A*, 312, 397
 Gavazzi, G., Boselli, A., Scodreggio, M., Pierini, D., Belsole, E., 1999, *MNRAS*, 304, 595
 Gavazzi, G., Franzetti, P., Scodreggio, M., Boselli, A., Pierini, D., 2000, *A&A*, 361, 863
 Gavazzi, G., Bonfanti, C., Sanvito, G., Boselli, A., Scodreggio, M., 2002, *ApJ*, 576, 135
 Gavazzi, G., Boselli, A., Pedotti, P., Gallazzi, A., Carrasco, L., 2002, *A&A*, 396, 449
 Gavazzi, G., Boselli, A., Donati, A., Franzetti, P., Scodreggio, M., 2003, *A&A*, 400, 451
 Gavazzi, G., Zaccardo, A., Sanvito, G., Boselli, A., Bonfanti, C., 2004, *A&A*, 417, 499
 Gavazzi, G., Boselli, A., Cortese, L., Arosio, I., Gallazzi, A., Pedotti, P., Carrasco, L., 2006, *A&A*, 446, 839
 Gavazzi, G., Savorgnan, G., Fumagalli, M., 2011, *A&A*, 534, 31
 Gilbank, D., Baldry, I., Balogh, M., Glazebrook, K., Bower, R., 2010, *MNRAS*, 405, 2594
 Gordon, K., Clayton, G., Witt, A., Misselt, K., 2000, *ApJ*, 533, 236
 Griffin, M., Abergel, A., Abreu, A., et al., 2010, *A&A*, 518, L3
 Groves, B., Brinchmann, J., Walcher, J., 2012, *MNRAS*, 419, 1402
 Guiderdoni, B., Hivon, E., Bouchet, F., Maffei, B., 1998, *MNRAS*, 295, 877
 Jansen, R., Fabricant, D., Franx, M., Caldwell, N., 2000, *ApJS*, 126, 331
 Jarrett, T., Chester, T., Cutri, R., Schneider, S., Huchra, J., 2003, *AJ*, 125, 525
 Johnson, B., Schiminovich, D., Seibert, M., et al., 2007, *ApJS*, 173, 392
 Hao C-N., Kennicutt, R., Johnson, B., Calzetti, D., Dale, D., Moustakas, J., 2011, *ApJ*, 741, 124
 Haynes, M., Giovanelli, R., 1984, *AJ*, 89, 758
 Hopkins, A., Connolly, A., Haarsma, D., Cram, L., 2001, *AJ*, 122, 288
 Hughes, T., Cortese, L., 2009, *MNRAS*, 396, L41
 Hughes, T., Cortese, L., Boselli, A., Gavazzi, G., Davies, J., 2012, *A&A*, in press (paper II)
 Kennicutt, R., 1983a, *AJ*, 88, 483
 Kennicutt, R., 1983b, *ApJ*, 272, 54
 Kennicutt, R., 1992a, *ApJS*, 79, 255
 Kennicutt, R., 1992b, *ApJ*, 388, 310
 Kennicutt, R., Tamblyn, P., Congdon, C., 1994, *ApJ*, 435, 22
 Kewley, L., Ellison, S., 2008, *ApJ*, 681, 1183
 Kewley, L., Groves, B., Kauffmann, G., Heckman, T., 2006, *MNRAS*, 372, 961
 Kobulnicky, H., Kennicutt, R., Pizagno, J., 1999, *ApJ*, 514, 544
 Koopmann, R., Kenney, J., Young, J., 2001, *ApJS*, 135, 125
 Iglesias-Paramo, J., Buat, V., Takeuchi, T., et al., 2006, *ApJ*, 164, 38
 Iglesias-Paramo, J., Buat, V., Hernandez-Fernandez, J., et al., 2007, *ApJ*, 670, 279
 Izotov, Y., Thuan, T., Lipovetsky, V., 1994, *ApJ*, 435, 647
 Le Borgne, D., Rocca-Volmerange, B., Prugniel P., Lancon, A., Fioc, M., Soubiran, C., 2004, *A&A*, 425, 881
 Lee, J., Gil de Paz, A., Tremonti, C., et al., 2009, *ApJ*, 706, 599
 Lequeux, J., Maucherat-Joubert, M., Deharveng, J.M., Kunth, D., 1981, *A&A*, 103, 305
 Ly, C., Malkan, M., Kashikawa, N., Ota, K., Shimasaku, K., Iye, M., Currie, T., 2012, *ApJ*, 747, L16
 Martin, C., Small, T., Schiminovich, D., et al., 2007, *ApJS*, 173, 415
 Massey, P., Strobel, K., Barnes, J., Anderson, E., 1988, *ApJ*, 328, 315
 McCall, M., Rybski, P., Shields, G., 1985, *ApJS*, 57, 1
 Meurer, G., Heckman, T., Calzetti, D., 1999, *ApJ*, 521, 64
 Moustakas, J., Kennicutt, R., 2006, *ApJS*, 164, 81
 Moustakas, J., Kennicutt, R., Tremonti, C., 2006, *ApJ*, 642, 775
 Moustakas, J., Kennicutt, R., Tremonti, C., Dale, D., Smith, J., Calzetti, D., 2010, *ApJS*, 190, 233
 Nilson, P., Uppsala general catalogue of galaxies, 1973, *Acta Universitatis Upsaliensis. Nova Acta Regiae Societatis Scientiarum Upsaliensis - Uppsala Astronomiska Observatoriums Annaler, Uppsala: Astronomiska Observatorium*
 Nolthenius, R., 1993, *ApJS*, 85, 1
 Oh, K., Sarzi, M., Schawinski, K., Yi, S., 2011, *ApJS*, 195, 13
 Osterbrock, D., Ferland, G., 2006, *Astrophysics of gaseous nebulae and active galactic nuclei*, Sausalito, CA: University Science Book
 Overzier, R., Heckman, T., Wang, J., et al., 2011, *ApJ*, 726, L7
 Perez-Gonzalez, P., Zamorano, J., Gallego, J., Aragon-Salamanca, A., Gil de Paz, A., 2003, *ApJ*, 591, 827
 Pettini, M., Pagel, B., 2004, *MNRAS*, 348, L59
 Pilbratt, G., Reidinger, J., Passvogel, T., et al., 2010, *A&A*, 518, L1
 Poggianti, B., Barbaro, G., 1997, *A&A*, 325, 1025
 Poggianti, B., Bridges, T., Mobasher, B., et al., 2001, *ApJ*, 562, 689
 Roehly, Y., Moreau, C., Buat, V., et al., 2012, *A&A*, in prep.
 Rosa-Gonzalez, D., Terlevich, E., Terlevich, R., 2002, *MNRAS*, 332, 283
 Salim, S., Rich, M., Charlot, S., et al., 2007, *ApJS*, 173, 267
 Schlegel, D., Finkbeiner, D., Davis, M., 1998, *ApJ*, 500, 525
 Seaton, M., 1979, *MNRAS*, 187, 73
 Skrutskie, M. F., Cutri, R. M., Stiening, R., Weinberg, M. D., Schneider, S., Carpenter, J. M., Beichman, C., Capps, R., et al., 2006, *AJ*, 131, 1163
 Smith, R., Lucey, J., Hudson, M., et al., 2009, *MNRAS*, 392, 1265
 Smith, D., Dunne, L., da Cunha, E., et al., 2012b, *MNRAS*, 427, 703
 Smith, M., Gomez, H., Eales, S., et al., 2012a, *ApJ*, 748, 123
 Stasinska, G., Mateus, A., Sodre, L., Szczerba, R., 2004, *A&A*, 420, 475
 Stasinska, G., Vale Asari, N., Cid Fernandes, R., et al., 2008, *MNRAS*, 391, 29
 Sullivan, M., Mobasher, B., Chan, B., Cram, L., Ellis, R., Treyer, M., Hopkins, A., 2001, *ApJ*, 558, 72

- Thomas, D., Maraston, C., Kron, A., 2004, MNRAS, 351, L19
Tremonti, C., Heckman, T., Kauffmann, G., et al., 2004, ApJ, 613, 898
Tully, R. B., Nearby galaxies catalog, 1988, Cambridge and New York, Cambridge University Press, 221
Xiao, T., Wang, T., Wang, H., Zhou, H., Lu, H., Dong, X., 2012, MNRAS, 421, 486
Xu, C., Buat, V., Boselli, A., Gavazzi, G., 1997, A&A, 324, 32
Vazdekis, A., Sanchez-Blazquez, P., Falcon-Barroso, J., Cenarro, A., Beasley, M., Cardiel, N., Gorgas, J., Peletier, R., 2010, MNRAS, 404, 1639
Wang, B., Heckman, T., 1996, ApJ, 457, 645
Warmels, R., 1986, PhD thesis, Groningem Rijksuniversiteit
Wijesinghe, D., da Cunha, E., Hopkins, A., et al., 2011, MNRAS, 415, 1002
Witt, A., Gordon, K., 2000, ApJ, 528, 799
Zwicky, F., Herzog, E., Wild, P., 1961-1968, Catalogue of Galaxies and of Clusters of Galaxies, Vol. I, California Institute of Technology.

Table 7. The general properties of observed late-type galaxies of the HRS sample.

HRS (1)	CGCG (2)	VCC (3)	UGC (4)	NGC (5)	IC (6)	R.A.(h m s) (7)	Dec.($^{\circ}$ '") (8)	D (Mpc) (9)	Type (10)	K_{Stot} (11)	$D_{25}(\prime)$ (12)	V (km s $^{-1}$) (13)	Member (14)	Run (15)	Phot. (16)	T_{exp}/s (17)
1	123035	-	-	-	-	10 17 39.6	+22 48 36.1	16.79	Pec	11.59	1.0	1175	Leo Cl.	O08	C	1 x 1800
2	124004	-	5588	-	-	10 20 57.2	+25 21 54.0	18.44	S?	11.03	0.52	1291	Leo Cl.	O08	P	1 x 1800
5	94052	-	-	-	610	10 26 28.4	+20 13 39.8	16.71	Sc	9.94	1.86	1170	Leo Cl.	O07	P	1 x 1200
10	183028	-	5738	-	-	10 34 29.8	+35 15 24.0	21.66	S?	11.31	0.91	1516	Leo Cl.	O09	C	1 x 1800
11	124038	-	5742	3287	-	10 34 47.3	+21 38 52.0	18.93	SB(s)d	9.78	2.09	1325	Leo Cl.	O07	P	1 x 1800
12	124041	-	-	-	-	10 35 42.0	+26 07 33.0	19.89	cI	11.98	0.59	1392	Leo Cl.	O08	C	1 x 1800
13	183030	-	5753	3294	-	10 36 16.2	+37 19 28.8	22.47	SA(s)c	8.38	3.55	1573	Leo Cl.	O07	P	1 x 1200
16	94116	-	5842	3346	-	10 43 38.9	+14 52 18.6	18.00	SB(rs)cd	9.59	2.69	1260	Leo Cl.	O07	P	1 x 1800
17	95019	-	5887	3370	-	10 47 04.0	+17 16 25.0	18.30	SA(s)c	9.43	3.16	1281	Leo Cl.	O07	P	1 x 1200
18	155015	-	5906	3380	-	10 48 12.1	+28 36 06.4	22.91	SBa	9.92	1.7	1604	Leo Cl.	O07	T	1 x 1200
19	184016	-	5909	3381	-	10 48 24.8	+34 42 41.0	23.29	SBpec	10.32	2.04	1630	Leo Cl.	O07	T	1 x 1800
21	155028	-	5958	-	-	10 51 15.8	+27 50 55.6	16.89	Sbc	11.56	1.45	1182	Leo Cl.	O07	P	1 x 1200
23	184028	-	5972	3424	-	10 51 46.3	+32 54 02.7	21.44	SB(s)b?:;HII	9.04	2.82	1501	Leo Cl.	O07	P	1 x 1200
24	184029	-	5982	3430	-	10 52 11.4	+32 57 02.0	22.64	SAB(rs)c	8.9	3.98	1585	Leo Cl.	O09	P	1 x 1800
25	125013	-	5995	3437	-	10 52 35.7	+22 56 04.0	18.24	SAB(rs)c:	8.88	2.51	1277	Leo Cl.	O07	P	1 x 1200
26	184031	-	5990	-	-	10 52 38.3	+34 28 59.3	22.41	Sab	11.71	1.35	1569	Leo Cl.	O08	C	1 x 1800
28	155035	-	6023	3451	-	10 54 20.9	+27 14 23.0	19.03	Sd	10.23	1.7	1332	Leo Cl.	O09	P	2 x 1800
29	95060	-	6026	3454	-	10 54 29.4	+17 20 38.0	15.73	SB(s)c?sp;HII	10.67	2.09	1101	Leo Cl.	O07	P	1 x 1200
30	95062	-	6028	3455	-	10 54 31.0	+17 17 05.0	15.79	(R)SAB(rs)b	10.39	2.38	1105	Leo Cl.	O08	P	1 x 1800
31	267027	-	6024	3448	-	10 54 39.0	+54 18 19.0	19.63	IO	9.47	5.62	1374	Ursa Major SS	O07	T	1 x 1800
32	95065	-	6030	3457	-	10 54 48.6	+17 37 16.4	16.54	S?	9.64	0.91	1158	Leo Cl.	O07	T	1 x 1200
33	95085	-	6077	3485	-	11 00 02.4	+14 50 29.0	20.46	SB(r)b:	9.46	2.1	1432	Leo Cl.	O07	P	1 x 1800
34	95097	-	6116	3501	-	11 02 47.2	+17 59 21.6	16.14	Scd	9.41	3.89	1130	Leo Cl.	O07	C	1 x 1800
37	155051	-	6128	3512	-	11 04 02.9	+28 02 12.0	19.61	SAB(rs)c	9.65	1.62	1373	Leo Cl.	O07	C	1 x 1800
38	38129	-	6167	3526	-	11 06 56.8	+07 10 28.0	20.27	SAcpecsp	10.69	1.91	1419	Leo Cl.	O07	P	1 x 1200
39	66115	-	6169	-	-	11 07 03.3	+12 03 36.1	22.24	Sb:	11.13	1.86	1557	Leo Cl.	O07	T	2 x 1800
40	67019	-	6209	3547	-	11 09 55.9	+10 43 15.0	22.63	Sb:	10.44	1.91	1584	Leo Cl.	O07	T	1 x 1800
42	96013	-	6277	3596	-	11 15 06.2	+14 47 13.2	17.04	SAB(rs)c	8.7	4.06	1193	Leo Cl.	O07	P	1 x 1800
44	96026	-	6320	-	-	11 18 17.2	+18 50 49.5	16.01	S?	10.99	0.89	1121	Leo Cl.	O08	P	1 x 1800
47	156064	-	6352	3629	-	11 20 31.8	+26 57 48.1	21.53	SA(s)cd:	10.5	2.29	1507	Leo Cl.	O07	T	1 x 1800
48	268021	-	6360	3631	-	11 21 02.8	+53 10 10.4	16.50	SA(s)c	7.99	5.01	1155	Ursa Major Cl.	O07	P	1 x 1800
50	96037	-	6396	3655	-	11 22 54.6	+16 35 24.1	21.43	SA(s)c;;HII	8.83	1.55	1500	Leo Cl.	O07	C	1 x 1200
51	96038	-	6405	3659	-	11 23 45.5	+17 49 07.2	18.56	SB(s)m?	10.28	2.09	1299	Leo Cl.	O08	P	1 x 1200
52	268030	-	6406	3657	-	11 23 55.6	+52 55 16.0	17.20	SAB(rs)cpec	10.29	1.45	1204	Ursa Major Cl.	O09	C	1 x 1800
53	67071	-	6420	3666	-	11 24 26.1	+11 20 32.0	15.14	SA(rs)c:	9.23	4.37	1060	Leo Cl.	O09	C	1 x 1800
54	96045	-	6445	3681	-	11 26 29.8	+16 51 47.0	17.77	SAB(r)bc;LINER	9.79	2.25	1244	Leo Cl.	O09	C	1 x 1800
55	96047	-	6453	3684	-	11 27 11.1	+17 01 48.6	16.54	SA(rs)bc;HII	9.28	2.89	1158	Leo Cl.	O07	P	1 x 1800
56	291072	-	6458	3683	-	11 27 31.8	+56 52 37.4	24.40	SB(s)c?:;HII	8.67	1.86	1708	Ursa Major Cl.	O07	T	1 x 1200
57	96049	-	6460	3686	-	11 27 43.9	+17 13 27.0	16.51	SB(s)bc	8.49	3.19	1156	Leo Cl.	O07	C	1 x 1800
58	96050	-	6464	3691	-	11 28 09.4	+16 55 14.0	15.24	SBB?	10.51	1.35	1067	Leo Cl.	O09	C	1 x 1800
59	67084	-	6474	3692	-	11 28 24.0	+09 24 27.4	24.53	Sb;LINER;HII	9.52	3.16	1717	Leo Cl.	O07	T	1 x 1800
60	268051	-	6547	3729	-	11 33 49.3	+53 07 32.0	15.14	SB(r)apec	8.73	2.82	991	Ursa Major Cl.	O09	T	1 x 1800
61	292009	-	6575	-	-	11 36 26.4	+58 11 29.0	17.39	Scd;;HII	11.40	1.95	1217	Ursa Major Cl.	O09	T	1 x 1800
62	186012	-	6577	3755	-	11 36 33.3	+36 24 37.2	22.44	SAB(rs)cpec	10.6	3.16	1571	Ursa Major SS	O08	P	1 x 1800
63	268063	-	6579	3756	-	11 36 48.0	+54 17 36.8	18.41	SAB(rs)bc	8.78	4.17	1289	Ursa Major Cl.	O07	C	1 x 1800
65	292019	-	6640	3794	-	11 40 53.4	+56 12 07.0	19.76	SAB(s)d	11.6	2.24	1383	Ursa Major Cl.	O09	T	1 x 1800
66	186024	-	6651	3813	-	11 41 18.6	+36 32 48.5	20.97	SA(rs)b:	8.86	2.24	1468	Ursa Major SS	O07	C	1 x 1200
67	268076	-	6706	-	-	11 44 14.8	+55 02 05.9	20.51	SB(s)m:	11.28	1.91	1436	Ursa Major Cl.	O08	P	1 x 1800
68	186045	-	-	-	-	11 46 26.0	+34 51 07.0	20.17	S?	11.44	0.32	1412	Ursa Major SS	O08	C	1 x 1800
69	268088	-	6787	3898	-	11 49 15.1	+56 05 05.0	16.73	SA(s)ab;LINE;HII	7.66	4.37	1171	Ursa Major Cl.	O07	P	1 x 1200

Continued on next page...

Table 7 – Continued

HRS (1)	CGCG (2)	VCC (3)	UGC (4)	NGC (5)	IC (6)	R.A.(h m s) (7)	Dec.(^o '") (8)	D (Mpc) (9)	Type (10)	K _S tot (11)	D ₂₅ (") (12)	V (km s ⁻¹) (13)	Member (14)	Run (15)	Phot. (16)	T _{exp} /s (17)
70	-	-	-	-	2969	11 52 30.1	-03 52 15.0	23.10	SB(r)bc?;HII	11.15	1.23	1617	Crater Cl.	O08	P	1 x 1800
72	-	-	-	3952	2972	11 53 40.5	-03 59 45.8	22.53	IBm:sp;HII	11.01	1.58	1577	Crater Cl.	O08	T	1 x 1200
74	269019	-	6918	3982	-	11 56 28.1	+55 07 31.0	15.83	SAB(r)b;HII;Sy2	8.85	2.34	1108	Ursa Major Cl.	O09	T	1 x 1800
75	269020	-	6919	-	-	11 56 37.5	+55 37 59.0	18.33	Sdm:	11.56	1.45	1283	Ursa Major Cl.	O09	T	1 x 1800
76	269022	-	6923	-	-	11 56 49.4	+53 09 37.0	15.27	Im:	11.32	2.0	1069	Ursa Major Cl.	O09	T	1 x 1800
77	13033	-	6993	4030	-	12 00 23.6	-01 06 00.3	20.83	SA(s)bc;HII	7.33	4.17	1458	Crater Cl.	O07	P	1 x 1200
78	98019	-	6995	4032	-	12 00 32.9	+20 04 28.0	18.13	Im:	10.45	1.86	1269	Coma I Cl.	O07	T	1 x 1800
79	69024	-	7001	4019	755	12 01 10.5	+14 06 13.5	21.54	SBb?sp	11.33	2.4	1508	Virgo Out.	O07	P	1 x 1200
80	69027	-	7002	4037	-	12 01 23.6	+13 24 03.6	17.00	SB(rs)b:	10.11	2.51	932	Virgo Out.	O08	P	1 x 1800
83	41031	-	7035	-	-	12 03 40.1	+02 38 28.3	17.60	SB(r)a;HII	11.82	1.1	1232	Crater Cl.	O08	T	1 x 1200
84	69036	-	7048	4067	-	12 04 11.5	+10 51 15.8	17.00	SA(s)b:	9.90	1.20	2424	Virgo Out.	O05	P	1 x 1800
86	41041	-	7111	4116	-	12 07 36.8	+02 41 32.0	17.00	SB(rs)dm	10.27	3.80	1309	Virgo Out.	O05	P	1 x 1800
88	41042	-	7116	4123	-	12 08 11.1	+02 52 41.8	17.00	SB(r)c;Sbrst;HII	8.79	5.00	1326	Virgo Out.	O05	P	1 x 1800
90	13104	-	7214	4179	-	12 12 52.1	+01 17 59.0	17.00	Sb(f)	7.92	3.8	1279	Virgo Out.	O09	T	1 x 1800
99	69123	213	7305	-	3094	12 16 56.0	+13 37 31.0	17.00	S;BCD	11.25	0.93	-162	Virgo N Cl.	O05	P	1 x 1800
103	42015	341	7361	4260	-	12 19 22.2	+06 05 55.2	23.00	SB(s)a	8.54	3.52	1935	Virgo B	O04	P	1 x 1200
107	42033	404	7387	-	-	12 20 17.3	+04 12 06.0	17.00	Sd(f)	10.74	1.89	1733	Virgo S Cl.	O07	T	1 x 1800
108	42037	434	-	4287	-	12 20 48.4	+05 38 23.4	23.00	Sc(f)	11.02	1.76	2155	Virgo B	O07	T	1 x 1800
109	42038	449	7403	4289	-	12 21 02.3	+03 43 20.0	17.00	SA(s)cd:sp	9.89	4.33	2541	Virgo S Cl.	O07	C	1 x 1800
112	42044	492	7413	4300	-	12 21 41.5	+05 23 05.4	23.00	Sa	9.53	2.16	2310	Virgo B	O05	C	1 x 1200
115	42047	517	7422	-	-	12 22 01.3	+05 06 00.0	17.00	SBab(s)	10.79	1.41	1864	Virgo S Cl.	O08	T	1 x 1200
121	70035	576	7447	4316	-	12 22 42.2	+09 19 56.9	23.00	Sbc	9.25	2.48	1254	Virgo B	O05	P	1 x 1800
122	99030	596	7450	4321	-	12 22 54.9	+15 49 20.6	17.00	SAB(s)bc;LINER;HII	6.59	9.12	1575	Virgo A	O05	P	1 x 1200
133	158099	-	7483	4359	-	12 24 11.4	+31 31 18.0	17.90	SB(rs)c?sp	10.81	3.6	1253	Coma I Cl.	O07	T	1 x 1800
140	42092	785	7497	4378	-	12 25 18.1	+04 55 30.2	17.00	(R)SA(s)a;Sy2	8.51	3.06	2557	Virgo S Cl.	O04	C	1 x 1200
147	42099	859	7522	-	-	12 25 58.3	+03 25 47.3	17.00	Sd(f)	10.18	2.92	1428	Virgo S Cl.	O05	T	1 x 1800
165	42117	1048	7579	-	-	12 27 55.4	+05 43 16.0	23.00	Sdm:	11.58	1.89	2252	Virgo B	O08	P	1 x 1200
169	99063	-	7595	-	3391	12 28 27.3	+18 24 54.0	24.30	Scd:	10.45	1.1	1701	Coma I Cl.	O09	T	1 x 1800
172	99065	1126	7602	-	3392	12 28 43.3	+14 59 58.2	17.00	SAB:	9.26	2.92	1687	Virgo A	O05	T	1 x 1800
187	42144	1375	7668	4505	-	12 31 39.2	+03 56 22.1	17.00	SB(rs)m	9.56	4.76	1732	Virgo S Cl.	O05	T	1 x 1800
195	99087	1479	7703	4516	-	12 33 07.5	+14 34 29.8	17.00	SB(rs)ab?	9.99	2.16	958	Virgo A	O07	C	1 x 1800
198	159016	-	7714	4525	-	12 33 51.1	+30 16 38.9	16.77	Scd:	9.99	3.0	1174	Coma I Cl.	O07	P	1 x 1800
204	42159	1555	7727	4535	-	12 34 20.3	+08 11 51.9	17.00	SAB(s)c;HII	7.38	8.33	1962	Virgo S Cl.	O05	P	1 x 1800
205	14068	1562	7732	4536	-	12 34 27.1	+02 11 16.4	17.00	SAB(rs)bc;HII;Sbrst	7.52	7.23	1807	Virgo S Cl.	O05	C	1 x 1800
212	99098	-	7768	4561	-	12 36 08.3	+19 19 20.0	20.14	SB(rs)dm	10.63	1.51	1410	Coma I Cl.	O07	P	1 x 1200
224	42187	1760	7804	4586	-	12 38 28.4	+04 19 08.8	17.00	SA(s)a: sp	8.47	4.33	792	Virgo S Cl.	O04	C	1 x 1800
225	70202	1778	7817	-	3611	12 39 04.1	+13 21 49.0	17.00	S?	11.42	1.76	2750	Virgo E Cl.	O09	T	1 x 1800
227	14091	-	7819	4592	-	12 39 18.7	-00 31 55.0	15.27	SA(s)dm:	10.22	5.75	1069	Virgo Out.	O08	P	1 x 1200
229	70204	1809	7825	-	3631	12 39 48.0	+12 58 26.0	17.00	S?	11.11	1.1	2839	Virgo E Cl.	O09	C	1 x 1800
237	42208	1923	7871	4630	-	12 42 31.1	+03 57 37.3	17.00	IB(s)m?	9.89	2.31	742	Virgo S Cl.	O05	P	1 x 1800
238	14109	-	7869	4629	-	12 42 32.6	-01 21 02.4	15.94	SAB(s)mpec	11.84	1.38	1116	Virgo Out.	O08	P	1 x 1800
252	15016	-	7931	4668	-	12 45 31.9	-00 32 08.6	23.13	SB(s)d;NLAGN	10.58	1.38	1619	Virgo Out.	O08	P	1 x 1800
261	43040	-	7982	-	-	12 49 50.2	+02 51 05.0	16.54	Sd(f)	10.17	3.39	1158	Virgo Out.	O09	P	1 x 1800
262	43041	-	7985	4713	-	12 49 57.9	+05 18 41.1	17.00	SAB(rs)d;LINER	9.75	3.20	652	Virgo Out.	O05	C	1 x 1800
264	15027	-	7991	-	-	12 50 38.9	+01 27 52.2	18.17	Sd(f)	11.61	1.7	1272	Virgo Out.	O08	P	1 x 1200
265	-	-	-	4720	-	12 50 42.8	-04 09 21.0	21.49	Pec	10.77	0.65	1504	Virgo Out.	O09	P	1 x 1800
266	-	-	-	4731	-	12 51 00.8	-06 23 28.4	21.30	SB(s)cd	9.79	6.61	1491	Virgo Out.	O07	T	1 x 1200
267	129028	-	8005	4747	-	12 51 45.9	+25 46 37.4	16.84	SBcd?pecsp	10.29	3.95	1179	Coma I Cl.	O07	T	1 x 1800
270	15029	-	8009	4753	-	12 52 22.0	-01 11 59.0	17.70	IO	6.72	6.03	1239	Virgo Out.	O07	P	1 x 900
271	100015	-	8014	4758	-	12 52 44.0	+15 50 55.9	17.00	Im.;HII	10.93	3.00	1240	Virgo Out.	O05	P	1 x 1800
273	15031	-	8020	4771	-	12 53 21.3	+01 16 09.0	17.00	SAd? sp;NLAGN	9.01	4.00	1119	Virgo Out.	O05	T	1 x 1800
274	15032	-	8021	4772	-	12 53 29.2	+02 10 06.0	17.00	SA(s)a;LINER;Sy3	8.36	2.90	1038	Virgo Out.	O05	T	1 x 1200
277	43060	-	-	4791	-	12 54 43.9	+08 03 10.6	17.00	cl	11.35	1.2	2529	Virgo Out.	O08	P	1 x 1800

Table 7 – Continued

HRS (1)	CGCG (2)	VCC (3)	UGC (4)	NGC (5)	IC (6)	R.A.(h m s) (7)	Dec.($^{\circ}$ '") (8)	D (Mpc) (9)	Type (10)	K_{Stot} (11)	$D_{25} (\prime)$ (12)	V (km s $^{-1}$) (13)	Member (14)	Run (15)	Phot. (16)	T_{exp}/s (17)
278	71071	-	8032	-	-	12 54 44.1	+13 14 14.1	16.01	S	10.39	2.75	1121	Virgo Out.	O07	T	1 x 1200
280	43066	-	8043	4799	-	12 55 15.5	+02 53 47.9	17.00	S?	9.89	1.60	2802	Virgo Out.	O05	P	1 x 1800
281	43068	-	8045	-	-	12 55 23.5	+07 54 35.0	17.00	IBm:	11.82	0.91	2801	Virgo Out.	O08	P	1 x 1200
282	43069	-	-	4803	-	12 55 33.7	+08 14 25.0	17.00	Comp	10.71	0.5	2664	Virgo Out.	O09	P	1 x 1800
284	-	-	-	-	3908	12 56 40.2	-07 33 27.1	18.51	SB(s)d?;HII	9.1	1.82	1296	Virgo Out.	O07	T	1 x 1800
285	15049	-	8078	4845	-	12 58 01.2	+01 34 33.0	17.00	SA(s)ab sp;HII	7.79	5.20	1097	Virgo Out.	O05	C	1 x 1800
287	15055	-	8121	4904	-	13 00 58.6	-00 01 39.4	17.00	SB(s)cd;Sbrst	9.5	2.4	1174	Virgo Out.	O07	P	1 x 1200
288	-	-	-	4941	-	13 04 12.8	-05 33 06.7	15.91	(R)SAB(r)ab::Sy2	8.22	3.63	1114	Virgo Out.	O07	P	1 x 1200
289	-	-	-	4981	-	13 08 48.7	-06 46 39.0	23.97	SAB(r)bc;LINER	8.49	2.75	1678	Virgo Out.	O09	C	1 x 1800
290	189037	-	8271	5014	-	13 11 31.2	+36 16 56.0	16.23	Sa?sp	10.11	1.7	1136	Canes Ven. Spur	O09	T	1 x 1800
291	217031	-	8388	5103	-	13 20 30.1	+43 05 01.3	18.53	Sab	9.49	1.45	1297	Canes Ven. Spur	O07	P	1 x 1200
292	218010	-	8439	5145	-	13 25 13.9	+43 16 02.1	17.50	S?;HII;Sbrst	9.33	2.0	1225	Canes Ven. Spur	O07	C	1 x 1200
293	16069	-	8443	5147	-	13 26 19.7	+02 06 03.0	15.60	SB(s)dm	9.73	1.91	1092	Virgo Out.	O07	T	1 x 1800
294	246017	-	8593	-	902	13 36 01.2	+49 57 39.0	22.97	Sb	10.42	2.19	1608	Canes Ven. Spur	O07	T	1 x 1800
297	246023	-	8711	5301	-	13 46 24.6	+46 06 25.4	21.54	SA(s)bc:sp	9.11	4.17	1508	Canes Ven. Spur	O07	C	1 x 1200
298	218047	-	8725	5303	-	13 47 45.0	+38 18 17.0	20.27	Pec	10.23	0.91	1419	Canes Ven. Spur	O09	T	1 x 1800
299	45108	-	8727	5300	-	13 48 16.0	+03 57 03.1	16.73	SAB(r)c	9.5	3.89	1171	Virgo-Libra Cl.	O07	P	1 x 1800
300	218058	-	8756	-	-	13 50 35.8	+42 32 29.5	19.34	Sab	10.34	1.7	1354	Canes Ven. Spur	O07	T	1 x 1200
301	17088	-	8790	5334	4338	13 52 54.4	-01 06 52.6	19.71	SB(rs)c:	9.94	4.17	1380	Virgo-Libra Cl.	O07	P	1 x 1800
302	45137	-	8821	5348	-	13 54 11.3	+05 13 39.0	20.61	SBbc:sp	10.87	3.55	1443	Virgo-Libra Cl.	O07	P	1 x 1800
303	295024	-	8843	5372	-	13 54 45.9	+58 40 00.7	24.53	S?	10.65	0.65	1717	Canes Ven-Came. Cl	O07	T	1 x 1800
304	46001	-	8831	5356	-	13 54 58.4	+05 20 01.4	19.57	SABbc:sp;HII	9.64	3.09	1370	Virgo-Libra Cl.	O08	P	1 x 1800
305	46003	-	8838	5360	958	13 55 38.7	+04 59 06.2	16.73	IO	11.15	2.19	1171	Virgo-Libra Cl.	O07	T	1 x 1800
308	46011	-	8857	-	-	13 56 26.6	+04 23 48.0	15.59	Sb(f)	11.93	0.91	1091	Virgo-Libra Cl.	O07	T	1 x 1800
309	272031	-	9036	5486	-	14 07 24.9	+55 06 11.0	19.76	SA(s)m:	11.95	1.86	1383	Canes Ven-Came. Cl	O07	P	1 x 1200
310	47010	-	9172	5560	-	14 20 04.4	+03 59 33.0	24.54	SB(s)bpec	9.98	3.72	1718	Virgo-Libra Cl.	O07	P	1 x 1200
313	47022	-	9187	5577	-	14 21 13.2	+03 26 10.0	21.29	SA(rs)bc:	9.75	3.39	1490	Virgo-Libra Cl.	O07	P	1 x 1800
314	19012	-	9215	-	-	14 23 27.1	+01 43 34.6	19.84	SB(s)d	10.54	2.19	1389	Virgo-Libra Cl.	O07	P	1 x 1800
315	220015	-	9242	-	-	14 25 21.0	+39 32 22.4	20.57	Sc	11.73	5.01	1440	Canes Ven. Spur	O07	C	1 x 1200
317	47066	-	9311	-	1022	14 30 01.8	+03 46 22.3	24.51	S?	11.7	1.1	1716	Virgo-Libra Cl.	O07	T	1 x 1800
318	47070	-	9328	5645	-	14 30 39.3	+07 16 30.0	19.57	SB(s)d	9.69	2.4	1370	Virgo-Libra Cl.	O09	P	1 x 1800
319	75064	-	9353	5669	-	14 32 44.0	+09 53 31.0	19.54	SAB(rs)cd	10.35	3.98	1368	Virgo-Libra Cl.	O07	P	1 x 1800
320	47090	-	9363	5668	-	14 33 24.3	+04 27 01.7	22.61	SA(s)d	11.71	3.31	1583	Virgo-Libra Cl.	O07	T	1 x 1800
321	47123	-	9427	5692	-	14 38 18.1	+03 24 37.1	22.59	S?	10.54	0.89	1581	Virgo-Libra Cl.	O07	T	1 x 1800
323	48004	-	9483	-	1048	14 42 58.0	+04 53 22.5	23.43	S	9.55	2.24	1640	Virgo-Libra Cl.	O07	P	1 x 1200

Table 8. Fluxes of the emission lines of the HRS galaxies.

HRS	ref	E(B-V) mag	C(H β)	Flux f(H α)=1									
				[OIII] λ 3727	H β λ 4861	[OIII] λ 4958	[OIII] λ 5007	[NII] λ 6548	H α λ 6563	[NII] λ 6584	[SII] λ 6717	[SII] λ 6731	
(1)	(2)	(3)	(4)	(5)	(6)	(7)	(8)	(9)	(10)	(11)	(12)	(13)	
1	1	0.031	1.20	0.22	0.15	-	0.06	0.10	1.00	0.29	0.18	0.12	
2	1	0.023	0.80	0.51	0.20	0.04	0.09	0.10	1.00	0.30	0.19	0.14	
4	6	0.023	-	-	-	-	-	-	-	-	-	-	
5	1	0.020	-	-	-	-	-	0.08	1.00	0.34	0.14	0.11	
10	1	0.027	0.47	0.75	0.25	0.08	0.24	0.06	1.00	0.24	0.21	0.15	
11	1	0.023	0.76	0.45	0.21	0.06	0.12	0.08	1.00	0.27	0.23	0.17	
12	1	0.023	0.43	0.91	0.26	0.11	0.33	0.07	1.00	0.17	0.22	0.17	
13	1	0.019	1.28	-	0.15	-	0.06	0.09	1.00	0.32	0.17	0.12	
16	1	0.027	0.83	-	0.20	-	0.09	0.08	1.00	0.31	0.20	0.17	
17	1	0.031	0.44	0.70	0.26	0.07	0.22	0.08	1.00	0.26	0.17	0.13	
18	1	0.025	1.11	1.06	0.16	-	0.23	0.13	1.00	0.40	0.22	0.17	
19	1	0.020	0.42	0.53	0.26	0.04	0.09	0.10	1.00	0.30	0.18	0.12	
20	4	0.025	0.25	0.87	0.29	0.13	0.40	0.07	1.00	0.21	0.20	0.13	
21	1	0.024	1.59	-	0.12	-	0.10	0.05	1.00	0.23	0.23	0.20	
23	1	0.023	1.98	0.29	0.09	-	0.11	0.12	1.00	0.43	0.23	0.17	
24	1	0.024	0.98	0.44	0.18	-	0.06	0.10	1.00	0.35	0.16	0.12	
25	1	0.019	0.89	0.25	0.19	0.06	0.11	0.10	1.00	0.33	0.19	0.14	
26	1	0.019	0.83	0.57	0.20	0.08	0.21	0.07	1.00	0.20	0.24	0.18	
27	4	0.018	0.32	0.57	0.28	0.05	0.16	0.10	1.00	0.31	0.19	0.13	
28	1	0.022	0.16	0.57	0.31	0.05	0.12	0.07	1.00	0.26	0.19	0.13	
29	1	0.034	0.32	0.58	0.28	0.07	0.20	0.07	1.00	0.23	0.21	0.17	
30	1	0.033	0.78	0.87	0.20	-	0.14	0.09	1.00	0.28	0.23	0.15	
31	1	0.012	0.38	0.79	0.27	0.20	0.57	0.04	1.00	0.13	0.18	0.13	
32	1	0.031	-	-	-	-	-	-	-	-	-	-	
33	1	0.021	0.64	1.11	0.23	-	0.09	0.10	1.00	0.35	0.19	0.14	
34	1	0.023	-	-	-	-	-	0.08	1.00	0.31	0.22	0.15	
35	5	0.009	-	-	-	-	-	-	-	-	-	-	
36	4	0.026	0.72	0.31	0.21	0.03	0.10	0.19	1.00	0.59	0.19	0.15	
37	1	0.028	0.65	0.65	0.22	-	0.09	0.14	1.00	0.42	0.19	0.14	
38	1	0.033	0.72	0.79	0.21	0.13	0.36	0.05	1.00	0.15	0.24	0.18	
39	1	0.015	0.97	-	0.18	0.08	0.15	0.08	1.00	0.25	0.22	0.16	
40	1	0.024	0.33	0.75	0.28	0.11	0.29	0.06	1.00	0.23	0.21	0.16	
42	1	0.027	0.76	-	0.21	-	-	0.10	1.00	0.36	0.17	0.11	
44	1	0.022	0.26	0.74	0.29	0.20	0.57	0.05	1.00	0.14	0.14	0.10	
47	1	0.018	0.64	0.92	0.22	0.12	0.31	0.06	1.00	0.20	0.25	0.17	
48	1	0.016	0.75	0.55	0.21	-	0.09	0.11	1.00	0.33	0.17	0.12	
50	1	0.025	1.05	0.26	0.17	-	0.05	0.10	1.00	0.34	0.14	0.11	
51	1	0.019	0.76	0.47	0.21	0.06	0.15	0.08	1.00	0.24	0.23	0.17	
52	1	0.017	1.28	1.12	0.15	-	0.40	0.10	1.00	0.34	0.19	0.14	
53	1	0.032	1.25	0.46	0.15	-	0.06	0.09	1.00	0.31	0.18	0.12	
55	1	0.026	0.91	0.31	0.19	-	0.07	0.10	1.00	0.34	0.17	0.14	
56	1	0.015	1.15	0.21	0.16	0.04	0.07	0.12	1.00	0.36	0.18	0.13	
57	1	0.024	0.70	-	0.22	-	-	0.09	1.00	0.34	0.15	0.10	
58	1	0.026	0.48	0.98	0.25	0.13	0.24	0.07	1.00	0.25	0.24	0.16	
59	1	0.032	1.27	-	0.15	-	0.11	0.11	1.00	0.36	0.22	0.16	
60	1	0.011	1.55	0.26	0.12	-	0.16	0.13	1.00	0.47	0.18	0.15	
61	1	0.015	0.24	1.04	0.30	0.17	0.58	0.04	1.00	0.12	0.18	0.13	
62	1	0.025	0.55	0.75	0.24	0.18	0.40	0.06	1.00	0.18	0.22	0.14	
63	1	0.011	-	-	-	-	-	0.09	1.00	0.35	0.16	0.14	
64	5	0.014	0.91	0.71	0.19	0.10	0.14	0.04	1.00	0.19	0.27	0.19	
65	1	0.013	0.40	0.87	0.27	0.15	0.43	0.04	1.00	0.15	0.17	0.12	
66	1	0.019	0.97	0.48	0.18	0.07	0.13	0.09	1.00	0.28	0.20	0.15	
67	1	0.013	0.19	1.30	0.31	0.15	0.50	0.04	1.00	0.14	0.19	0.13	
68	1	0.020	0.48	0.66	0.25	0.26	0.74	0.04	1.00	0.11	0.13	0.09	
69	1	0.021	-	-	-	-	-	0.30	1.00	0.41	-	-	
70	1	0.027	0.00	0.56	0.35	0.14	0.41	0.05	1.00	0.15	0.20	0.14	
72	1	0.025	0.60	0.61	0.23	0.23	0.68	0.04	1.00	0.09	0.12	0.08	
73	4	0.030	0.25	0.35	0.30	0.00	0.01	0.13	1.00	0.39	0.17	0.09	
74	1	0.014	0.59	0.40	0.23	0.10	0.16	0.11	1.00	0.35	0.15	0.11	
75	1	0.014	-	-	-	-	-	-	1.00	0.23	0.25	0.19	
76	1	0.026	0.12	1.00	0.32	0.24	0.77	0.03	1.00	0.11	0.15	0.12	
77	1	0.027	1.32	-	0.14	-	-	0.09	1.00	0.32	0.12	0.09	
78	1	0.035	0.63	0.23	0.23	0.12	0.31	0.05	1.00	0.18	0.23	0.17	
79	1	0.032	0.18	0.27	0.31	0.21	0.64	0.04	1.00	0.12	0.18	0.13	
80	1	0.029	1.11	0.73	0.16	-	-	0.09	1.00	0.30	0.19	0.12	
81	2	0.022	-	-	-	-	-	0.02	1.00	0.46	-	-	
83	1	0.027	0.55	0.95	0.24	0.15	0.42	0.04	1.00	0.15	0.19	0.14	
84	1	0.025	1.26	-	0.15	-	-	0.11	1.00	0.39	0.17	0.14	
85	4	0.023	0.65	0.39	0.22	0.03	0.11	0.14	1.00	0.43	0.21	0.14	
86	1	0.022	0.00	-	0.35	0.03	0.14	0.07	1.00	0.22	0.24	0.16	

Continued on next page. . .

Table 8 – Continued

HRS	ref	E(B-V) mag	C(H β)	Flux f(H α)=1								
				[OIII] λ 3727	H β λ 4861	[OIII] λ 4958	[OIII] λ 5007	[NII] λ 6548	H α λ 6563	[NII] λ 6584	[SII] λ 6717	[SII] λ 6731
(1)	(2)	(3)	(4)	(5)	(6)	(7)	(8)	(9)	(10)	(11)	(12)	(13)
88	1	0.020	0.62	-	0.23	0.05	0.08	0.14	1.00	0.43	0.19	0.15
89	2	0.028	0.68	-	0.22	0.12	0.33	-	1.00	0.18	0.25	0.18
91	2	0.035	1.50	-	0.12	-	0.05	0.20	1.00	0.39	0.25	0.09
92	2	0.037	0.57	-	0.24	-	0.11	0.08	1.00	0.29	0.22	0.14
94	2	0.032	0.22	-	0.30	-	0.20	0.10	1.00	0.24	0.20	0.15
95 ^a	2	0.017	1.50	-	0.13	-	0.06	0.10	1.00	0.27	0.19	0.14
96	2	0.033	1.02	-	0.17	-	-	0.09	1.00	0.33	0.17	0.09
97	2	0.032	-	-	-	-	-	-	1.00	0.28	0.04	0.04
98	2	0.031	1.17	0.66	0.16	0.06	0.16	0.07	1.00	0.23	0.23	0.16
99	1	0.035	0.37	-	0.27	-	0.10	0.07	1.00	0.26	0.19	0.12
100	2	0.030	-	-	-	-	-	-	1.00	0.26	0.08	0.11
102	2	0.039	0.74	-	0.21	-	0.05	0.10	1.00	0.32	0.13	0.09
103	1	0.023	-	-	-	-	-	-	1.00	0.44	-	-
106	2	0.029	-	0.46	-	-	-	0.08	1.00	0.23	0.13	0.25
107	1	0.022	-	-	-	-	-	0.10	1.00	0.30	0.22	0.16
108	1	0.019	1.23	-	0.15	-	-	0.11	1.00	0.30	0.23	0.16
109	1	0.019	-	-	-	-	0.18	0.07	1.00	0.33	0.23	0.17
110	2	0.034	0.06	0.84	0.34	0.16	0.43	0.05	1.00	0.15	0.22	0.15
111	2	0.035	-	-	-	-	-	0.18	1.00	0.30	0.14	-
112	1	0.022	-	-	-	-	-	-	1.00	0.43	-	-
113	2	0.035	-	-	-	-	-	-	-	-	-	-
114 ^a	2	0.022	0.66	0.32	0.22	-	0.07	0.12	1.00	0.39	0.15	0.10
115	1	0.020	-	-	-	-	-	0.10	1.00	0.38	-	-
116	2	0.042	-	-	-	-	-	-	-	-	-	-
118	2	0.024	0.08	1.27	0.33	0.29	0.84	0.04	1.00	0.10	0.16	0.10
119	2	0.027	-	-	-	-	-	0.09	1.00	0.29	0.10	0.06
121	1	0.022	-	-	-	-	-	0.09	1.00	0.31	0.18	0.14
122	1	0.026	0.79	-	0.20	-	-	0.12	1.00	0.36	0.08	0.06
124	2	0.024	-	-	-	-	0.08	-	1.00	0.22	0.19	0.16
127	2	0.021	-	-	-	-	-	0.07	1.00	0.29	0.09	0.09
128	2	0.022	0.72	0.48	0.21	-	-	0.05	1.00	0.15	0.21	0.27
130	2	0.029	0.31	-	0.28	0.05	0.14	0.08	1.00	0.26	0.23	0.15
132	2	0.025	0.05	0.77	0.34	0.15	0.45	0.08	1.00	0.21	0.22	0.10
133	1	0.025	1.05	0.70	0.17	0.10	0.27	0.05	1.00	0.19	0.24	0.18
134	2	0.027	-	-	-	-	-	-	1.00	0.44	-	-
136	2	0.024	-	-	-	-	-	-	-	-	-	-
139	2	0.023	0.06	0.73	0.34	0.14	0.35	0.08	1.00	0.21	0.25	0.17
141	2	0.024	-	-	-	-	-	0.09	1.00	0.35	0.12	0.08
142	2	0.024	0.28	0.71	0.29	0.12	0.27	0.08	1.00	0.25	0.27	0.14
143	2	0.026	0.48	1.05	0.25	0.16	0.48	0.07	1.00	0.19	0.19	0.12
144	2	0.033	0.69	0.93	0.22	0.39	1.12	0.13	1.00	0.43	0.28	0.22
145 ^a	2	0.031	0.64	1.01	0.23	-	0.23	0.06	1.00	0.21	0.22	0.14
146	2	0.029	1.00	-	0.18	-	0.15	0.07	1.00	0.23	0.26	0.17
147	1	0.023	-	-	-	-	-	0.11	1.00	0.32	0.27	0.17
148 ^b	2	0.026	0.64	0.72	0.23	0.10	0.25	0.07	1.00	0.19	0.26	0.18
149	2	0.029	2.02	-	0.09	-	-	0.05	1.00	0.31	0.14	0.11
151	2	0.032	1.11	-	0.16	-	-	0.11	1.00	0.31	0.17	0.15
152	2	0.018	0.71	0.59	0.21	-	0.08	0.12	1.00	0.40	0.18	0.12
153 ^a	2	0.025	0.70	0.56	0.22	-	0.05	0.12	1.00	0.31	0.19	0.11
154 ^a	2	0.029	0.52	1.30	0.25	-	0.12	0.08	1.00	0.24	0.22	0.15
156	2	0.033	-	-	-	-	-	0.15	1.00	0.62	0.17	0.15
157	2	0.018	0.49	0.52	0.25	0.09	0.17	0.07	1.00	0.25	0.19	0.13
158	2	0.021	0.41	1.28	0.26	0.22	0.54	-	1.00	0.10	0.21	0.14
159	2	0.021	0.72	0.52	0.21	-	-	0.22	1.00	0.65	0.25	0.19
160	2	0.019	1.27	0.49	0.15	-	-	0.13	1.00	0.38	0.22	0.13
163	2	0.028	-	-	-	-	-	0.38	1.00	0.98	0.41	0.39
164	2	0.027	-	-	-	-	-	-	-	-	-	-
165	1	0.020	1.04	0.70	0.17	0.05	0.18	0.08	1.00	0.20	0.23	0.16
167	2	0.024	-	-	-	-	-	0.09	1.00	0.37	0.13	0.11
168	2	0.021	0.34	1.00	0.28	0.23	0.67	-	1.00	0.10	0.19	0.11
169	1	0.032	1.85	1.10	0.10	0.20	0.42	0.06	1.00	0.15	0.23	0.19
170	2	0.028	-	-	-	-	-	0.19	1.00	0.47	0.20	0.20
171	2	0.019	0.88	0.38	0.19	-	0.04	0.10	1.00	0.30	0.19	0.13
172	1	0.037	-	-	-	-	-	0.07	1.00	0.30	0.11	0.10
173	2	0.022	-	-	-	-	-	0.18	1.00	0.62	0.28	0.22
177	2	0.024	0.48	0.76	0.25	0.08	0.14	0.06	1.00	0.25	-	-
182 ^a	2	0.024	0.15	0.28	0.32	-	0.08	0.08	1.00	0.23	0.16	0.16
184	2	0.042	-	-	-	-	-	-	1.00	-	0.26	-
185	2	0.025	-	-	-	-	-	-	-	-	-	-
187	1	0.024	0.34	-	0.28	0.07	0.15	0.08	1.00	0.26	0.19	0.14
188	2	0.029	0.13	-	0.32	-	0.10	0.17	1.00	0.26	0.20	0.14

Continued on next page...

Table 8 – Continued

HRS	ref	E(B-V) mag	C(H β)	Flux f(H α)=1								
				[OIII] λ 3727	H β λ 4861	[OIII] λ 4958	[OIII] λ 5007	[NII] λ 6548	H α λ 6563	[NII] λ 6584	[SII] λ 6717	[SII] λ 6731
(1)	(2)	(3)	(4)	(5)	(6)	(7)	(8)	(9)	(10)	(11)	(12)	(13)
189	2	0.031	0.43	0.73	0.26	-	0.09	0.08	1.00	0.25	0.20	0.14
190	2	0.038	2.07	-	0.08	-	-	0.10	1.00	0.37	0.11	0.11
191	2	0.029	0.14	-	0.32	0.17	0.35	0.07	1.00	0.19	0.24	0.17
192	2	0.029	-	-	-	-	-	-	1.00	0.19	0.11	0.11
193	2	0.036	0.02	-	0.35	0.06	0.15	0.08	1.00	0.24	0.21	0.14
194 ^a	2	0.024	0.84	-	0.20	-	0.19	0.06	1.00	0.22	0.23	0.14
195	1	0.036	-	-	-	-	-	-	-	-	-	-
196	2	0.020	0.62	0.84	0.23	0.16	0.29	0.08	1.00	0.21	0.19	0.14
197	2	0.021	1.54	0.56	0.12	-	0.08	0.07	1.00	0.33	0.23	0.22
198	1	0.023	0.83	-	0.20	0.10	0.17	0.06	1.00	0.22	0.25	0.21
199	2	0.038	0.66	0.71	0.22	-	0.07	0.09	1.00	0.28	0.23	0.16
201	2	0.022	1.89	-	0.10	-	-	0.13	1.00	0.40	0.13	0.20
203	2	0.021	0.33	0.88	0.28	0.20	0.57	0.04	1.00	0.12	0.18	0.13
204	1	0.019	1.19	-	0.15	-	-	0.12	1.00	0.37	0.15	0.10
205	1	0.018	1.28	-	0.14	-	0.12	0.12	1.00	0.37	0.20	0.16
206	2	0.022	0.64	-	0.23	-	0.02	0.09	1.00	0.29	0.14	0.10
207	2	0.035	1.47	-	0.13	-	-	0.10	1.00	0.30	0.21	0.14
208	2	0.038	-	-	-	-	-	0.07	1.00	0.34	0.07	0.10
212	1	0.026	0.13	0.85	0.32	0.25	0.70	0.05	1.00	0.11	0.18	0.14
215	2	0.033	1.61	-	0.12	-	0.00	0.09	1.00	0.29	0.11	0.09
216	2	0.032	1.48	-	0.13	-	0.02	0.10	1.00	0.32	0.12	0.08
217	2	0.047	-	-	-	-	-	0.09	1.00	0.57	0.15	0.17
220	2	0.041	-	-	-	-	-	0.20	1.00	0.72	0.38	0.23
221	2	0.024	-	-	-	-	-	0.07	1.00	0.32	0.08	0.09
222	2	0.037	-	-	-	-	-	0.13	1.00	0.31	0.14	0.14
223	2	0.029	0.79	0.84	0.20	0.25	0.30	-	1.00	0.07	0.29	0.05
224	1	0.037	-	-	-	-	-	0.30	1.00	0.66	-	-
225	1	0.036	0.80	1.00	0.20	-	0.20	0.11	1.00	0.37	0.26	0.22
227	1	0.022	0.45	1.23	0.26	0.13	0.40	0.04	1.00	0.15	0.22	0.15
229	1	0.038	-	-	-	-	-	-	-	-	-	-
230	2	0.037	0.73	-	0.21	-	0.14	0.08	1.00	0.27	0.23	0.15
232	2	0.032	-	-	-	-	-	0.07	1.00	0.33	0.15	0.13
233	2	0.032	1.99	-	0.09	-	-	0.08	1.00	0.33	0.20	0.17
237	1	0.030	0.46	0.53	0.26	-	0.05	0.09	1.00	0.27	0.16	0.11
238	1	0.037	0.70	0.74	0.22	0.17	0.43	-	1.00	0.13	0.22	0.18
239 ^a	2	0.028	1.32	-	0.14	-	0.07	0.10	1.00	0.37	0.20	0.14
242 ^a	2	0.026	1.70	0.53	0.11	-	0.14	0.14	1.00	0.41	0.17	0.14
244	2	0.026	1.02	-	0.17	-	-	0.09	1.00	0.27	0.12	0.07
246 ^a	2	0.027	0.84	-	0.20	-	0.08	0.11	1.00	0.37	0.18	0.11
247	2	0.026	0.50	-	0.25	-	0.10	0.08	1.00	0.28	0.16	0.08
249	2	0.029	-	-	-	-	-	-	-	-	-	-
252	1	0.025	0.63	1.29	0.23	0.15	0.44	0.06	1.00	0.16	0.20	0.14
254	2	0.023	1.68	-	0.11	-	-	0.09	1.00	0.30	0.11	0.11
257	2	0.026	-	-	-	-	-	-	-	-	-	-
259	2	0.029	0.85	0.68	0.20	0.12	0.19	-	1.00	0.23	0.18	0.10
261	1	0.035	0.31	-	0.28	-	-	0.06	1.00	0.26	0.19	0.15
262	1	0.028	0.04	1.51	0.34	0.14	0.36	0.06	1.00	0.20	0.20	0.13
263	3	0.012	-	-	-	-	-	-	-	-	-	-
264	1	0.025	1.60	-	0.12	-	-	-	1.00	0.18	0.23	0.17
265	1	0.026	0.31	0.87	0.28	0.19	0.56	0.04	1.00	0.14	0.16	0.12
266	1	0.032	0.48	0.75	0.25	0.06	0.21	0.07	1.00	0.22	0.23	0.15
267	1	0.010	0.77	0.39	0.21	0.11	0.32	0.07	1.00	0.20	0.17	0.12
268	2	0.036	0.92	0.71	0.19	0.08	0.20	0.07	1.00	0.32	0.21	0.14
270	1	0.033	-	-	-	-	-	-	-	0.00	-	-
271	5	0.026	0.96	0.71	0.18	0.14	0.17	0.04	1.00	0.16	0.28	0.20
273	1	0.020	2.16	0.63	0.08	-	-	0.13	1.00	0.32	0.17	0.13
274	1	0.027	-	-	-	-	-	-	1.00	0.30	-	-
275	6	0.025	0.00	1.05	0.35	0.13	0.41	0.06	1.00	0.21	0.00	0.35
277	1	0.034	-	-	-	-	-	0.11	1.00	0.37	0.23	0.18
278	1	0.036	-	-	-	-	-	-	1.00	0.35	0.16	0.16
280	1	0.034	1.11	-	0.16	-	-	0.14	1.00	0.36	0.18	0.14
281	1	0.041	0.80	0.82	0.20	-	0.13	0.09	1.00	0.26	0.20	0.11
282	1	0.031	-	-	-	-	-	-	-	-	-	-
283	2	0.037	0.62	0.66	0.23	0.10	0.17	0.13	1.00	0.39	0.26	0.15
284	1	0.035	1.94	-	0.09	-	0.05	0.10	1.00	0.35	0.22	0.18
285	1	0.020	-	-	-	-	-	0.18	1.00	0.95	-	-
287	1	0.031	0.80	-	0.20	0.07	0.14	0.10	1.00	0.29	0.21	0.15
288	1	0.036	-	-	-	0.41	0.65	0.24	1.00	0.72	0.15	0.19
289	1	0.042	1.48	0.15	0.13	-	-	0.10	1.00	0.38	0.16	0.11
290	1	0.008	0.99	0.46	0.18	-	0.14	0.08	1.00	0.29	0.19	0.14
291	1	0.018	-	-	-	-	-	-	-	-	-	-

Continued on next page...

Table 8 – Continued

HRS	ref	E(B-V) mag	C(H β)	Flux f(H α)=1								
				[OIII] λ 3727	H β λ 4861	[OIII] λ 4958	[OIII] λ 5007	[NII] λ 6548	H α λ 6563	[NII] λ 6584	[SII] λ 6717	[SII] λ 6731
(1)	(2)	(3)	(4)	(5)	(6)	(7)	(8)	(9)	(10)	(11)	(12)	(13)
292	1	0.012	1.44	-	0.13	-	-	0.11	1.00	0.37	0.13	0.10
293	1	0.027	0.22	-	0.30	0.10	0.31	0.07	1.00	0.21	0.19	0.14
294	1	0.011	1.26	0.48	0.15	-	0.08	0.08	1.00	0.28	0.24	0.17
295	6	0.035	0.46	0.25	0.26	0.01	0.04	0.12	1.00	0.37	0.00	0.25
297	1	0.017	1.23	0.79	0.15	0.07	0.16	0.06	1.00	0.25	0.20	0.15
298	1	0.014	0.52	0.65	0.24	0.09	0.21	0.08	1.00	0.27	0.15	0.11
299	1	0.023	0.93	-	0.19	-	0.10	0.07	1.00	0.28	0.21	0.17
300	1	0.014	-	-	-	-	-	0.09	1.00	0.35	0.19	0.15
301	1	0.046	0.80	-	0.20	-	0.18	0.05	1.00	0.30	0.24	0.17
302	1	0.029	1.08	0.97	0.17	-	0.21	0.07	1.00	0.17	0.23	0.17
303	1	0.010	0.62	0.46	0.23	0.05	0.12	0.11	1.00	0.34	0.20	0.14
304	1	0.025	-	-	-	-	-	-	1.00	0.31	0.21	0.15
305	1	0.029	1.03	-	0.17	0.02	0.05	0.08	1.00	0.28	0.20	0.15
308	1	0.033	1.82	-	0.10	-	0.18	-	1.00	0.19	0.23	0.18
309	1	0.020	0.05	1.49	0.34	0.15	0.52	0.03	1.00	0.14	0.21	0.13
310	1	0.030	1.05	0.45	0.17	-	0.07	0.11	1.00	0.34	0.18	0.13
313	1	0.040	1.04	-	0.17	-	0.11	0.07	1.00	0.23	0.22	0.17
314	1	0.032	0.33	1.13	0.28	0.16	0.52	0.06	1.00	0.18	0.21	0.15
315	1	0.010	0.13	0.83	0.32	0.25	0.77	-	1.00	0.09	0.16	0.10
317	1	0.033	0.66	-	0.22	0.11	0.19	0.07	1.00	0.24	0.24	0.16
318	1	0.027	0.46	1.16	0.25	0.13	0.35	0.05	1.00	0.17	0.26	0.16
319	1	0.027	0.67	0.71	0.22	0.08	0.28	0.07	1.00	0.22	0.23	0.17
320	1	0.036	0.35	0.53	0.28	0.05	0.25	0.07	1.00	0.22	0.22	0.15
321	1	0.037	0.42	0.61	0.26	0.09	0.20	0.09	1.00	0.26	0.20	0.15
323	1	0.037	1.80	-	0.10	-	0.06	0.08	1.00	0.29	0.22	0.16

Notes:

- a) spurious detections in the [OIII] λ 4959 line in Gavazzi et al. (2004).
b) new measurements on the original Gavazzi et al. (2004) data.

Table 9. Equivalent widths of the main emission lines of the HRS galaxies.

HRS	ref	E(B-V) mag	EW(Å)									
			[OII] λ3727	Hβ λ4861	[OIII] λ4958	[OIII] λ5007	[NII] λ6548	Hα λ6563	[NII] λ6584	[SII] λ6717	[SII] λ6731	Hβ _{abs} λ4861
(1)	(2)	(3)	(4)	(5)	(6)	(7)	(8)	(9)	(10)	(11)	(12)	(13)
1	1	0.031	6.53	3.11	-	1.19	2.28	22.12	6.65	4.20	2.73	-5.37
2	1	0.023	21.36	5.66	1.18	2.85	3.81	36.76	11.31	7.20	5.18	-5.87
4	6	0.023	10.00	4.00	2.33	7.00	0.00	34.80	0	0.00	5.00	-
5	1	0.020	-	-	-	-	0.68	9.03	3.04	1.21	1.00	-
10	1	0.027	22.40	6.11	2.12	6.04	2.13	33.64	8.05	7.57	5.38	-5.16
11	1	0.023	18.10	4.90	1.34	3.04	2.42	30.78	8.38	7.16	5.30	-6.09
12	1	0.023	34.24	7.02	3.06	9.13	2.44	37.57	6.53	8.76	6.60	-5.39
13	1	0.019	-	3.09	-	1.46	2.26	24.69	8.16	4.20	2.96	-4.30
16	1	0.027	-	2.78	-	1.27	1.42	18.08	5.75	3.59	3.06	-3.42
17	1	0.031	34.52	7.06	1.86	6.16	2.97	36.44	9.69	6.32	5.23	-5.20
18	1	0.025	23.78	1.75	-	2.61	1.78	13.77	5.64	3.16	2.37	-5.10
19	1	0.020	17.28	6.58	0.94	2.52	3.60	37.39	11.56	7.05	4.71	-5.23
20	4	0.025	39.50	12.65	6.24	18.71	4.82	66.70	14.47	13.72	9.22	-
21	1	0.024	-	1.54	-	1.38	0.69	14.52	3.41	3.29	2.77	-4.38
23	1	0.023	8.75	1.40	-	1.76	1.90	15.88	6.98	3.79	2.77	-3.79
24	1	0.024	19.36	3.35	-	1.22	2.32	22.56	8.1	3.81	2.77	-7.06
25	1	0.019	8.31	6.00	1.83	3.71	3.91	38.21	12.68	7.24	5.36	-6.15
26	1	0.019	15.27	4.56	1.96	5.13	2.10	28.21	5.86	6.84	5.05	-5.05
27	4	0.018	24.40	10.12	2.14	6.42	5.33	50.40	15.99	10.08	7.00	-
28	1	0.022	20.99	7.88	1.27	3.06	2.31	32.46	8.54	6.67	4.53	-5.94
29	1	0.034	16.70	6.22	1.61	4.76	1.81	27.65	6.33	5.75	4.68	-6.63
30	1	0.033	15.53	5.64	-	4.13	2.94	34.52	8.72	8.52	6.06	-4.71
31	1	0.012	24.53	10.09	7.53	22.17	2.32	56.44	7.56	10.07	7.19	-5.70
32	1	0.031	-	-	-	-	-	-	-	-	-	-
33	1	0.021	69.31	3.49	-	1.50	2.03	19.96	7.03	3.71	3.00	-4.55
34	1	0.023	-	-	-	-	1.11	13.28	4.1	2.92	1.97	-
35	5	0.009	3.10	-	-	-	-	1.80	0.6	0.30	0.30	-
36	4	0.026	13.50	5.68	0.93	2.79	5.92	30.30	17.76	5.82	4.72	-
37	1	0.028	13.96	3.84	-	1.60	2.90	21.09	9.02	3.98	3.16	-3.81
38	1	0.033	12.63	3.93	2.53	6.89	1.24	27.08	4.11	6.32	4.72	-5.28
39	1	0.015	-	3.31	1.51	2.92	1.80	21.84	5.5	4.99	3.48	-4.52
40	1	0.024	20.87	8.07	3.17	8.99	2.81	44.46	10.58	9.71	7.30	-5.63
42	1	0.027	-	3.59	-	-	2.14	21.09	7.66	3.58	2.53	-4.31
44	1	0.022	54.58	20.64	14.54	43.26	4.76	104.90	14.47	14.79	10.79	-4.96
47	1	0.018	16.91	3.59	2.00	5.30	1.45	25.90	5.37	6.36	4.36	-6.81
48	1	0.016	16.08	4.35	-	2.00	3.24	30.14	10.07	5.12	3.76	-5.69
50	1	0.025	9.03	4.24	-	1.33	3.21	30.78	10.63	4.34	3.12	-4.54
51	1	0.019	18.86	5.11	3.90	8.69	1.54	29.04	5.05	6.16	4.16	-2.91
52	1	0.017	19.46	1.23	-	3.50	0.92	9.24	3.26	1.83	1.41	-4.54
53	1	0.032	13.95	2.94	-	1.24	1.91	21.54	6.78	4.07	2.72	-6.12
55	1	0.026	5.97	3.40	-	1.36	2.41	24.14	8.47	4.28	3.32	-4.52
56	1	0.015	12.46	5.69	1.35	2.47	4.05	34.36	12.6	6.20	4.46	-5.62
57	1	0.024	-	3.53	-	-	1.94	20.60	7.16	3.25	2.25	-4.19
58	1	0.026	22.81	-4.38	2.38	4.27	1.59	22.51	5.66	5.44	3.80	-4.54
59	1	0.032	-	1.86	-	1.45	1.47	12.93	4.8	2.91	2.17	-4.50
60	1	0.011	7.93	1.20	-	1.65	1.58	11.92	5.77	2.28	1.92	-5.71
61	1	0.015	180.20	7.45	4.50	15.16	1.45	39.41	4.69	7.39	5.17	-5.22
62	1	0.025	35.98	5.00	14.02	41.85	3.30	84.36	8.5	11.82	8.33	-3.05
63	1	0.011	-	-	-	-	1.05	11.82	4.12	1.89	1.62	-
64	5	0.014	14.20	2.50	1.20	1.80	0.70	14.20	2.6	3.70	2.60	-
65	1	0.013	64.61	6.16	3.72	10.95	1.29	31.92	4.87	5.74	4.16	-8.47
66	1	0.019	17.20	4.74	1.87	3.54	3.05	35.02	10.12	7.19	5.11	-5.11
67	1	0.013	53.10	9.74	5.00	16.90	1.99	47.36	6.85	9.19	6.48	-5.92
68	1	0.020	34.62	13.20	13.82	40.71	3.67	84.13	9.08	11.54	8.40	-5.70
69	1	0.021	-	-	-	-	0.95	3.15	1.28	-	-	-
70	1	0.027	30.95	13.87	5.67	16.55	2.47	47.11	6.84	9.18	6.70	-7.06
72	1	0.025	23.55	13.48	2.97	2.89	2.21	24.53	6.79	5.68	3.71	-5.86
73	4	0.030	6.30	2.72	0.05	0.14	1.17	9.16	3.52	1.61	0.90	-
74	1	0.014	13.43	6.17	2.62	4.46	4.09	37.27	13.34	6.01	4.55	-5.40
75	1	0.014	-	-	-	-	-	10.28	2.39	2.74	2.07	-
76	1	0.026	35.41	7.86	6.17	19.91	1.02	39.99	4.5	6.43	4.84	-6.17
77	1	0.027	-	2.54	-	-	1.89	19.93	6.53	2.32	1.68	-6.07
78	1	0.035	3.65	4.23	2.30	5.81	1.30	23.92	4.32	5.29	3.78	-3.48
79	1	0.032	9.55	12.84	9.40	28.08	2.82	71.96	8.99	12.45	9.30	-4.78
80	1	0.029	16.51	2.44	-	-	1.73	18.26	5.62	3.63	2.30	-3.02
81	2	0.022	-	-	-	-	0.37	14.30	6.6	-	-	-
83	1	0.027	27.69	6.68	4.34	12.30	1.64	38.34	5.91	7.70	5.57	-5.08
84	1	0.025	-	1.39	-	-	1.41	12.46	5.02	2.16	1.81	-6.32
85	4	0.023	10.20	3.28	0.55	1.66	2.13	15.18	6.39	3.26	2.18	-
86	1	0.022	-	10.71	1.02	4.45	2.50	37.87	8.39	8.84	5.94	-8.72

Continued on next page...

Table 9 – Continued

HRS	ref	E(B-V) mag	EW(Å)									
			[OII] $\lambda 3727$	H β $\lambda 4861$	[OIII] $\lambda 4958$	[OIII] $\lambda 5007$	[NII] $\lambda 6548$	H α $\lambda 6563$	[NII] $\lambda 6584$	[SII] $\lambda 6717$	[SII] $\lambda 6731$	H β_{abs} $\lambda 4861$
(1)	(2)	(3)	(4)	(5)	(6)	(7)	(8)	(9)	(10)	(11)	(12)	(13)
88	1	0.020	-	3.80	0.77	1.49	2.96	21.65	9.5	4.14	3.36	-6.12
89	2	0.028	-	5.27	2.99	8.41	-	32.89	6	8.15	5.81	-5.41
91	2	0.035	-	1.03	-	0.46	1.80	9.06	3.56	2.19	0.79	-4.88
92	2	0.037	-	3.74	-	1.81	1.53	19.31	5.63	4.25	2.60	-7.85
94	2	0.032	-	5.13	-	3.85	1.88	18.90	4.59	3.93	2.96	-
95 ^a	2	0.017	-	2.45	-	1.18	1.92	19.00	5.17	3.63	2.67	-6.10
96	2	0.033	-	2.97	-	-	1.86	19.66	6.54	3.21	1.98	-5.52
97	2	0.032	-	-	-	-	-	4.97	1.43	0.21	0.22	-
98	2	0.031	18.91	3.08	1.20	3.18	1.57	23.69	5.4	5.64	3.85	-5.16
99	1	0.035	-	4.04	-	1.45	1.50	21.36	5.57	4.28	2.78	-6.91
100	2	0.030	-	-	-	-	-	12.14	3.15	1.04	1.31	-
102	2	0.039	-	4.86	-	1.18	3.09	31.49	10.2	4.22	3.03	-5.36
103	1	0.023	-	-	-	-	-	2.95	1.23	-	-	-
106	2	0.029	11.53	-	-	-	1.45	18.48	4.28	2.36	4.66	-
107	1	0.022	-	-	-	-	1.13	11.64	3.5	2.57	1.93	-
108	1	0.019	-	2.50	-	-	2.02	18.03	5.57	4.25	3.02	-5.71
109	1	0.019	-	-	-	2.28	0.81	11.03	3.62	2.47	1.83	-
110	2	0.034	26.38	12.51	6.36	16.31	2.22	51.16	7.7	11.61	8.36	-5.87
111	2	0.035	-	-	-	-	2.59	14.04	4.3	1.72	-	-4.51
112	1	0.022	-	-	-	-	-	3.15	1.29	-	-	-
113	2	0.035	-	-	-	-	-	-	-	-	-	-
114 ^a	2	0.022	7.81	5.36	-	1.69	3.76	31.40	12.56	4.83	3.36	-4.60
115	1	0.020	-	-	-	-	0.52	5.15	1.97	-	-	-
116	2	0.042	-	-	-	-	-	-	-	-	-	-
118	2	0.024	49.08	11.56	10.29	31.34	2.01	55.52	6.08	9.20	6.03	-6.35
119	2	0.027	-	-	-	-	0.70	7.37	2.25	0.79	0.51	-
121	1	0.022	-	-	-	-	1.16	12.22	3.75	2.13	1.68	-
122	1	0.026	-	3.05	-	-	2.42	20.00	7.21	1.79	1.25	-5.40
124	2	0.024	-	-	-	0.64	-	9.37	2.07	1.85	1.60	-
127	2	0.021	-	-	-	-	0.40	6.20	1.81	0.56	0.59	-3.70
128	2	0.022	11.11	3.07	-	-	0.88	16.75	2.59	3.55	4.78	-6.15
130	2	0.029	-	4.73	0.91	2.45	2.21	26.81	6.99	6.01	4.05	-5.39
132	2	0.025	42.28	13.00	6.32	18.09	3.41	48.15	10.04	10.37	5.07	-11.27
133	1	0.025	8.06	2.43	1.54	4.11	1.03	20.76	4.05	5.09	3.77	-6.11
134	2	0.027	-	-	-	-	-	7.78	3.4	-	-	-2.60
136	2	0.024	-	-	-	-	-	-	-	-	-	-4.20
139	2	0.023	43.61	14.12	6.12	14.70	3.28	46.17	9.65	11.37	7.90	-9.99
141	2	0.024	-	-	-	-	0.65	6.77	2.37	0.84	0.59	-
142	2	0.024	38.95	11.33	4.54	10.68	3.56	40.86	10.46	11.24	5.80	-8.26
143	2	0.026	35.86	8.65	5.71	17.40	3.05	45.09	8.46	8.78	5.82	-8.56
144	2	0.033	30.91	7.09	12.91	37.46	4.72	36.50	15.64	10.32	8.28	-3.28
145 ^a	2	0.031	25.90	4.15	-	4.63	1.64	26.65	5.65	5.89	3.99	-5.00
146	2	0.029	-	3.00	-	2.73	1.63	22.22	5.05	5.68	3.73	-6.58
147	1	0.023	-	-	-	-	0.93	8.12	2.57	2.18	1.36	-
148 ^b	2	0.026	15.23	5.75	2.60	6.74	2.29	35.05	6.56	9.42	6.42	-4.88
149	2	0.029	-	0.93	-	-	0.61	11.94	3.75	1.71	1.34	-5.80
151	2	0.032	-	2.25	-	-	2.07	19.01	5.97	3.41	2.80	-4.33
152	2	0.018	16.50	4.06	-	1.48	3.17	26.34	10.66	4.67	3.14	-4.40
153 ^a	2	0.025	20.35	3.45	-	0.85	2.80	22.83	7.05	4.20	2.78	-5.92
154 ^a	2	0.029	41.06	3.17	-	1.60	1.53	18.88	4.55	4.22	2.99	-3.91
156	2	0.033	-	-	-	-	0.69	4.49	2.78	0.78	0.69	-
157	2	0.018	18.48	7.25	2.72	5.31	3.09	40.58	10.44	8.14	5.75	-6.75
158	2	0.021	37.71	6.03	5.23	12.81	-	31.81	3.33	7.15	4.73	-5.18
159	2	0.021	13.42	3.24	-	-	3.78	17.03	11.12	4.42	3.34	-5.68
160	2	0.019	10.89	2.11	-	-	2.24	16.96	6.58	3.89	2.12	-4.27
163	2	0.028	-	-	-	-	1.78	4.63	4.56	1.90	1.80	-2.80
164	2	0.027	-	-	-	-	-	-	-	-	-	-3.64
165	1	0.020	28.01	4.28	1.16	4.61	2.32	29.74	6.12	7.13	4.83	-3.50
167	2	0.024	-	-	-	-	0.49	5.11	1.88	0.67	0.56	-
168	2	0.021	44.02	9.85	8.40	24.94	-	48.99	4.99	9.28	5.69	-5.41
169	1	0.032	5.60	0.61	1.03	2.23	0.49	7.57	1.16	1.90	1.53	-6.21
170	2	0.028	-	-	-	-	0.70	3.65	1.7	0.76	0.77	-2.00
171	2	0.019	9.33	3.41	-	0.76	2.01	21.81	6.53	4.41	2.99	-4.96
172	1	0.037	-	-	-	-	0.58	8.36	2.49	0.92	0.87	-
173	2	0.022	-	-	-	-	1.08	5.89	3.67	1.68	1.32	-6.91
177	2	0.024	24.56	6.45	2.08	3.71	1.98	31.12	7.71	-	-	-6.70
182 ^a	2	0.024	13.89	8.25	-	2.25	1.87	24.21	5.49	3.81	3.77	-10.36
184	2	0.042	-	-	-	-	-	8.19	-	2.12	-	-5.05
185	2	0.025	-	0.85	-	-	-	-	-	-	-	-3.37
187	1	0.024	-	6.59	1.67	3.76	2.46	32.22	8.35	6.27	4.76	-4.33
188	2	0.029	-	5.98	-	1.96	4.44	25.53	6.59	4.86	3.30	-8.51

Continued on next page...

Table 9 – Continued

HRS	ref	E(B-V) mag	EW(Å)		[OIII] λ4958	[OIII] λ5007	[NII] λ6548	Hα λ6563	[NII] λ6584	[SII] λ6717	[SII] λ6731	Hβ _{abs} λ4861
			[OII] λ3727	Hβ λ4861								
(1)	(2)	(3)	(4)	(5)	(6)	(7)	(8)	(9)	(10)	(11)	(12)	(13)
189	2	0.031	23.74	6.96	-	2.33	3.08	38.66	9.79	8.35	5.70	-5.24
190	2	0.038	-	0.76	-	-	0.92	9.40	3.55	1.10	1.11	-2.75
191	2	0.029	-	6.13	3.15	6.98	1.70	24.33	4.6	5.72	4.16	-4.12
192	2	0.029	-	-	-	-	-	5.55	1.06	0.64	0.63	-1.72
193	2	0.036	-	12.63	2.08	5.83	4.44	57.24	13.36	11.96	8.05	-7.50
194 ^a	2	0.024	-	2.84	-	2.92	0.93	15.94	3.56	3.86	2.32	-5.06
195	1	0.036	-	-	-	-	-	-	-	-	-	-
196	2	0.020	14.81	4.76	3.50	6.54	2.50	31.95	6.74	6.40	4.57	-6.36
197	2	0.021	14.64	2.01	-	1.37	1.33	18.84	6.29	4.18	3.95	-4.41
198	1	0.023	-	2.16	1.11	1.93	0.88	13.95	3.07	3.61	2.98	-3.18
199	2	0.038	19.81	5.35	-	1.62	3.19	34.31	9.72	8.07	5.43	-3.52
201	2	0.022	-	1.48	-	-	1.90	14.59	5.99	2.10	2.98	-3.82
203	2	0.021	47.60	17.43	12.98	38.11	3.96	98.97	11.49	17.44	12.06	-5.28
204	1	0.019	-	1.61	-	-	1.67	13.42	5.07	2.06	1.34	-4.15
205	1	0.018	-	3.08	-	2.65	3.06	26.22	9.78	5.31	4.19	-4.12
206	2	0.022	-	7.29	-	0.68	3.83	41.15	11.97	6.01	4.24	-4.74
207	2	0.035	-	1.36	-	-	1.38	13.43	4.15	2.92	1.93	-4.33
208	2	0.038	-	-	-	-	0.36	4.87	1.69	0.36	0.48	-4.05
212	1	0.026	20.17	9.47	7.60	22.32	2.08	40.50	4.52	7.42	5.56	-5.17
215	2	0.033	-	1.44	-	0.02	1.47	16.27	4.76	1.82	1.50	-4.39
216	2	0.032	-	2.53	-	0.37	2.15	21.26	6.83	2.46	1.65	-4.18
217	2	0.047	-	-	-	-	0.41	4.81	2.75	0.74	0.84	-6.91
220	2	0.041	-	-	-	-	1.01	4.88	3.52	1.90	1.14	-6.27
221	2	0.024	-	-	-	-	0.54	8.26	2.71	0.64	0.72	-1.11
222	2	0.037	-	-	-	-	0.93	7.32	2.32	1.04	1.00	-3.85
223	2	0.029	28.84	5.05	6.57	7.70	-	31.46	2.34	9.03	1.87	-6.45
224	1	0.037	-	-	-	-	0.98	3.28	2.18	-	-	-
225	1	0.036	-0.00	1.48	-	3.02	2.65	23.00	8.65	6.30	5.26	-
227	1	0.022	73.78	7.94	4.06	13.24	1.99	45.48	7	10.17	6.86	-5.69
229	1	0.038	-	-	-	-	-	-	-	-	-	-
230	2	0.037	-	2.97	-	2.14	1.50	20.24	5.49	4.70	3.07	-5.22
232	2	0.032	-	-	-	-	0.45	5.85	2.06	0.97	0.85	-
233	2	0.032	-	1.04	-	-	0.99	11.57	3.88	2.44	1.96	-4.96
237	1	0.030	15.66	7.91	-	1.47	3.90	44.79	12.4	7.61	5.23	-6.19
238	1	0.037	6.58	2.15	1.81	4.56	-	14.63	1.87	3.18	2.69	-3.94
239 ^a	2	0.028	-	2.32	-	1.26	1.95	19.41	7.19	4.18	2.86	-5.88
242 ^a	2	0.026	6.52	0.98	-	1.30	1.45	10.22	4.2	1.88	1.53	-2.83
244	2	0.026	-	4.11	-	-	2.77	29.77	8.31	3.48	2.44	-6.33
246 ^a	2	0.027	-	2.43	-	1.03	1.69	15.19	5.74	2.79	1.85	-4.01
247	2	0.026	-	8.00	-	3.33	3.28	37.86	10.44	6.26	3.41	-
249	2	0.029	-	-	-	-	-	-	-	-	-	-5.53
252	1	0.025	35.00	4.47	3.24	9.41	1.66	28.73	4.8	5.95	4.24	-5.87
254	2	0.023	-	1.66	-	-	1.71	17.99	5.49	2.04	1.94	-4.88
257	2	0.026	-	-	-	-	0.85	-	1.35	0.53	0.53	-3.41
259	2	0.029	32.87	6.70	4.21	6.87	-	44.04	10.6	8.21	5.13	-6.29
261	1	0.035	-	1.26	-	-	0.68	11.68	3.08	2.27	1.77	-
262	1	0.028	42.77	11.17	4.51	12.65	3.65	59.40	11.77	12.19	7.93	-8.74
263	3	0.012	-	-	-	-	-	-	-	-	-	-
264	1	0.025	-	1.36	-	-	-	12.31	2.26	2.85	2.23	-3.60
265	1	0.026	41.98	10.02	6.83	20.49	2.05	54.15	7.47	9.30	6.59	-5.20
266	1	0.032	26.50	7.56	1.93	6.67	3.05	44.12	9.83	9.74	6.56	-4.38
267	1	0.010	19.01	10.91	5.84	17.70	4.55	68.50	13.91	11.09	8.38	-5.29
268	2	0.036	36.68	7.35	3.36	8.49	2.64	43.26	13.84	8.84	5.73	-
270	1	0.033	-	-	-	-	-	-	0.63	-	-	-
271	5	0.026	18.70	3.50	2.40	2.90	0.80	18.10	2.8	5.10	3.70	-
273	1	0.020	6.79	0.85	-	-	1.32	10.30	3.39	1.86	1.46	-4.42
274	1	0.027	-	-	-	-	-	3.07	0.9	-	-	-
275	6	0.025	35.00	11.00	4.67	14.00	3.17	46.10	9.526	0.00	17.00	-
277	1	0.034	-	-	-	-	0.85	7.51	2.79	1.83	1.46	-
278	1	0.036	-	-	-	-	-	5.67	1.96	0.90	0.90	-
280	1	0.034	-	2.10	-	-	1.92	14.12	5.21	2.65	2.06	-4.66
281	1	0.041	31.50	3.41	-	2.32	2.13	23.82	6.29	4.65	2.63	-7.66
282	1	0.031	-	-	-	-	-	-	-	-	-	-
283	2	0.037	26.94	6.98	3.24	5.47	4.82	36.71	14.17	9.52	5.67	-7.15
284	1	0.035	-	3.18	-	1.83	2.75	26.10	9.39	5.62	4.45	-4.37
285	1	0.020	-	-	-	-	0.65	3.64	3.45	-	-	-
287	1	0.031	-	3.89	1.49	2.74	2.59	25.05	7.47	5.13	3.72	-4.92
288	1	0.036	-	-	2.91	4.65	1.78	7.27	5.21	1.12	1.41	-
289	1	0.042	2.71	1.70	-	-	1.36	13.65	5.32	2.27	1.57	-4.75
290	1	0.008	11.96	3.05	-	2.62	1.79	22.27	6.7	4.47	3.26	-5.40
291	1	0.018	-	-	-	-	-	-	-	-	-	-

Continued on next page...

Table 9 – Continued

HRS	ref	E(B-V) mag	EW(Å)		[OIII] $\lambda 4958$	[OIII] $\lambda 5007$	[NII] $\lambda 6548$	H α $\lambda 6563$	[NII] $\lambda 6584$	[SII] $\lambda 6717$	[SII] $\lambda 6731$	H β_{abs} $\lambda 4861$
			[OII] $\lambda 3727$	H β $\lambda 4861$								
(1)	(2)	(3)	(4)	(5)	(6)	(7)	(8)	(9)	(10)	(11)	(12)	(13)
292	1	0.012	-	5.17	-	-	3.77	33.82	12.9	4.34	3.42	-6.37
293	1	0.027	-	13.51	4.79	14.29	5.19	69.15	14.42	12.85	9.39	-5.07
294	1	0.011	27.95	2.62	-	1.55	1.60	19.73	5.66	4.85	3.48	-4.45
295	6	0.035	9.00	6.00	0.33	1.00	2.78	22.67	8.346	0.00	6.00	-
297	1	0.017	18.70	2.56	1.36	3.03	1.13	20.31	5.2	4.18	3.01	-6.73
298	1	0.014	27.62	7.49	2.68	6.85	3.53	44.51	12.16	7.34	5.31	-4.79
299	1	0.023	-	2.29	-	1.33	1.07	14.83	4.28	3.26	2.54	-2.95
300	1	0.014	-	-	-	-	0.33	3.91	1.36	0.77	0.60	-
301	1	0.046	-	2.48	-	2.33	0.88	16.72	5.02	4.06	2.92	-4.29
302	1	0.029	11.29	2.29	-	3.00	1.26	18.76	3.33	4.42	3.30	-4.48
303	1	0.010	19.24	7.74	1.82	4.18	5.17	46.49	16.18	9.20	6.73	-4.71
304	1	0.025	-	-	-	-	-	9.28	2.89	2.03	1.42	-
305	1	0.029	-	2.38	0.32	0.75	1.47	17.94	5.19	3.66	2.79	-4.88
308	1	0.033	-	0.63	-	1.14	-	7.39	1.45	1.74	1.36	-2.77
309	1	0.020	23.64	7.32	3.23	12.11	0.93	34.65	4.79	7.43	4.71	-4.52
310	1	0.030	7.77	2.88	-	1.28	2.07	19.25	6.66	3.44	2.59	-4.28
313	1	0.040	-	2.18	-	1.41	1.13	15.38	3.54	3.42	2.62	-5.53
314	1	0.032	31.65	7.24	4.42	14.27	2.50	43.04	7.61	9.19	6.47	-4.15
315	1	0.010	73.98	16.20	13.58	42.31	-	79.23	7.49	12.61	8.32	-7.21
317	1	0.033	-	3.68	1.90	3.34	1.59	21.79	5.39	5.35	3.61	-4.31
318	1	0.027	63.21	5.14	2.62	7.34	1.37	29.70	5.2	7.85	5.02	-5.10
319	1	0.027	23.13	4.73	1.91	6.68	2.40	32.84	7.27	7.42	5.58	-6.00
320	1	0.036	6.72	5.31	1.00	5.16	1.93	29.43	6.38	6.74	4.66	-6.34
321	1	0.037	17.05	6.67	2.37	5.41	3.19	37.23	9.77	7.54	5.64	-5.27
323	1	0.037	-	1.79	-	1.05	1.42	17.48	5.26	3.87	2.90	-4.30

Notes:

- a) spurious detections in the [OIII] $\lambda 4959$ line in Gavazzi et al. (2004).
b) new measurements on the original Gavazzi et al. (2004) data.

Table 10. HRS galaxies with data in the literature: equivalent widths (in Å).

K92										This work									
HRS	[OII] λ3727	Hβ λ4861	[OIII] λ4959	[OIII] λ5007	[NII] λ6548	Hα λ6563	[NII] λ6584	[SII] λ6717	[SII] λ6731	run	[OII] λ3727	Hβ λ4861	[OIII] λ4959	[OIII] λ5007	[NII] λ6548	Hα λ6563	[NII] λ6584	[SII] λ6717	[SII] λ6731
4	10	5	2.3	7	0	34.8	0	-	5	-	-	-	-	-	-	-	-	-	-
20	44	16	7.7	23	4.5	77.0	13.3	-	32	-	-	-	-	-	-	-	-	-	-
275	35	11	4.7	14	3.2	46.1	9.6	-	17	-	-	-	-	-	-	-	-	-	-
295	9	6	0.3	1	2.8	22.7	8.3	-	6	-	-	-	-	-	-	-	-	-	-
J00										This work									
HRS	[OII] λ3727	Hβ λ4861	[OIII] λ4959	[OIII] λ5007	[NII] λ6548	Hα λ6563	[NII] λ6584	[SII] λ6717	[SII] λ6731	run	[OII] λ3727	Hβ λ4861	[OIII] λ4959	[OIII] λ5007	[NII] λ6548	Hα λ6563	[NII] λ6584	[SII] λ6717	[SII] λ6731
29	23.2	5.9	2.4	4.6	1.7	26.3	5.4	5.7	4.2	1	16.7	6.2	1.6	4.8	1.8	27.6	6.3	5.7	4.7
35	3.1	-	-	-	-1	1.8	0.6	0.3	0.3	-	-	-	-	-	-	-	-	-	-
64	14.2	2.5	1.2	1.8	0.7	14.2	2.6	3.7	2.6	-	-	-	-	-	-	-	-	-	-
67	44.9	9.9	5.8	13.8	1.4	40.9	5.2	9	5.8	1	53.1	9.7	5	16.9	2.0	47.4	6.8	9.2	6.5
271	18.7	3.5	2.4	2.9	0.8	18.1	2.8	5.1	3.7	-	-	-	-	-	-	-	-	-	-
MK06										This work									
HRS	[OII] λ3727	Hβ λ4861	[OIII] λ4959	[OIII] λ5007	[NII] λ6548	Hα λ6563	[NII] λ6584	[SII] λ6717	[SII] λ6731	run	[OII] λ3727	Hβ λ4861	[OIII] λ4959	[OIII] λ5007	[NII] λ6548	Hα λ6563	[NII] λ6584	[SII] λ6717	[SII] λ6731
20	39.5	12.65	6.24	18.71	4.82	66.70	14.47	13.72	9.22	-	-	-	-	-	-	-	-	-	-
27	24.4	10.12	2.14	6.42	5.33	50.40	15.99	10.08	7.00	-	-	-	-	-	-	-	-	-	-
36	13.5	5.68	0.93	2.79	5.92	30.30	17.76	5.82	4.72	-	-	-	-	-	-	-	-	-	-
60	7.5	2.56	0.55	1.648	1.56	10.45	4.68	2.26	1.72	1	7.93	1.20	-	1.65	1.58	11.92	5.77	2.28	1.92
73	6.3	2.72	0.05	0.14	1.17	9.16	3.52	1.61	0.90	-	-	-	-	-	-	-	-	-	-
74	13.42	6.40	1.41	4.24	3.84	30.60	11.53	5.90	4.20	1	13.43	6.17	2.62	4.46	4.09	37.27	13.34	6.01	4.55
76	26.4	7.31	4.94	14.81	0.96	30.70	2.87	5.85	3.23	1	35.41	7.86	6.17	19.91	1.02	39.99	4.50	6.43	4.84
85	10.2	3.28	0.55	1.66	2.13	15.18	6.39	3.26	2.18	-	-	-	-	-	-	-	-	-	-
102	10.21	6.06	0.63	1.88	3.81	33.50	11.44	4.8	3.14	2	-	4.86	-	1.18	3.09	31.49	10.20	4.22	3.03
114	9.46	6.26	0.81	2.43	4.33	31.30	13	4.76	3.66	2	7.81	5.36	3.31	1.69	3.76	31.40	12.56	4.83	3.36
122	3	3.09	0.47	1.42	2.34	19.76	7.01	1.84	0.98	1	-	3.05	-	-	2.42	20.00	7.21	1.79	1.25
217	3.1	0.30	0.37	1.12	0.95	3.71	2.86	1.42	0.81	2	-	-	-	-	0.41	4.81	2.75	0.74	0.84
246	13.6	3.65	0.96	2.88	1.92	15.28	5.75	3.69	2.78	2	-	2.43	0.62	1.03	1.69	15.19	5.74	2.79	1.85
250	17.4	5.36	1.13	3.38	3.27	25.80	9.82	5.38	4.34	-	-	-	-	-	-	-	-	-	-
262	39.5	11.20	4.34	13.03	3.94	54.10	11.82	11.58	7.74	1	42.77	11.17	4.51	12.65	3.65	59.40	11.77	12.19	7.93
290	13.4	4.17	0.99	2.97	2.19	18.45	6.57	4.94	3.26	1	11.96	3.05	2.07	2.62	1.79	22.27	6.70	4.47	3.26
M10										This work									
HRS	[OII] λ3727	Hβ λ4861	[OIII] λ4959	[OIII] λ5007	[NII] λ6548	Hα λ6563	[NII] λ6584	[SII] λ6717	[SII] λ6731	run	[OII] λ3727	Hβ λ4861	[OIII] λ4959	[OIII] λ5007	[NII] λ6548	Hα λ6563	[NII] λ6584	[SII] λ6717	[SII] λ6731
102	5.00	5.14	0.39	1.16	2.97	30.39	8.92	3.56	2.57	2	-	4.86	-	1.18	3.09	31.49	10.2	4.22	3.03
122	4.98	3.22	0.27	0.81	2.24	17.09	6.73	2.36	1.73	1	-	3.05	-	-	2.42	20.00	7.21	1.79	1.25
170	7.10	0.46	0.37	1.12	0.54	2.09	1.63	0.94	0.66	2	-	-	-	-	0.70	3.65	1.70	0.76	0.77
205	13.60	3.30	0.42	1.27	3.04	20.61	9.12	5.07	3.81	1	-	3.08	-	2.65	3.06	26.22	9.78	5.31	4.19
211	-	0.62	-	-	-	-	-	-	-	2	-	-	-	-	-	-	-	-	-
217	3.45	0.43	0.31	0.94	1.36	4.18	4.07	1.28	0.94	2	-	-	-	-	0.41	4.81	2.75	0.74	0.84
220	9.57	0.78	0.53	1.60	1.33	2.96	3.99	2.01	1.14	2	-	-	-	-	1.01	4.88	3.52	1.90	1.14
263	-	1.00	-	-	0.50	-	1.50	-	-	-	-	-	-	-	-	-	-	-	-

Notes to Table :

a: References are K92 - Kennicutt (1992b); J00 - Jansen et al. (2000); MK06 - Moustakas & Kennicutt (2006); M10 - Moustakas et al. (2010).

b: for consistency with our work, the original data of Kennicutt (1992b) are corrected for the underlying Balmer absorption in $H\beta$ (5 Å) and $H\alpha$ (2.8 Å). The $[OIII]\lambda 4959$ and the $[NII]\lambda 6548$ equivalent widths are inferred from the $[OIII]\lambda 5007$ and the $[NII]\lambda 6584$ measurements assuming a standard ratio $[OIII]\lambda 5007/[OIII]\lambda 4959=3$ and $[NII]\lambda 6584/[NII]\lambda 6548=3$ (Osterbrock & Ferland 2005). The $[SII]\lambda 6731$ equivalent width includes the emission of both $[SII]\lambda 6717$ and $[SII]\lambda 6731$ lines.

c: the original data of Jansen et al. (2000) are corrected only for the underlying Balmer absorption in $H\alpha$ (2.8 Å), but not for that in $H\beta$ given that the spectral resolution of these data, comparable to our, allows the direct measurement of the underlying absorption.

d: the $[OIII]\lambda 4959$ and the $[NII]\lambda 6548$ equivalent widths of Moustakas et al. (2010) and Moustakas & Kennicutt (2006) are inferred from the $[OIII]\lambda 5007$ and the $[NII]\lambda 6584$ measurements assuming a standard ratio $[OIII]\lambda 5007/[OIII]\lambda 4959=3$ and $[NII]\lambda 6584/[NII]\lambda 6548=3$ (Osterbrock & Ferland 2005).

Table 11. HRS galaxies with data in the literature: fluxes normalised to H α .

K92											This work											
HRS	C(H β)	[OIII] λ 3727	H β λ 4861	[OIII] λ 4959	[OIII] λ 5007	[NII] λ 6548	H α λ 6563	[NII] λ 6584	[SII] λ 6717	[SII] λ 6731	run	C(H β)	[OIII] λ 3727	H β λ 4861	[OIII] λ 4959	[OIII] λ 5007	[NII] λ 6548	H α λ 6563	[NII] λ 6584	[SII] λ 6717	[SII] λ 6731	
4	-	0.13	-	0.07	0.20	-	1	-	-	0.16	-	-	-	-	-	-	-	-	-	-	-	-
20	0.30	0.80	0.28	0.13	0.39	0.06	1	0.17	-	0.39	-	-	-	-	-	-	-	-	-	-	-	-
275	0.00	1.15	0.37	0.14	0.43	0.07	1	0.21	-	0.35	-	-	-	-	-	-	-	-	-	-	-	-
295	0.46	0.25	0.25	0.01	0.04	0.12	1	0.37	-	0.25	-	-	-	-	-	-	-	-	-	-	-	-
J00											This work											
HRS	C(H β)	[OIII] λ 3727	H β λ 4861	[OIII] λ 4959	[OIII] λ 5007	[NII] λ 6548	H α λ 6563	[NII] λ 6584	[SII] λ 6717	[SII] λ 6731	run	C(H β)	[OIII] λ 3727	H β λ 4861	[OIII] λ 4959	[OIII] λ 5007	[NII] λ 6548	H α λ 6563	[NII] λ 6584	[SII] λ 6717	[SII] λ 6731	
29	0.58	0.68	0.23	0.11	0.21	0.06	1	0.21	0.22	0.16	1	0.32	0.58	0.28	0.07	0.20	0.07	1	0.23	0.21	0.17	0.17
35	-	-	0.56	-	-	-	1	-	-	-	-	-	-	-	-	-	-	-	-	-	-	-
64	0.92	0.70	0.19	0.10	0.15	0.05	1	0.19	0.27	0.19	-	-	-	-	-	-	-	-	-	-	-	-
67	0.12	1.32	0.32	0.22	0.51	0.04	1	0.13	0.22	0.14	1	0.19	1.31	0.31	0.15	0.50	0.04	1	0.14	0.19	0.13	0.13
271	0.97	0.71	0.18	0.14	0.17	0.05	1	0.16	0.28	0.20	-	-	-	-	-	-	-	-	-	-	-	-
MK06											This work											
HRS	C(H β)	[OIII] λ 3727	H β λ 4861	[OIII] λ 4959	[OIII] λ 5007	[NII] λ 6548	H α λ 6563	[NII] λ 6584	[SII] λ 6717	[SII] λ 6731	run	C(H β)	[OIII] λ 3727	H β λ 4861	[OIII] λ 4959	[OIII] λ 5007	[NII] λ 6548	H α λ 6563	[NII] λ 6584	[SII] λ 6717	[SII] λ 6731	
20	0.26	0.86	0.29	0.13	0.40	0.07	1	0.21	0.20	0.13	-	-	-	-	-	-	-	-	-	-	-	-
27	0.33	0.56	0.28	0.06	0.17	0.10	1	0.31	0.19	0.13	-	-	-	-	-	-	-	-	-	-	-	-
36	0.73	0.31	0.21	0.03	0.10	0.19	1	0.59	0.19	0.15	-	-	-	-	-	-	-	-	-	-	-	-
60	0.45	0.36	0.26	0.05	0.15	0.15	1	0.45	0.21	0.16	1	1.55	0.26	0.12	-	0.16	0.13	1	0.47	0.18	0.15	0.15
73	0.25	0.35	0.29	0.00	0.01	0.13	1	0.39	0.17	0.09	-	-	-	-	-	-	-	-	-	-	-	-
74	0.48	0.36	0.25	0.05	0.16	0.12	1	0.37	0.18	0.13	1	0.59	0.40	0.23	0.10	0.16	0.11	1	0.35	0.15	0.11	0.11
76	0.09	0.98	0.33	0.21	0.64	0.03	1	0.10	0.19	0.10	1	0.12	1.00	0.32	0.24	0.77	0.03	1	0.11	0.15	0.12	0.12
85	0.65	0.39	0.22	0.04	0.11	0.14	1	0.43	0.21	0.14	-	-	-	-	-	-	-	-	-	-	-	-
102	0.65	0.27	0.22	0.02	0.06	0.11	1	0.34	0.14	0.09	2	0.74	-	0.21	-	0.05	0.10	1	0.32	0.13	0.09	0.09
114	0.46	0.31	0.25	0.03	0.10	0.14	1	0.41	0.14	0.11	2	0.66	0.32	0.22	0.13	0.07	0.12	1	0.39	0.15	0.10	0.10
122	1.05	0.10	0.17	0.02	0.07	0.11	1	0.33	0.09	0.05	1	0.79	-	0.20	-	-	0.12	1	0.36	0.08	0.06	0.06
217	2.00	0.43	0.09	0.10	0.31	0.26	1	0.77	0.37	0.21	2	-	-	-	-	-	0.09	1	0.57	0.15	0.17	0.17
246	0.37	0.55	0.27	0.07	0.20	0.13	1	0.38	0.24	0.18	2	0.84	-	0.20	0.05	0.08	0.11	1	0.37	0.18	0.11	0.11
250	0.85	0.31	0.19	0.04	0.12	0.13	1	0.38	0.20	0.16	-	-	-	-	-	-	-	-	-	-	-	-
262	0.20	0.92	0.30	0.11	0.34	0.07	1	0.22	0.21	0.14	1	0.04	1.15	0.34	0.14	0.36	0.06	1	0.20	0.20	0.13	0.13
290	0.43	0.52	0.26	0.06	0.17	0.13	1	0.35	0.26	0.17	1	0.99	0.46	0.18	0.12	0.14	0.08	1	0.29	0.19	0.14	0.14
M10											This work											
HRS	C(H β)	[OIII] λ 3727	H β λ 4861	[OIII] λ 4959	[OIII] λ 5007	[NII] λ 6548	H α λ 6563	[NII] λ 6584	[SII] λ 6717	[SII] λ 6731	run	C(H β)	[OIII] λ 3727	H β λ 4861	[OIII] λ 4959	[OIII] λ 5007	[NII] λ 6548	H α λ 6563	[NII] λ 6584	[SII] λ 6717	[SII] λ 6731	
102	1.38	0.07	0.14	0.01	0.03	0.10	1	0.29	0.12	0.08	2	0.74	-	0.21	-	0.05	0.10	1	0.32	0.13	0.09	0.09
122	1.24	0.10	0.15	0.01	0.04	0.13	1	0.39	0.14	0.10	1	0.79	-	0.20	-	-	0.12	1	0.36	0.08	0.06	0.06
170	1.23	0.74	0.15	0.12	0.37	0.25	1	0.76	0.43	0.31	2	-	-	-	-	-	0.19	1	0.47	0.20	0.20	0.20
205	1.66	0.19	0.11	0.01	0.04	0.15	1	0.44	0.25	0.19	1	1.28	-	0.14	-	0.12	0.12	1	0.37	0.20	0.16	0.16
211	-	-	1.00	-	-	-	1	-	-	-	2	-	-	-	-	-	-	-	-	-	-	-
217	2.25	0.22	0.07	0.05	0.16	0.32	1	0.96	0.30	0.23	2	-	-	-	-	-	0.09	1	0.57	0.15	0.17	0.17
220	0.93	0.74	0.18	0.13	0.38	0.44	1	1.33	0.66	0.37	2	-	-	-	-	-	0.20	1	0.72	0.38	0.23	0.23
263	-	-	-	-	-	-	1	-	-	-	-	-	-	-	-	-	-	-	-	-	-	-

Notes to Table :

a: References are K92 - Kennicutt (1992b); J00 - Jansen et al. (2000); MK06 - Moustakas & Kennicutt (2006); M10 - Moustakas et al. (2010).

b: for consistency with our work, the original data of Kennicutt (1992b) are corrected for the underlying Balmer absorption in $H\beta$ (5 Å) and $H\alpha$ (2.8 Å). The $[OIII]\lambda 4959$ and the $[NII]\lambda 6548$ fluxes are inferred from the $[OIII]\lambda 5007$ and the $[NII]\lambda 6584$ measurements assuming a standard ratio $[OIII]\lambda 5007/[OIII]\lambda 4959=3$ and $[NII]\lambda 6584/[NII]\lambda 6548=3$ (Osterbrock & Ferland 2005). The $[SII]\lambda 6731$ flux includes the emission of both $[SII]\lambda 6717$ and $[SII]\lambda 6731$ lines.

c: the original data of Jansen et al. (2000) are corrected only for the underlying Balmer absorption in $H\alpha$ (2.8 Å), but not for that in $H\beta$ given that the spectral resolution of these data, comparable to our, allows the direct measurement of the underlying absorption.

d: the $[OIII]\lambda 4959$ and the $[NII]\lambda 6548$ fluxes of Moustakas et al. (2010) and Moustakas & Kennicutt (2006) are inferred from the $[OIII]\lambda 5007$ and the $[NII]\lambda 6584$ measurements assuming a standard ratio $[OIII]\lambda 5007/[OIII]\lambda 4959=3$ and $[NII]\lambda 6584/[NII]\lambda 6548=3$ (Osterbrock & Ferland 2005). In the original works of Moustakas et al. (2010) and Moustakas & Kennicutt (2006) fluxes are absolute values (not normalised) representative of the whole galaxies. The galaxy HRS 211 in Moustakas et al. (2010) is detected only in the $H\beta$ line.

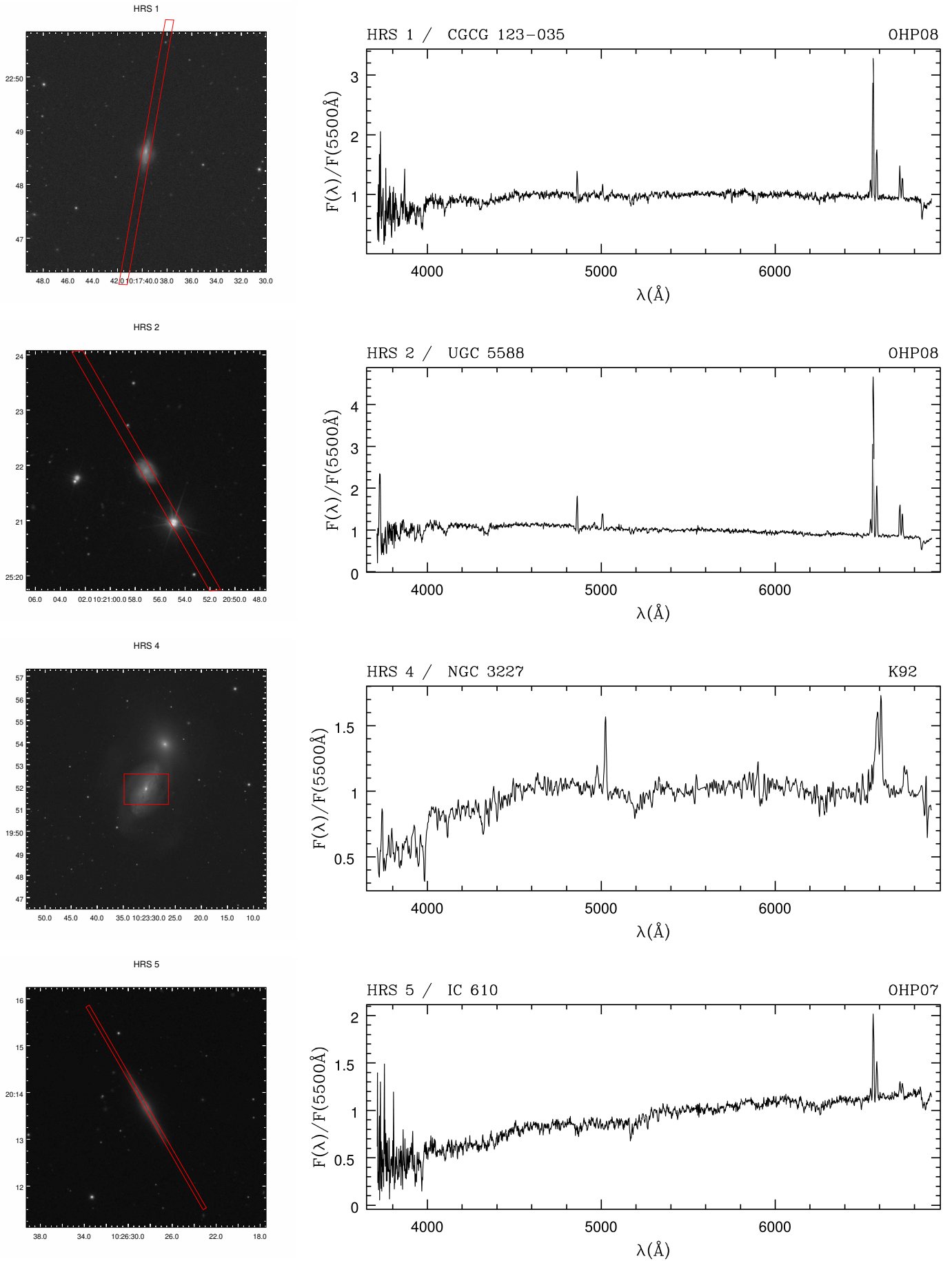


Fig. 19. Integrated spectral atlas of the HRS galaxies, in order of increasing HRS name. Left: the *r* band SDSS image of the observed galaxies with overlaid the position covered by the slit during the observations (red solid line). Right: observed spectra normalised to their mean intensity between $\lambda = 5400 - 5600 \text{ \AA}$. The full atlas is available in electronic format on the HeDaM database.